UNIVERSIDAD NACIONAL AUTÓNOMA DE MÉXICO
POSGRADO EN CIENCIAS FÍSICAS
INSTITUTO DE CIENCIAS FÍSICAS

DECOHERENCE, ENTANGLEMENT, AND QUANTUM INFORMATION WITH TWO-QUBIT SYSTEMS

TESIS QUE PARA OPTAR POR EL GRADO DE:
DOCTOR EN CIENCIAS (FÍSICA)

PRESENTA:

CARLOS ANDRES GONZALEZ GUTIERREZ

TUTOR PRINCIPAL:

DR. THOMAS HENRY SELIGMAN SCHURCH
INSTITUTO DE CIENCIAS FÍSICAS

MIEMBROS DEL COMITÉ TUTOR:

DR. CARLOS FRANCISCO PINEDA ZORRILLA
INSTITUTO DE FÍSICA

DR. THOMAS GORIN
UNIVERSIDAD DE GUADALAJARA

CIUDAD DE MÉXICO, ENERO 2019

'There is no authority who decides what is a good idea.'

The Meaning of it All.

Richard Feynman

Contents

Abstract

In this thesis we present some results about decoherence, entanglement dynamics, and quantum information employing one and two-qubit systems. We start by introducing the Kicked Ising model (KI) as a quantum chaotic Hamiltonian model to describe decoherence and entanglement decay in one and two non-interacting spin systems in the presence of a near and far KI environments. We show that these nested spin-environments can assist the protection of coherence and entanglement (measured by purity and concurrence) by tuning the coupling between near and far environments, a mechanism that could be further exploited for quantum information processing and quantum computation based in spin systems. We then turn our attention to the study of decoherence in light-matter scenarios considering a two-atom system interacting with a single-mode of the electromagnetic field. For different initial states of the field, we found very specific analytical relations between purity and concurrence for Tavis-Cummings as well as photon-dependent and dephasing interactions. These results allowed to compute concurrence thresholds for the necessary entanglement to realize a teleportation protocol with quantum speedup depending on the specific interaction. The problem of microscopic dissipation is also discussed for the simple case of the Jaynes-Cummings interaction for which a general Lindblad master equation in the dressed state basis was obtained and solved in the limit of single-excitation. Phase space analysis beyond this single-excitation manifold showed that field relaxation to equilibrium is better described by the microscopic approach instead of the common formulation using the standard phenomenological approach. The final chapter of this thesis considers the implementation of a complete atomic-Bell measurement based on the nonlinear light-matter interaction provided by the two-photon Dicke model. It turns out that a convenient way to express the time evolution of the system in terms of Bell and coherent states of the field can be found and exploited in order to achieved the complete discrimination and postselection of the full Bell basis by performing projective measurements on the field in an optical two-stage Ramsey setup. The experimental feasibility of the protocol is discussed in the context of cavity-QED, circuit-QED, and trapped ions setups.

Resumen

En esta tesis se aborda el estudio de la decoherencia, entrelazamiento e información cuántica en sistemas de uno y dos qubits. En la primera parte de la tesis se introduce el modelo de Ising pateado (KI); un sistema que presenta caos en el sentido de la teoría de matrices aleatorias (RMT), para describir la dinámica de uno y dos qubits no interactuantes en presencia de entornos caóticos anidados, los cuales llamamos entorno cercano y lejano. El resultado principal en esta parte se basa en un efecto encontrado, en el cual entornos anidados pueden ayudar a proteger la coherencia y el entrelazamineto de sistemas de qubits aprovechando el control de la interacción entre dichos entornos, cernano y lejano. Este fenómeno podría ser explotado para el procesamiento de información cuántica basada en sistemas de espines y en sistemas de iones atrapados. En la segunda parte de la tesis tratamos el tema de decoherencia en el contexto de la interacción de la luz con la materia. Consideramos un sistema de dos atomos de dos niveles (qubits) interactuando con un solo modo de radiación electromagnética en una cavidad. Se estudiala dinámica de los qubits para distintos estados iniciales del modo de radiación y se obtienen expresiones analíticas generales entre la pureza de los qubits y su entrelzamiento usando tres tipos de interacción: Jaynes-Cummings, Buck-Sukumar e interacción espin-bosón. Los resultados obtenidos permiten calcular valores umbrales para el entrelazamiento necesario para llevar a cabo el algoritmo de teleportación cuántica de manera eficiente dependiendo del tipo de interacción estudiada. En este contexto también se estudia el problema de disipación desde el punto de vista microscópico en el caso de una interacción de tipo Jaynes-Cummings y se deriva una ecuación maestra en forma de Lindblad. Una solución analítica a ésta ecuación se deriva en límite de una sola excitación y se realiza un análisis detallado de la dinńamica del sistema en el espacio fase para el caso de mas de una excitación. Un resultado interesante es que la dinámica de relajación del campo electromagnético hacia el estado de equilibrio resulta ser más adecuada por el enfoque microscópico en comparación del tratamiento común usando el enfoque fenomenológico estandar. La parte final de la tesis trata el tema de información cuántica en electrodinámica cuántica de cavidades. Se propone la implementación de una medición completa de Bell usando una interacción no lineal de dos fotones de dos átomos en una cavidad usando el modelo de Dicke y se encuentran expresiones aproximadas para la evolución del sistema en el límite de muchos photones. Resulta interesante que dicha solución puede ser expresada en términos de estados de Bell atómicos y estados coherentes del campo, cual se puede aprovechar para discriminar y postseleccionar sin ambiguedad cada uno de los cuatro estados de la base de Bell con ayuda de mediciones proyectivas realizadas sobre el modo electromagnético en un esquema tipo Ramsey con dos cavidades. Por último se discute la posibilidad de implementar experimentalmente el protocolo propuesto en experimentos de electrodinámica cuántic de cavidades, circuitos superconductores y también el la arquitectura de iones atrapados en potenciales armónicos.

Agradecimientos

Finalmente he llegado a este punto donde las palabras no serán suficientes para agradecer a tantas personas, instituciones y proyectos, sin los cuales concluir esta tesis no hubiera sido posible.

Agradezco con mucho cariño a mi familia en Barranquilla-Colombia, que desde la distancia siempre enviaban sus buenos deseos y mensajes que me inspiraban a seguir adelante. En especial a mi madre Adela, mi hermana Ena Luz y mi abuela Donatila.

Quiero expresar mi más profundo agradecimiento a Adriana Lozano, quien ha sido testigo de todos los momentos felices y tristes que he vivido durante el posgrado. Sin su apoyo hubiera sido imposible.

Quiero agradecer especialmente a mi asesor Thomas H. Seligman por su excelente labor como tutor y por sus consejos siempre acertados. También por todo el apoyo que me brindó para realizar estancias de investigación durante el doctorado en México, Eslovenia y Alemania.

A todos los investigadores con quienes tomé clases, trabajé o estuve visitando durante estancias, quienes me brindaron mucho conocimiento en cada una de sus áreas: Carlos Pineda, Thomas Gorin, Tomaž Prosen, Blas Rodriguez, Mauricio Torres, Pablo Barberis, François Leyvraz, Hernán Larralde, Luis Mochán, Max Aldana, Bernardo Wolf, Armando Pérez-Leija, Octavio de los Santos, Luis Benet, Thomas Stegmann, Manan Vyas, Jianming Cai.

Al Dr. José Récamier, mi asesor de licenciatura y con quien he colaborado hasta la fecha. Infinitas gracias por todo su apoyo durante todos estos años, amdemás por sus buenos comentarios en esta tesis.

A todos los científicos con quien tuve la oportunidad de charlar en el Centro Internacional de Ciencias en Cuernavaca, un lugar donde conocí gente impresionante y donde se discutia física de primer nivel.

Muchas gracias a todos mis amigos del Instituto de Ciencias Físicas de la UNAM en Cuernavaca, con quienes compartí momentos inolvidables. En especial a Ricardo, David (Poshin) y Roberto (Mota). Será dificil mencionarlos a todos, pero aqui van: Mayra, Luisana, Bertha, Cristina, Karla, Héctor, Moisés, Jorge, Paulino, Susana, Raksha, Tanu, Yenni, Adrian, Alfredo, Diego, Braulio.

A Mauricio Torres, quien es practicamente co-asesor de esta tesis. Gracias Mau por brindarme tu amistad y permitirme trabajar contigo.

Agradezco a los sinodales de esta tesis: François Leyvraz, Mauricio Torres, Pablo Barberis y a Roberto de León por sus excelentes sugerencias y correcciones.

Al Dr. Blas Rodriguez Lara, quién influyó de manera muy positiva en un momento clave de mi doctorado y cuyo trabajo también se ve reflejado en esta tesis.

A los nuevos amigos: Ivan Kukuljan y Ralf Betzholz por sus atenciones y hospitalidad en Ljubljana y en Wuhan.

Publications

All results presented in this thesis are based on the following publications:

- C. González-Gutiérrez, E. Villaseñor, C. Pineda, and T. H. Seligman, "Stabilizing coherence with nested environments: a numerical study using kicked Ising models", *Phys. Scr.*, **91**(8), 083001, (2016).

- C. González-Gutiérrez, R Román-Ancheyta, D. Espitia, and R. Lo Franco, "Relations between entanglement and purity in non-Markovian dynamics", *Int. J. Quantum Inform.*, **14**, 1650031, (2016).

- C. González-Gutiérrez, D. Solís-Valles, and B. M. Rodríguez-Lara, "Microscopic approach to field dissipation in the Jaynes-Cummings model", *J. Phys. A: Math. Theor.*, **51**, 015301 (2018).

- Carlos A. González-Gutiérrez and Juan Mauricio Torres, "Atomic Bell measurement via two-photon interactions", *arXiv preprint*, arXiv:1811.06176 (2018)
  (Submitted to Physical Review A)

Other publications (not included in this thesis):

- R. Román-Ancheyta, C. González-Gutiérrez, and J. Récamier, "Photon-added nonlinear coherent states for a one-mode field in a Kerr medium", *J. Opt. Soc. Am. B*, **31**(1), 38-44, (2014).

- O. de los Santos-Sánchez, C. González-Gutiérrez, and J. Récamier, "Nonlinear Jaynes-Cummings model for two interacting two-level atoms." *J. Phys. B: At. Mol. Opt. Phys.*, **49,** 165503, (2016).

- R. Román-Ancheyta, C. González-Gutiérrez, and J. Récamier, "Influence of the Kerr nonlinearity in a single nonstationary cavity mode", *J. Opt. Soc. Am. B*, **34**(6), 1170-1176, (2017).

- R. Román-Ancheyta, O. de los Santos-Sánchez, C. González-Gutiérrez, "Damped Casimir radiation and photon correlation measurements", *J. Opt. Soc. Am. B*, **35**(3), 523-527, (2018).

- C. González-Gutiérrez, O. de los Santos-Sánchez, R. Román-Ancheyta, M. Berrondo, and J. Récamier, "Lie algebraic approach to a nonstationary atom-cavity system", *J. Opt. Soc. Am. B*, **35**(8), 1979-1984, (2018).

Chapter 1

Introduction

We are living the so called *second quantum revolution*, in which quantum phenomena like superposition and entanglement allow practical applications such as quantum computing, quantum teleportation, quantum cryptography, quantum metrology, quantum communication, and more recently, quantum sensing [1, 2]. The identification of quantum entanglement as a technological tool was first pointed out by Peter Shor in 1994 [3], establishing that a quantum computer (a machine based on quantum mechanics), harnessing the non-local properties of such correlations as a consequence of entanglement, provides an exponential speedup in the computational power for some intractable numerical problems. Entanglement and the behaviour of quantum systems in general, are now important technological tools and not just curiosity, or a consequence of the non complete status of quantum theory as Einstein, Podolsky, and Rosen pointed out in their famous EPR paradox [4].

Nowadays there are plenty of options for the physical encoding of quantum information. Some of them more promising than others for future large scale implementations, but all of them showing a big step towards the precise control and manipulation of quantum systems. In this thesis we deal mainly with spin systems [5], atomic qubits in high finesse optical cavities [6], or trapped ions in harmonic potentials [7,8]. The main limiting factor for the implementation of these technologies is the fact that quantum systems are very sensitive to their surroundings and every perturbation might deteriorate quantum coherence and entanglement (see Ref. [9] for an example in cavity-QED). One of the key ingredients in a quantum processor is therefore the conservation of quantum coherence and entanglement for long times, at least long enough in order to perform quantum operations and process quantum information. Dynamics of composite quantum systems interacting with their surroundings is therefore of central interest for understanding how quantum features are affected by the environment and for controlling them in view of their exploitation as quantum information resources [10–14]. In this sense, exactly solvable Hamiltonian models for the interaction between the system and the environment are useful in the general understanding of open quantum systems. One of the first phenomenological models for decoherence was proposed by Caldeira and Leggett (CL) considering a harmonic oscillator immersed in a bath of independent harmonic oscillators at finite temperature [15, 16]. In particular, the situation provided in the CL model is appropriate for the study of the dynamics of meso or nanoscopic superconducting devices which in turn are useful for testing quantum theory at the the macroscopic scale. Despite of the fact this model can reproduce generic features of decoherence in various real systems, it does not capture the actions of different environments, for instance, there are reservoirs whose dynamics can be better mimicked by a set of two-level systems or spins instead of harmonic oscillators [16,17]. In this context we have introduced a model for the study of decoherence in one and two qubit systems in the presence of a spin environment in Chapter 3. One of the main goals is to understand the generic features of the dynamics in this kind of enironments so we can find clever strategies to control and use this information in our favor. In many situations the immediate environment surrounding a quantum system can be well controlled in order to isolate the system for unwanted external interactions. The following questions then arise: what about the

influence of the rest of the universe?, i.e., the environment that is not immediately accessible to the system. Can it affect the decoherence process due to the interaction with the immediate environment? can it slow down decoherence (or equivalently, protect coherence) in the system? It turns out that the answer to these questions is affirmative as we will see in Chapter 3 where the implementation of a particular dynamics using the presence of a nested spin environment is described.

A quantum system made of two qubits is the simplest theoretical platform to analyze entanglement and coherence evolution from the perspective of the theory of open quantum systems [18, 19]. The study of this simple system is of special relevance as it constitutes the basic building block for quantum gates and quantum teleportation protocols [20, 21] which can be affected by external undesired interactions. Physical models in the context of quantum optics have been widely used in the study of *intrinsic* decay of quantum coherences for one or more qubits due to the interaction with the quantized electromagnetic radiation field. For instance, the Jaynes-Cummings model or its generalization to a collection of N two-level atoms (or qubits) known as the Tavis-Cummings model are typical settings [22, 23]. The study of bipartite entanglement between one qubit and the field [6, 24, 25] or of multipartite entanglement among qubits [26, 27], has led to discover many interesting phenomena and also to experimental proposals for quantum protocols. Some examples are entanglement in simple quantum phase transitions [28], protocols for Bell state measurements [29, 30], physical implementation of quantum gates [20, 31, 32] and generation of quantum correlations in qubit networks [33].

One of the main drawbacks encountered when two qubits locally interact with their own Markovian (memoryless) environment is the so-called entanglement sudden death (ESD), that is the complete disappearance of entanglement at a finite time [34–41]. This phenomenon has been proven experimentally [44, 45] and has motivated the development of efficient strategies to avoid it [46–53] or delay it [54–61], typically based on suitable non-Markovian (memory-keeping) environments and local operations. In chapter 4 we provide new insights about the non-Markovian dynamics of the quantum correlations captured by entanglement from the perspective of its interplay with purity, which identifies the degree of mixedness of a quantum state being related to coherence. Such a study is still little addressed in the literature but there has been interesting works with chaotic environments [39–41, 62] and other non-Markovian environments [63].

Knowledge of relationships between entanglement and purity in specific dynamical contexts is important not only from a fundamental viewpoint but also from a practical one. In fact, it would provide quantitative thresholds of entanglement for a given purity at a certain time which allow quantum protocols, like teleportation [64, 65], entanglement swapping [66] and entanglement percolation [67]. To this aim our strategy is to consider a two-qubit *central system* using the so-called *spectator configuration* [62], where one of the qubits is isolated and acts as a *probe*. This idealized configuration is a convenient way to investigate non-trivial dynamics of entanglement versus purity for two qubits without any type of interaction between them. On the other hand, the characterization of quantum processes under particular channels or operations within this simple open quantum system can be implemented experimentally. Realizations of unital and nonunital (both Markovian and non-Markovian) channels acting on one of two qubits are possible using all-optical setups [49, 55, 68, 69] and are also achievable in circuit-QED devices [23, 25]. For our analysis we shall also employ the concurrence-purity (*C-P*) plane [42], which is a powerful tool that brings a general overview of the system dynamics. We focus on three models which shall allow us to obtain exact analytical results with a consequent better understanding of the system evolution, namely: Tavis-Cummings (TC), Buck-Sukumar (BS) and spin-boson (SB) models. In the second part of Chapter 4 we study the problem of microscopic dissipation in the simplest model of light-matter interaction, the Jaynes-Cummings model. Traditional treatments of dissipation involve a dynamical description in terms of a Markovian Lindblad master equation that considers only dissipation due to photonic or field losses. We derive a general Markovian Lindblad master equation from the exact eigenstates, known as a the dressed basis, from which dissipation is caused by transitions or channels induced by the external environment. Purity and entropy are analyzed as a function of detuning between the qubit and field

frequencies and the qubit-field entanglement in the single excitation manifold is studied. It turns out that for initial semiclassical states of the field, we show that the microscopic approach, in phase space, provides an evolution to thermal equilibrium that is smoother than the one provided by the standard phenomenological approach.

In chapter 5 we address the issue of implementing quantum information algorithms using quantum optical setups, in particular those based on cavity-QED. In this last part of the thesis we describe how to implement a complete Bell measurement scheme employing projective measurements of multiphotonic coherent fields in a model of two qubits interacting with one mode of a radiation field trough two-photon transitions. The concept of Bell measurement is crucial to implement quantum information protocols such as quantum teleportation, superdense coding, and entanglement swapping [20, 71]. These protocols play a key role in the nodes of a quantum repeater and to establish long-distance communication in a quantum network [72, 73]. In a complete Bell measurement a two-qubit system is probabilistically projected onto one of the four Bell states. For photonic qubits, it is possible to identify two of the four Bell states, i.e. a 50%-efficient Bell measurement, using interference effects with linear optics [74–76]. The capability to surpass this limit relies either on more resourceful techniques [77, 78] or on higher order optical interactions [79] that report low efficiency in the experiment [80]. In the case of atomic qubits, most experimental realizations of quantum teleportation consider the implementation of a complete Bell measurement through entangling gates, such as a controlled-NOT or controlled-phase gate, that together with single qubit gates can map Bell sates onto product states in the computational basis [81–83]. A problem with this approach, however, is that high fidelity two-qubit gates are still experimentally difficult to achieve [84–86].

Motivated by the hybrid quantum repeater [72] that employs material qubits and multiphoton coherent signals, a recently proposed alternative is to explore atom-photon interaction models that directly generate Bell states of the atoms correlated with states of the field. Using this approach, it was shown that unambiguous Bell state projections can be implemented within the framework of the two-atom Tavis-Cummings model [29, 30, 87]. There, the state of the atoms is postselected by projecting the states of the field onto nearly orthogonal coherent states. The great benefit is that the atomic states are not directly measured and their projection occurs as postselection of the measured field. An imperfect efficiency relies on the fact that initial coherent states of the field in the Tavis-Cummings model do not evolve coherently during the interaction [29, 88]. This is clearly manifested in the non-perfect revivals of Rabi oscillations of atomic observables, similar to the well known collapse and revival phenomena in the Jaynes-Cummings model [89]. The natural question that arises is whether an atom-field model presenting perfect revivals of Rabi oscillations could better assist in the postselection of atomic Bell states. The answer to this question turns out to be positive as we shall demonstrate. In this context we propose a complete atomic Bell measurement based on the two-photon two-atom Dicke model in the rotating wave approximation [90] that presents nearly perfect revivals of Rabi oscillations. Similar to previous work [29, 30], the states of the qubits are encoded in a pair of two-level atoms that interact resonantly and sequentially with the field inside two optical cavities and the atomic state is postselected by measuring the optical field. The considered two-photon atom-field interaction model was first introduced as a generalization of the Jaynes-Cummings model [91–93], and later extended to multiatomic systems [90, 94]. It has been proposed theoretically, but its experimental feasibility has been analyzed in well controllable quantum optical systems [95]. Although we focus on a cavity QED implementation, two-photon or two-phonon interactions have also been studied and proposed in circuit QED and trapped ions [96, 97], thus making our proposal attractive to other architectures involving matter-field interaction.

This thesis is based mainly in four publications [61, 99–101]. We shall present all the results in chronological order and hope that the reader may find some of the work presented here useful.

Chapter 2

Fundamental concepts

In this chapter we review some of the basic concepts employed along this thesis. We introduce the main mathematical tools and models describing the physical systems and prepare the ground for the subsequent analysis in order to make the content of this manuscript self contained. For technical and specific details we will refer to the reader to the corresponding references.

2.1 Entanglement

Entanglement is a fundamental concept that distinguishes quantum theory from classical wave theory. Nowadays entanglement is considered a fundamental resource for many applications and lies at the heart of quantum computation, quantum teleportation, and quantum cryptography [102]. Amazing experimental progress has been achieved in production, manipulation, and detection of entangled states in a great variety of physical systems, just to mention a few: trapped ions in harmonic potentials, photons, nuclear magnetic resonance, atoms in optical cavities, artificial superconducting qubits in quantum circuits, etc [6, 82, 103–105]. It has been even argued that entanglement plays a significant role in the efficiency of the energy transfer process in light-harvesting complexes and photosynthetic reaction centers [106]. The first attempt to prove the non-local correlations of measurement results was made by Jhon Bell, who derived experimentally testable inequalities for the discrimination of correlations due to entanglement in contrast to those described by hidden variable theories [107]. Many experiments have been performed in order to check if Bell's inequalities can be violated, being perhaps the experiment reported by Aspect *et. al.* in 1982 one of the most popular and in which EPR pairs of photons were employed [108]. In quantum information theory, entangled states are considered as valuable resources for information tasks and therefore their classification and quantification is a very active research topic. Here we are not interested in the whole world of entanglement theory and we just provide the necessary concepts and tools for the understanding of the forthcoming chapters. For the reader interested in entanglement theory see for example Ref . [109].

Bipartite entanglement

A quantum system composed of two subsystems is called a *bipartite* quantum system. The Hilbert space of such a system $\mathscr{H}$ is given by the tensor product of the associated individual Hilbert spaces $\mathscr{H}_1 \otimes \mathscr{H}_2$, each of which denotes one subsystem. For pure states two kinds of quantum states can be identified, product states (or separable) and entangled states. A state $|\psi\rangle$ is called a product state or separable, if one is able to write it in the form

$$|\psi\rangle = |\varphi\rangle \otimes |\phi\rangle, \tag{2.1}$$

where $|\varphi\rangle \in \mathcal{H}_1$ and $|\phi\rangle \in \mathcal{H}_2$. The information content in the state 2.1 is exactly the same as the contained by the individual states in each subsystem. Any measurement performed on one of the subsystems has no effect on the other subsystem, i.e., measurement outcomes on different subsystems are uncorrelated. On the other hand correlations arise for entangled states, in other words, states that can not be written as the product of independent subsystem states. In this situation a local measurement affects the entire bipartite system and a description in terms of individual states for each subsystem is no longer possible. For general mixed states the situation becomes more complicated. In this case product states and separable states are not the same, a product state can still be written as a tensor product of subsystem state ρ_1 and ρ_2

$$\rho = \rho_1 \otimes \rho_2, \tag{2.2}$$

whereas a separable state is a convex sum of product states in the form

$$\rho = \sum_i p_i \rho_1^i \otimes \rho_2^i, \tag{2.3}$$

where $\sum_i p_i = 1$. Such separable states illustrate a situation where correlations between subsystems are consequence of the incomplete knowledge about the state of the full system and are completely characterized by classical probabilities p_i. Mixed entangled states are defined by the non-existence of a convex decomposition as the one given in Eq.2.3, i.e., a general mixed state ρ is entangled if [109]

$$\rho \neq \sum_i p_i \rho_1^i \otimes \rho_2^i. \tag{2.4}$$

Correlations in entangled states can not be characterized by a set of classical probabilities and have no analogue in classical systems.

2.1.1 Bell states

The maximally entangled two-qubit states are known as *Bell states* or *EPR states*. These states are defined as

$$|\Phi^+\rangle = \frac{1}{\sqrt{2}} \left(|00\rangle + |11\rangle \right), \tag{2.5}$$

$$|\Phi^-\rangle = \frac{1}{\sqrt{2}} \left(|00\rangle - |11\rangle \right), \tag{2.6}$$

$$|\Psi^+\rangle = \frac{1}{\sqrt{2}} \left(|01\rangle + |10\rangle \right), \tag{2.7}$$

$$|\Psi^-\rangle = \frac{1}{\sqrt{2}} \left(|01\rangle - |10\rangle \right). \tag{2.8}$$

If any of the above states represents the state of two qubits, one can see that perfect correlations can be found between local measurements performed on both systems, independently of the distance between them. These correlations can not be explained without quantum mechanics as was shown by J. Bell in 1964 [107]. The set of Bell states constitutes a basis for the four-dimensional Hilbert space of a two-qubit system.

2.1.2 von Neumann entropy and purity

Given the above definition of a general entangled state in Eq.2.4, the problem of deciding whether a quantum state is separable or not is definitely not an easy task. This question constitutes the so-called *separability problem*, a topic of current intense research [110]. Another issue with the given criterion is

that quantification of entanglement becomes also difficult at the time of practical applications, so having a practical quantitative way of computing the degree of entanglement becomes essential. It tuns out that an entropy function can be a useful tool to evaluate the amount of entanglement in a bipartite system. From the point of view of statistical mechanics and information theory, entropy can be seen as a lack of information measure, i.e, the information that would be gained if a perfect measurement of the system could be made. The von Neumann entropy for a density oparator ρ is defined as

$$S(\rho) = -\operatorname{Tr}\rho\ln\rho. \tag{2.9}$$

For a pure state $S(|\psi\rangle\langle\psi|) = 0$ and posterior measurements on the state of the system result in no gain of new information. For a mixed state we have that in general $S(\rho) > 1$. The von Neumann entropy is not easy to compute in general, but instead we can make use of a simpler function called *Purity*, which is defined via

$$P(\rho) = \operatorname{Tr}\rho^2. \tag{2.10}$$

This quantity varies from one for pure states to $1/\dim(\rho)$ for the totally mixed state. If in the above formulas ρ is the partial trace of a pure state, i.e.,

$$\rho = \operatorname{Tr}_2|\Psi\rangle\langle\Psi|, \tag{2.11}$$

where $|\Psi\rangle \in \mathscr{H}_1 \otimes \mathscr{H}_2$ and Tr_2 is the partial trace operation over $\mathscr{H}_2$, then both quantities, the von Neumann entropy and purity can be employed as measures of the entanglement between the two subsystems implied in the partial trace operation. Purity is just one of a large number of convex functions that can describe decoherence as interpreted as entanglement with the other subsystem. Its main advantage is the simple analytic structure which allows to compute it without previous diagonalization of the density matrix. Partial orders can be obtained using all or complete sets of positive functions [111–113]. Any of these convex functions reveal, in general, different aspects of decoherence. In fact, for a single qubit they are all equivalent and for larger systems, near pure states, they also tend to be equivalent. In this thesis we will use purity as our main measure for coherence of a quantum system in interaction with its environment. The reason for this choice is the fact that the square is holomorphic and often allows closed solutions, as mentioned above.

2.1.3   Entanglement measures

Before defining a concrete measure for the entanglement of a two-qubit system we first list the conditions that any entanglement measure must fulfill [109]. If E is an entanglement measure then:

- $E(\rho)$ is zero for separable states.

- *Additivity:* entanglement of n copies of a state ρ is given by $E(\rho^{\otimes n}) = nE(\rho)$.

- *Subadditivity:* entanglement of two states does not exceed the sum of the entanglement of both independent states, $E(\rho \otimes \rho') \leq E(\rho) + E(\rho')$.

- *Convexity:* $E(\lambda\rho + (1-\lambda)\rho') \leq \lambda E(\rho) + (1-\lambda)E(\rho')$, with $0 \leq \lambda \leq 1$.

Concurrence

In its original definition, *concurrence* was an auxiliary quantity used to compute the entanglement of formation for a system composed by two qubits [109]. For a pure state $|\psi\rangle$ concurrence is defined as follows

$$C(\psi) = |\langle\psi^*|\sigma_y \otimes \sigma_y|\psi\rangle|, \tag{2.12}$$

where σ_y is the Pauli matrix and the state $|\psi^*\rangle$ is the complex conjugate of $|\psi\rangle$ with respect to the computational basis $\{|00\rangle, |01\rangle, |10\rangle, |11\rangle\}$. For mixed states, the concurrence is generalized trough the corresponding convex roof extension

$$C(\rho) = \inf_{\{p_i, \psi_i\}} \sum_i p_i C(\psi_i), \quad \text{with } p_i > 0, \ \rho = \sum_i p_i |\psi_i\rangle\langle\psi_i|. \tag{2.13}$$

It turns out that this infimum can be computed exactly as was shown by Wootters in Ref. [114]. Concurrence can then be expressed in a more practical way as

$$C(\rho) = \max\{0, \tilde{\lambda}_1 - \sum_{i=2}^{4} \tilde{\lambda}_i\}, \tag{2.14}$$

where $\tilde{\lambda}_i$ are the square roots of the eigenvalues of $\rho\tilde{\rho}$ in decreasing order. The operator $\tilde{\rho}$ is the result of applying a *spin flip* operation on ρ, i.e., $\tilde{\rho} = (\sigma_y \otimes \sigma_y)\rho^*(\sigma_y \otimes \sigma_y)$. Again the complex conjugate is taken in the computational basis of two qubits.

2.2 Microscopic description of open quantum systems

Any practical description of a quantum system must take into account the unavoidable influence of the external environment. We use the term *open quantum system* for a quantum system $\mathscr{S}$ which is coupled to another quantum system called the *environment* $\mathscr{E}$. In general we assume that the combined system $\mathscr{S} + \mathscr{E}$ is closed and can be well described by a Hamiltonian dynamics. To describe the state of the subsystem $\mathscr{S}$, however, we need to include the effects of the surroundings, and such Hamiltonian description is no longer appropriate. It turns out that, as a consequence of the system-environment interaction, correlations between both systems appear and the dynamics in $\mathscr{S}$ must be described by a reduced system dynamics. In the following we will briefly describe in some detail how we can study the dynamics of general weakly coupled open quantum systems in the Markovian regime using the microscopic master equation approach as described in Ref. [18].

Let $\mathscr{H}_S$ and $\mathscr{H}_E$ be the Hilbert spaces corresponding to the system and and the environment, respectively. The Hilbert space of the total system is given by $\mathscr{H} = \mathscr{H}_S \otimes \mathscr{H}_E$. The Hamiltonian of the closed system is

$$H = H_S + H_E + H_{\text{int}}. \tag{2.15}$$

The unitary evolution of the total system is then dictated by the von Neumann equation in the interaction picture

$$\frac{d\rho(t)}{dt} = -i[H_{\text{int}}(t), \rho(t)]. \tag{2.16}$$

Integrating (2.16) we have

$$\rho(t) = \rho(0) - i \int_0^t ds [H_{\text{int}}(t), \rho(s)]. \tag{2.17}$$

Inserting (2.17) into (2.16)

$$\frac{d\rho(t)}{dt} = -i[H_{\text{int}}(t), \rho(0)] - \int_0^t ds [H_{\text{int}}(t), [H_{\text{int}}(s), \rho(s)]]. \tag{2.18}$$

Taking now the partial trace operation over the degrees of freedom of the environment we get

$$\frac{d\rho_S(t)}{dt} = -i\text{Tr}_E[H_{\text{int}}(t), \rho(0)] - \int_0^t ds \text{Tr}_E[H_{\text{int}}(t), [H_{\text{int}}(s), \rho(s)]]. \tag{2.19}$$

Without loss of generality we can assume that the first term on the right hand vanishes and Eq.(2.19)

becomes

$$\frac{d\rho_S(t)}{dt} = -\int_0^t ds \mathrm{Tr}_E[H_{\mathrm{int}}(t), [H_{\mathrm{int}}(s), \rho(s)]]. \tag{2.20}$$

At this point the dynamical equation 2.20 is exact. However, in order to derive the master equation we need to use some approximations:

- *Born-approximation*: this approximation assumes that the coupling between the system and the environment is weak, the presence of the system S is practically irrelevant for the environment. The density operator of the total system is then a product state at all times:

$$\rho(t) \approx \rho_S(t) \otimes \rho_E(0). \tag{2.21}$$

- *Markov-approximation*: the environmental excitations decay over time scales that can not be resolved.

Replacing (2.21) in (2.20) we obtain an integro-differential equation for the reduced density matrix of our system of interest

$$\frac{d\rho_S(t)}{dt} = -\int_0^t ds \mathrm{Tr}_E[H_{\mathrm{int}}(t), [H_{\mathrm{int}}(s), \rho_S(s) \otimes \rho_E]]. \tag{2.22}$$

Now we perform the Markov approximation replacing $\rho_S(s)$ by $\rho_S(t)$ in the last equation. In this way the state of the system at any time t only depends on the present state

$$\frac{d\rho_S(t)}{dt} = -\int_0^t ds \mathrm{Tr}_E[H_{\mathrm{int}}(t), [H_{\mathrm{int}}(s), \rho_S(t) \otimes \rho_E]]. \tag{2.23}$$

The equation 2.23 is the so called *Redfield master equation*. It is local in time but it is not Markovian at this point. Note that the time evolution is still dependent of the initial preparation at $t = 0$ (the semigroup property is not yet fulfilled). In order to achieve this, we can make the substitution $s \to t - s$ in Eq. (2.23) and let the upper limit of the integral to extend to infinity. This is justified provided the integrand disappears sufficiently fast for $s \gg \tau_E$, being τ_E the typical correlation time for the environment. Finally we obtain the Markovian master equation

$$\frac{d\rho_S(t)}{dt} = -\int_0^\infty ds \mathrm{Tr}_E[H_{\mathrm{int}}(t), [H_{\mathrm{int}}(t-s), \rho_S(t) \otimes \rho_E]]. \tag{2.24}$$

- *Secular-approximation*: it consists in averaging over the rapidly oscillating terms in the master equation and it is also known as the rotating-wave approximation (it should not be confused with the usual RWA in the context of light-matter interaction).

Usually the interaction Hamiltonian in the Schrödinger representation has the following separable form

$$H_{\mathrm{int}} = \sum_\alpha A_\alpha \otimes E_\alpha, \tag{2.25}$$

where $A_\alpha = A_\alpha^\dagger$ and $E_\alpha = E_\alpha^\dagger$ are hermitian operators acting on the Hilbert space of the system and environment, respectively. It is convenient to decompose the interaction Hamiltonian H_{int} into eigenoperators of the system Hamiltonian H_s. Let ε be an eigenvalue of H_S and the projection operator on this eigenspace belonging to the eigenvalue ε by $\Pi(\varepsilon)$. We define the decomposition of any operator on the system in its eigenmodes as

$$A_\alpha(\omega) \equiv \sum_{\varepsilon' - \varepsilon = \omega} \Pi(\varepsilon) A_\alpha \Pi(\varepsilon'). \tag{2.26}$$

This sum is extended over all energy eigenvalues ε' and ε of H_s wit a fixed energy difference ω. As a consequence of Eq. (2.26) we have the following commutation relations

$$[H_S, A_\alpha(\omega)] = -\omega A_\alpha(\omega), \text{ and } [H_S, A_\alpha^\dagger(\omega)] = +\omega A_\alpha^\dagger(\omega). \tag{2.27}$$

The system operators in the interaction picture read

$$e^{iH_S t} A_\alpha(\omega) e^{-iH_S t} = e^{-i\omega t} A_\alpha(\omega), \quad e^{iH_S t} A_\alpha^\dagger(\omega) e^{-iH_S t} = e^{+i\omega t} A_\alpha^\dagger(\omega). \tag{2.28}$$

We can then write the interaction Hamiltonian H_{int} in the following form

$$H_{\text{int}} = \sum_{\alpha,\omega} A_\alpha(\omega) \otimes E_\alpha = \sum_{\alpha,\omega} A_\alpha^\dagger(\omega) \otimes E_\alpha^\dagger. \tag{2.29}$$

The last equation represents the decomposition of the interaction into eigenoperators of the system Hamiltonian. The interaction picture Hamiltonian can now be written in the form

$$H_{\text{int}}(t) = \sum_{\alpha,\omega} e^{-i\omega t} A_\alpha(\omega) \otimes E_\alpha(t) = \sum_{\alpha,\omega} e^{i\omega t} A_\alpha^\dagger(\omega) \otimes E_\alpha^\dagger(t), \tag{2.30}$$

where

$$E_\alpha(t) = e^{iH_E t} E_\alpha e^{-iH_E t}, \tag{2.31}$$

is the interaction representation of the environment operators. The condition assumed before, i.e., $\text{Tr}_E[H_{\text{int}}(t), \rho(0)] = 0$ is equivalent to have $\langle E_\alpha(t) \rangle = 0$. Inserting now Eq. (2.30) in the Markovian master equation (2.24) we obtain

$$\frac{d\rho_S(t)}{dt} = \int_0^\infty ds \text{Tr}_E \{H_{\text{int}}(t-s)\rho_S(t)\rho_E H_{\text{int}}(t) - H_{\text{int}}(t)H_{\text{int}}(t-s)\}\rho_S(t)\rho_E + \text{h.c.}$$

$$= \sum_{\omega,\omega',\alpha,\beta} e^{i(\omega'-\omega)t} \Gamma_{\alpha,\beta}(\omega) \left(A_\beta(\omega)\rho_S(t)A_\alpha^\dagger(\omega') - A_\alpha^\dagger(\omega')A_\beta(\omega)\rho_S(t) \right) + \text{h.c.} \tag{2.32}$$

In the above expression we have introduced the Fourier transforms of the environment correlation functions

$$\Gamma_{\alpha,\beta} \equiv \int_0^\infty ds e^{i\omega s} \langle E_\alpha^\dagger(t)E_\beta(t-s) \rangle. \tag{2.33}$$

It turns out that whenever the typical timescale for the system evolution is short in comparison with the relaxation time, we can neglect the terms for which $\omega \neq \omega'$ since they are rapidly oscillating factors. This condition is typically satisfied in quantum optical systems. Then

$$\frac{d\rho_S(t)}{dt} = \sum_{\omega,\alpha,\beta} \Gamma_{\alpha,\beta}(\omega) \left(A_\beta(\omega)\rho_S(t)A_\alpha^\dagger(\omega) - A_\alpha^\dagger(\omega)A_\beta(\omega)\rho_S(t) \right) + \text{h.c.} \tag{2.34}$$

It is convenient to decompose the Fourier transforms of the environment correlation functions as follows

$$\Gamma_{\alpha,\beta}(\omega) = \frac{1}{2}\gamma_{\alpha,\beta}(\omega) + iS_{\alpha,\beta}(\omega), \tag{2.35}$$

where

$$S_{\alpha,\beta} = \frac{1}{2i} \left(\Gamma_{\alpha,\beta}(\omega) - \Gamma_{\beta,\alpha}^*(\omega) \right), \tag{2.36}$$

and

$$\gamma_{\alpha,\beta}(\omega) = \Gamma_{\alpha,\beta}(\omega) + \Gamma_{\beta,\alpha}^*(\omega) = \int_{-\infty}^\infty ds e^{i\omega s} \langle E_\alpha^\dagger(s)E_\beta(0) \rangle. \tag{2.37}$$

With these definitions we arrive to the master equation in the interaction picture

$$\frac{d\rho_S(t)}{dt} = \sum_{\omega,\alpha,\beta} \gamma_{\alpha,\beta}(\omega) \left(A_\beta(\omega)\rho_S(t)A_\alpha^\dagger(\omega) - \frac{1}{2}\{A_\alpha^\dagger(\omega)A_\beta(\omega),\rho_S(t)\} \right). \qquad (2.38)$$

Notice that in Eq. (2.38) we are not taking into account the Lamb shift contribution induced by the environment on the system of interest. The equation (2.38) is not yet in the standard Lindblad form. However we can diagonalize de matrix defined by the coefficients $\gamma_{\alpha,\beta}$. This diagonalization is always possible because, as one can show, this matrix is positive and the master equation can be rewritten in the diagonal form

$$\frac{d\rho_S(t)}{dt} = \sum_{\omega,k} \gamma_k(\omega) \left(A_k(\omega)\rho_S(t)A_k^\dagger(\omega) - \frac{1}{2}\{A_k^\dagger(\omega)A_k(\omega),\rho_S(t)\} \right). \qquad (2.39)$$

Transforming back to the Schrodinger picture, the final Markovian master equation has the general form

$$\frac{d\rho_S(t)}{dt} = -i[H_S,\rho_S(t)] + \sum_{\omega,k} \gamma_k(\omega) \left(A_k(\omega)\rho_S(t)A_k^\dagger(\omega) - \frac{1}{2}\{A_k^\dagger(\omega)A_k(\omega),\rho_S(t)\} \right). \qquad (2.40)$$

In Chapter 4 we will make use of the microscopic open system approach to arrive to a general Markovian master equation for the Jaynes-Cummings model in terms of its dressed states.

2.3   The kicked Ising spin chain

We now describe a paradigmatic model upon which the next chapter is based. It is the *kicked Ising spin chain* (KI), a system of N interacting qubits (or spin-1/2 particles) driven by a external pulsed uniform magnetic field. This model was introduced by T. Prosen [115] as an example of a quantum many-body system in which a general relation between integrability and the dynamics of correlation functions is well defined, and therefore establishing a criterion for the integrability of the model in terms of its dynamics as captured by the fidelity of an initial generic state. In general, the Hamiltonian model describing the system can be written as

$$H_{\mathrm{KI}}(t) = \sum_{j>k}^{N_0} J_{j,k}\sigma_z^j\sigma_z^k + K(t)\sum_j^N \vec{b}_j \cdot \vec{\sigma}^j, \qquad (2.41)$$

where $J_{j,k}$ is the strength of the Ising interaction between spin pairs at positions j and k. $\sigma_{x,y,z}^j$ are the spin-1/2 Pauli matrices at the spin j. The operator vector $\vec{\sigma}^j = \left(\sigma_x^j,\sigma_y^j,\sigma_z^j\right)$ and the magnetic field is $\vec{b}_j = (b_x,b_y,b_z)$. The time dependent function $K(t) = \sum_{n\in\mathbb{Z}}\delta(t-n)$ is a superposition of Dirac-Delta pulses of unit period. Two cases should be distinguished: *i)* $N_0=N$ (periodic boundary condition) and *ii)* $N_0=N-1$ (open boundary condition). In its original formulation, the model is a ring (or a chain in the case of open boundaries) with homogeneous Ising coupling strengths such that $J_{j,k}=J\delta_{j+1,k}$ and the magnetic field vector lies on the *x-z* plane, i.e., $\vec{b}_j = (b_x,0,b_z)$. The model is then described by a three-parameter independent set (J,b_x,b_z) which one can tune and obtain a variety of dynamics. The Hamiltonian 2.41 is trivially integrable in the case of a magnetic field parallel to the direction of the Ising interaction. Non-trivial integrability arise when the magnetic field is orthogonal to the Ising coupling, in which case the model can be solved trough the so-called Jordan-Wigner transformation mapping the spin system into a system of free non-interacting fermions [116, 117].

As the system is periodically driven in time, its dynamics can be characterized trough the Floquet unitary propagator in one period of time. During the free evolution (no magnetic kick), the system evolves

according the following propagator corresponding to the Ising interaction

$$U_{\text{Ising}} = \exp\left(-i\sum_{j>k}^{N_0} J_{j,k}\sigma_z^j\sigma_z^k\right) = \prod_{j>k}^{N_0}\exp\left(-iJ_{j,k}\sigma_z^j\sigma_z^k\right),\tag{2.42}$$

where we have assumed $\hbar = 1$. The propagator due to the magnetic kick is given by

$$U_{\text{Kick}} = \exp\left(-i\sum_{j=1}^{N}\vec{b}_j\cdot\vec{\sigma}^j\right) = \prod_{j=1}^{N}\exp\left(-i\vec{b}_j\cdot\vec{\sigma}^j\right),\tag{2.43}$$

and the complete Floquet map for one period can be easily constructed by the product of exponentials

$$U_{\text{KI}} = U_{\text{Ising}}U_{\text{Kick}}.\tag{2.44}$$

2.3.1 Symmetries and spectral statistics of the KI model

As we mention above, the KI model can show a very rich behavior concerning its spectral statistics as a function of the parameters (J, b_x, b_z). The model can be driven from a completely integrable situation to a fully chaotic one corresponding to an ensemble of random matrices taken from a Gaussian Orthogonal Ensemble (GOE). In order to characterize the spectral statistics, the eigenenergies of the system must be computed. In the case of driven systems, eigenenergies are called *cuasienergies* and can be obtained trough exact diagonalization of the Floquet unitary propagator (Eq.2.44) in the appropriate basis. In the computational basis $\{|s_1\rangle, |s_2\rangle, ..., |s_N\rangle\}$, where the state $|s_i\rangle$ represents spin state at position i, this problem reduces to diagonalize a unitary matrix of size $2^N \times 2^N$. The eigenvalues of this matrix are complex numbers of unit magnitude $e^{-i\phi_j}$ whose phases (or cuasienergies) ϕ_j are uniformly distributed over the unit circle in the interval $[-\pi, \pi]$.

Symmetries play an important role at the time of computing correlations between eigenenergies. If we consider an open chain, there exists a discrete reflection symmetry R such that $[H_{\text{KI}}, R] = 0$, and hence $[U_{\text{KI}}, R] = 0$. The double application of a reflection leaves the system invariant, i.e., $R^2 = \mathbb{1}$ with eigenvalues ± 1. This symmetry separates the spectrum into two subspaces with different parity. In the left panel of Fig.2.1 part of the spectrum (even parity) of cuasienergies is shown for the KI model as a function of the x component of the magnetic field b_x. For small values of b_x the spectrum is highly degenerate (trivial integrability). As we increase the intensity of this component symmetries break up and the system is driven to a nonintegrable situation which is reflected in the typical avoided crossings observed in the spectrum. It is important to mention that in the case of periodic boundary conditions there exists an additional symmetry T such that $[T, R]=0$ and whose action is the rotation of a spin to the next position. A detailed discussion about symmetries in the KI model can be found in Ref. [118].

According part of to the quantum chaos community, a quantum system is chaotic if its spectral statistics coincides with that of random matrix theory (RMT) [119]. In this context the so called nearest-neibourgh spacing distribution (NNSD) is often used as an indicator of quantum chaos, which for quantum chaotic systems is given by the Wigner-Dyson distribution $P_{WD}(s) = \frac{\pi}{2}s\exp\left(-\pi s^2/4\right)$[1] when an ensemble of random matrices taken from a GOE (Gaussian Orthogonal Ensemble). eigenenergies of a quantum chaotic system are correlated and avoided crossings between levels are present. On the other hand, integrable systems can be characterized by a Posisson NNSD of the form $P_P(s) = \exp\left(-s\right)$ indicating no correlation at all between levels with no restriction about the crossings. In the right panel of Fig.2.1 we show the transition from integrable regime to fully chaotic regime. This transition is shown in terms of the NNSD for the KI model for three special values of the horizontal magnetic component as can

---

[1]This result was obtained by E. Wigner for a 2×2 random matrix sampled from a Gaussian Orthogonal Ensemble (GOE) [119]
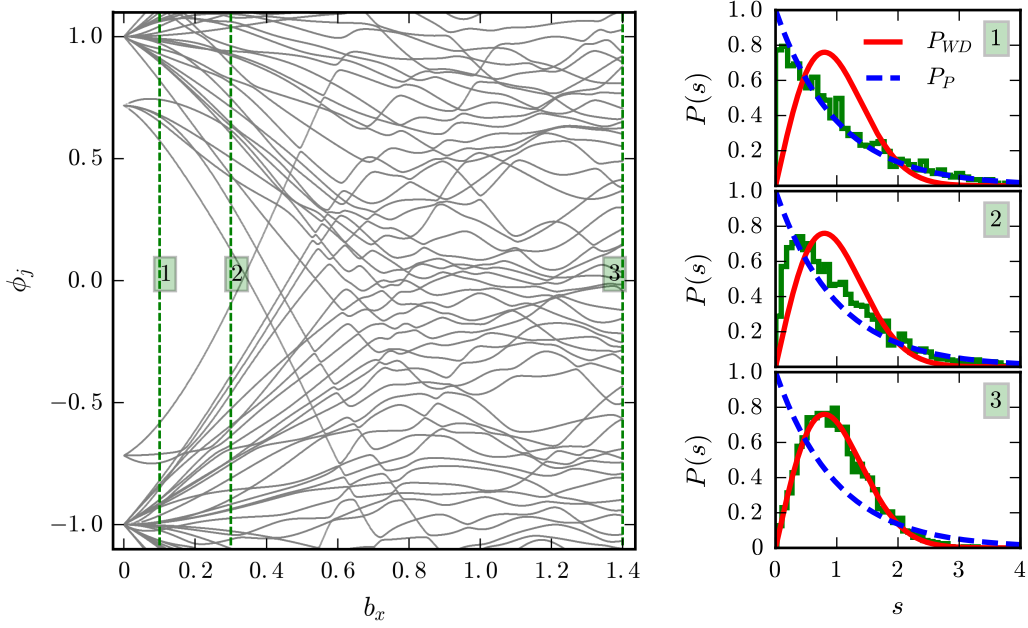
Figure 2.1: Left panel: spectrum of cuasienergies (even parity subspace) in the KI model as function of the magnetic component b_x. Vertical dashed lines indicate values of $b_x = \{0.1, 0.3, 1.4\}$. Right panel: transition to nonintegrability of the KI model as shown by the Wigner surmise for the values $b_x = \{0.1, 0.3, 1.4\}$. The spectral statistics is the result of performing independent averaging in each subspace (even and odd). Parameters: $\{J, b_z, N\} = \{1.0, 1.0, 12\}$.

be seen in the figure indicated by the vertical dashed lines. The system undergoes a clear transition from Poissonian behaviour going trough an intermediate case of mixed dynamics and finally reaching the chaotic regime described by a Wigner-Dyson NNSD. The relation between spectral statistics of the KI model and RMT implies somehow the applicability of a random model to this many-body quantum system. However we must emphasize that the KI model, as we have defined here, does not include any disorder and randomness in the Hamiltonian. It is just a many-body Hamiltonian with homogeneous two-body interactions and one-body local operations driven by uniform external magnetic field. Another important family of models is obtained when instead of having a fixed, and small, number of parameters, one allows some of these parameters to be random (though static). In particular, the random two-body interaction Hamiltonians used in Ref. [120] can readily be included in our framework, by considering nearest neighbour interactions with random strength plus a single particle term (in our case not random, for simplicity).

Chapter 3

Coherence and entanglement of one and two-qubits in spin environments

3.1 Two nested spin environments

Regarding the qubits as nodes, and non-zero Ising couplings as connections, we can consider the KI model as a quantum graph. While the analysis of an arbitrary graph will be of interest in the light of recent results for complete quantum graphs in the context of random matrix theory (RMT) [121], such a generalization will not be the subject of the present analysis. If we further allow to have two different types of connections (in our case strong an weak couplings), we can have a collection of connected graphs. We will play with the Ising interactions in order to obtain the formal structure of a central system and nested environments we need. To be more precise, we shall work in a Hilbert space structured as

$$\mathscr{H} = \mathscr{H}_{\mathrm{c}} \otimes \mathscr{H}_{\mathrm{e}} \otimes \mathscr{H}_{\mathrm{e}'}, \tag{3.1}$$

 with respective Hilbert spaces denoting central system, near environment and far environment. With respect to the spin environments, we shall consider that within each Hilbert space, there is strong coupling, and from the space of the central system to the near environment weak coupling is assumed, see Fig.3.1. We want to investigate the effect of different coupling regimes from the space of near environment to the far environment on the weakly coupled central system. We shall limit the central system $\mathscr{H}_{\mathrm{c}}$ to simple cases of one or two qubits. The former is obviously the simplest non-trivial system we can have and the latter is the building block for quantum information systems, as quantum gates involving pairs of qubits are sufficient to represent a universal quantum computer [20]. Furthermore, as we are not interested in the operation of quantum gates, we shall actually turn off the interaction between these two qubits, i.e.,
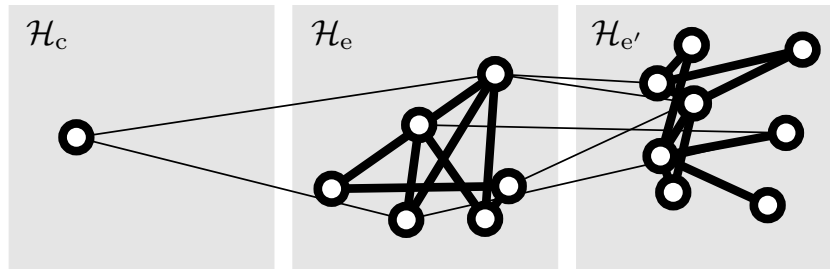
Figure 3.1: Example of a tripartite configuration of qubits systems. Each of the Hilbert spaces composing the total space 3.1, is displayed as a shaded area. The open circles represent the different qubits, thick lines represent strong interactions, and thin ones weak interaction.

treat a quantum memory, which for weak decoherence can be understood entirely in terms of single-qubit decoherence [39]. We shall separate the rest of the system into two sets of qubits forming $\mathcal{H}_e$ and $\mathcal{H}_{e'}$, respectively. For example, these qubits can be organized in an open chain where $\mathcal{H}_e$ will be connected to the central system at one spin and to the far environment by connecting a spin of this environment to another (or the same) spin of the central system. $\mathcal{H}_{e'}$ will have no connections to $\mathcal{H}_c$. Within each of these strings we shall consider nearest-neighbour interaction. We will also present some results for additional couplings within each subset, which for quantum chaotic situations result rather irrelevant, as may be expected following universality arguments. For the coupling between the two subsets we will vary from a single coupling to many interacting pairs. We can reorganize the Hamiltonian in Eq.2.41, and write it as

$$H = H_0 + \lambda V_{ce} + \gamma V_{ee'}, \tag{3.2}$$

with

$$H_0 = H_c + H_e + H_{e'}, \tag{3.3}$$

where the indices denote the Hilbert spaces in which the operators act non-trivially. λ and γ are real non negative coupling parameters between central system and near environment and between near environment and far environment, respectively. The Hamiltonian H_0 represents the internal dynamics of the central system, the near environment and the far environment. The operators V_{ce} and $V_{ee'}$ represent the interaction between each shaded area in Fig.3.1. To be more precise, we can label the set of spins belonging to $\mathcal{H}_\kappa$ as S_κ with $\kappa = \{c, e, e'\}$. Then,

$$H_\kappa = J \sum_{j>k\in S_\kappa} I^{(\kappa)}_{j,k} \sigma^j_z \sigma^k_z + K(t) \sum_{j\in S_\kappa} \vec{b}_\kappa \cdot \vec{\sigma}^j, \tag{3.4}$$

and $I^{(\kappa)}_{j,k}$ is a matrix of zeros and ones containing the configuration of the subsystem (adjacency matrix of the corresponding graph). The *open chain* system where $I^{(\kappa)}_{j,k} = \delta_{k+1,k}$ will be of particular interest. The interaction between central system and near environment and the one between near and far environment are given by the Ising terms

$$V_{ce} = \sum_{j\in S_c, k\in S_e} I^{(1)}_{jk} \sigma^j_z \sigma^k_z, \quad V_{ee'} = \sum_{j\in S_e, k\in S_{e'}} I^{(2)}_{jk} \sigma^j_z \sigma^k_z, \tag{3.5}$$

respectively, where in this case $I^{(1,2)}_{jk}$ are other matrices with zeros or ones, containing the particular configurations of the interactions. Notice that the propagator 2.42 is periodic (up to a global phase) in $J_{j,k}$, as $\exp[i(J_{jk} + \pi)\sigma^j_z \sigma^k_z] = -\exp[iJ_{jk}\sigma^j_z \sigma^k_z]$, so the behavior of all observables will also be periodic in γ and λ with period π. We have also observed a symmetry of the channel induced in the central system with respect to sign changes, both in γ and λ, so it will suffice to study, with respect to both parameters, the interval $[0, \pi/2]$. We however will show one example for a full period of γ to illustrate the effect. Taking into account that both the free and the kicked part can be decomposed in a simple multiplication of one and two qubit operations, we can see that this model can be numerically evolved efficiently. The memory requirements are set by the size of the state to be evolved (2^N, where N is the total number of qubits), and the speed of the algorithm is also linear with respect to the size of the Hilbert space, for each time step to be evolved. We have used efficient tools [122] developed for GPUs (graphics processing unit) to perform our numerical experiments. The dynamics of the central system is obtained by tracing over both environments, which leads to the reduced density operator

$$\rho_c(t) = \text{Tr}_{e,e'}\rho(t), \tag{3.6}$$

where the total density operator evolves unitarily as $\rho(t) = U_{KI}\rho(0)U^\dagger_{KI}$ for each discrete time step. We also assume the absence of initial quantum correlations between subsystems, i.e., the initial state for the

total system is a product state of the form

$$\rho(0) = \rho_c \otimes \rho_e \otimes \rho_{e'}. \tag{3.7}$$

In all numerical results we will present, two kinds of initial pure states for the central system are used. For one qubit as the central system, $\rho_c(0)$ will be taken as an eigenstate of the operator σ_x, while for a two qubit central system we shall use the Bell state $\rho_c = |\Phi^+\rangle\langle\Phi^+|$, which gives us the opportunity to study the evolution of internal entanglement within the central system. In order to emulate a high-temperature spin bath, the initial state of the environments is chosen as a product of two random pure states, one for each environment.

3.2 One-qubit in a nested spin environment

We shall first explore the effect of nested environments with the simplest central system possible, namely a single qubit. The coupling between the central system and the near environment will be chosen to be weak, while the coupling of the near environment to the far environment will range from weak to strong but always stronger that the former. As in previous works we neglect any coupling between the central system and the far environment, but we will test this assumption in a typical situation. Throughout the chapter, we shall choose the dimensions as large as we can for both the near and far environments without having excessive computation times. We also set the parameters of the model in a regime where the dynamics of the chains are in the quantum chaotic regime [115], so as to mimic universal results [119]. Specifically, we set $\dim(\mathscr{H}_e) = 2^6$, $\dim(\mathscr{H}_{e'}) = 2^{10}$, $J = 1.0$ and $\vec{b}_e = \vec{b}_{e'} = (1.0, 0., 1.0)$ in Eq. (3.4). This implies that the kicked magnetic field has an angle of $\pi/4$ with respect to the Ising coupling, and the field strength is chosen appropriately. The coupling between the central system and the near environment, shall be fixed to $\lambda = 0.01$ unless otherwise stated. Similarly, the size of the near and far environments shall be fixed as in Fig. 3.2, except when we analyse the effect of the dimensions in the environments. Finally we choose for most of this section a dephasing coupling between near and far environment ($\vec{b}_c = 0$). This is inspired by the observation [123] that it will lead to a measurable fidelity amplitude for the open near environment using the central qubit as a probe as in the original quantum optical proposal [124–126] for the measurement of fidelity decay, but now applied to an open system, which results by adding the far environment. We obtain the dephasing case by dropping the kicked magnetic field for the central qubit, whose Hamiltonian then commutes with the Ising coupling to the near environment. Another advantage of the dephasing case is that it involves no energy transport, and thus clearly distinguishes decoherence behavior from results for energy transfer. Towards the end of this section we shall lift this restriction.

Our model depends on the configuration of the connections used within each environment, the configuration of the connections between environments and the number of such connections as well as on their strength. Our main object is to study the behaviour of purity on the aforementioned details. The exploration cannot be exhaustive; rather we tested typical changes and in each of these cases the behavior of decoherence.

The configuration we first consider is characterized by including a single connection between both, the central system and the near environment (an open chain), and between the latter and the far environment (also an open chain), see Fig.3.2. The decay of the purity of the central system as a function of time for fixed λ and for different values of γ is shown in Fig.3.2. This picture shows the main feature we wish to highlight in this section: *larger values of γ lead to slower decoherence in the central system.* At this point we repeat the same calculation as in Fig.3.2, but adding a weak Ising coupling of 0.01λ between one qubit in the far environment and the central qubit. As expected, the resulting plot is indistinguishable from the aforementioned one, and thus we do not present it. We shall now proceed to look at what details of our model affect this result. First we shall explore how the configuration of the internal connections
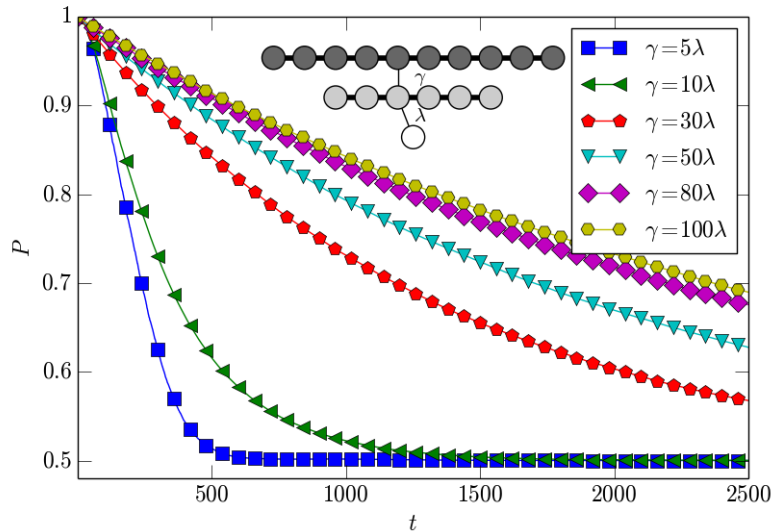
Figure 3.2: Purity decay of the central system (open circle) for $\lambda = 0.01$ and different values of γ, for the configu-ration illustrated in the upper part of this figure. Larger values of the coupling between the near (grey circles) and far (black circles) environments induce less decoherence of the central system.

in each of the environments with unchanged connections between the subsystems impact on the results. In Fig.3.3 we show the configurations, in the upper part, and plot the purity reached at a given time as a function of γ for each of these configurations. We limit γ to the interval $[-\pi/2, \pi/2]$ as the function must be periodic with period π. The figure shows that adding more internal connections in the environments does not change, at least qualitatively, the behavior of purity. As we allow γ to become larger we see that the tendency is reversed due to the reflection symmetry discussed in 2.3.1. Note that we see a peak near $\gamma = 0$. This is not a contradiction but rather confirms that we need $\gamma > \lambda$ to assure that we observe the effect of coherence protection.

We have also tested to what extent more connections between environments have an effect in the deco-herence process. We have found an interesting result: additional connections between the environments appears to have a small effect over purity decay, except for the implicit strengthening of the coupling. This can be compensated by the approximate scaling of γ with $1/\sqrt{\nu}$, i.e., the decays are very similar for a number ν of connections chosen randomly, if simultaneously γ is replaced by $\gamma' = \gamma/\sqrt{\nu}$, as we show in Fig.3.4. An interesting phenomenon appears as we take the random connections between environments, while conserving a fixed total number ν. We found that the configuration of the connections appears to have a definite effect, specially for large values of γ. In Fig.3.5 we show how different topologies affect the decay in different ways. One can notice that, in this case, different topologies cluster around three different behaviors, one with a flat plateau, with respect to γ, other with a slight, but noticeable maximum around $\gamma = \pi/4$, and finally another one with a skew behavior. This is not so for other configurations of the internal connections, as can be seen in Fig.3.3, but it is also true for more connections between the environments, as is shown in Fig.3.6. We were not successful in determining the pattern that lead to one or the other behavior. Additionally Fig.3.6 shows how for different ν the configuration of the connections is what really has an impact on purity decay, and not the number of connections, as long as they are compensated by the proper rescaling.

We next study the effect of the dimensions of the environments on purity decay. In Fig.3.7 we show for a single direct connection (see Fig.3.2) how, as the dimension increases, the maxima for purity becomes ever broader. Maybe this is even hinting the possibility of this happening for all non zero values of γ in the case where the dimensions of the environments go to infinite, but we shall later see, that there is strong indication that we must also relax the dephasing condition in order to reach that limit. As a final
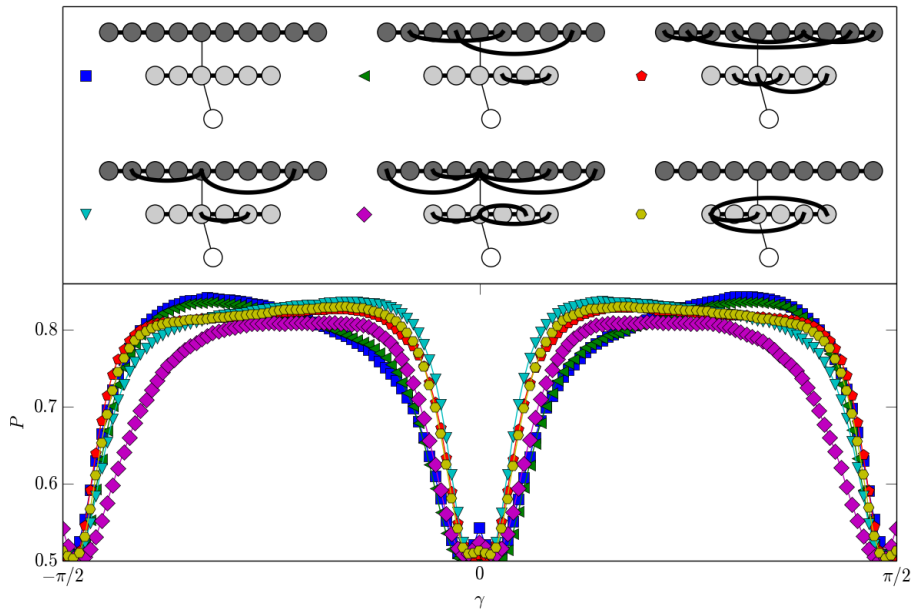
Figure 3.3: Purity as a function of γ for a fixed time $t = 1000$. The dimensions and parameters are the same as in 3.2. Six cases are shown, the first of the simple direct connection and additional five ones where additional two body connections are made within the environments as the diagrams show. Results show a plateau where a maximum purity value is reached. We see how the extra connections within the environments appear to have little effect in the overall phenomena.
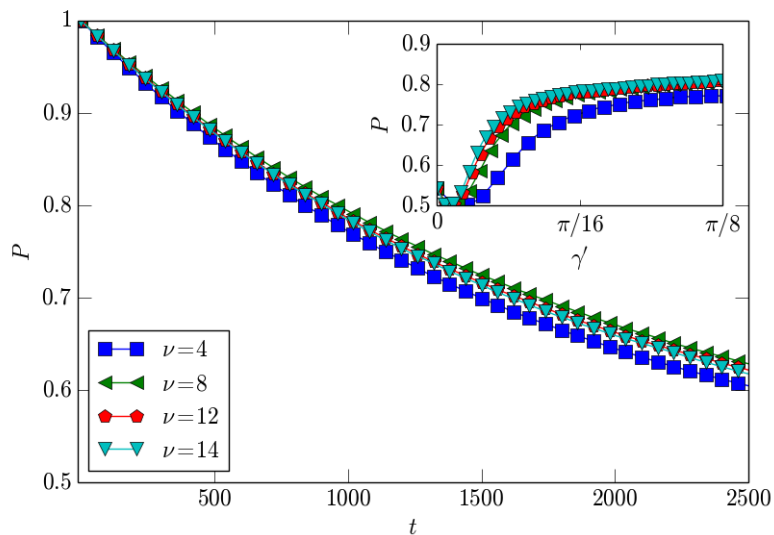
Figure 3.4: Purity decay over time for different number of connections. In each case the parameter $\gamma' = \gamma/\sqrt{\nu}$ is used. The inset shows purity, for $t = 1000$, as a function of γ'. We see how using the value γ', for sufficiently large values of γ' there is no gain in increasing the number of connections as all the cases show basically the same behaviour.
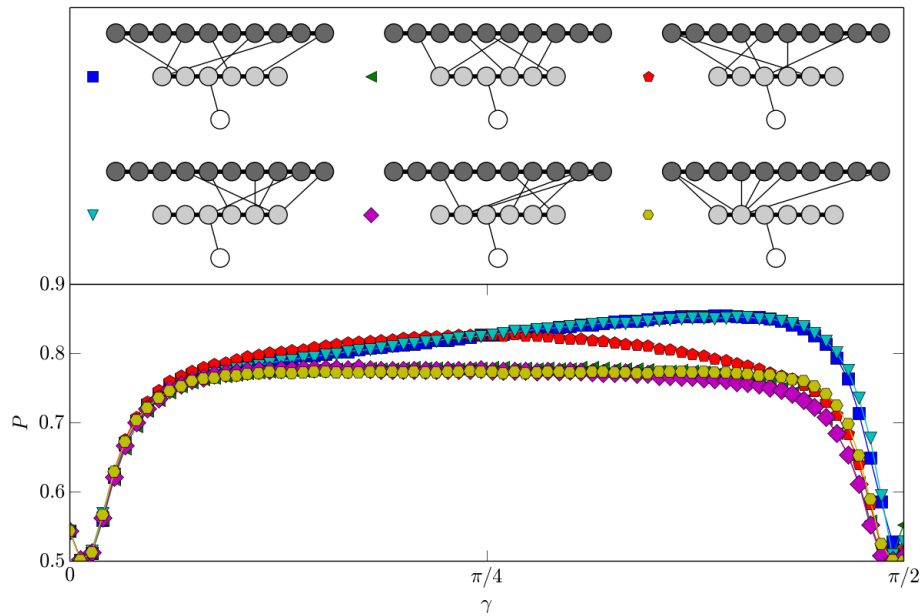
Figure 3.5: *Purity as a function of γ for a fixed number of connections ν = 6. In each case a different configuration of connections is used between environments, each shown in as a diagram. Results show the existence of three qualitatively different behaviours for the purity depending strongly on the configuration. The first one corresponds to a flat plateau, the second one to an increasing but symmetric in π/4 shape and the last one to a increasing non symmetric shape.*
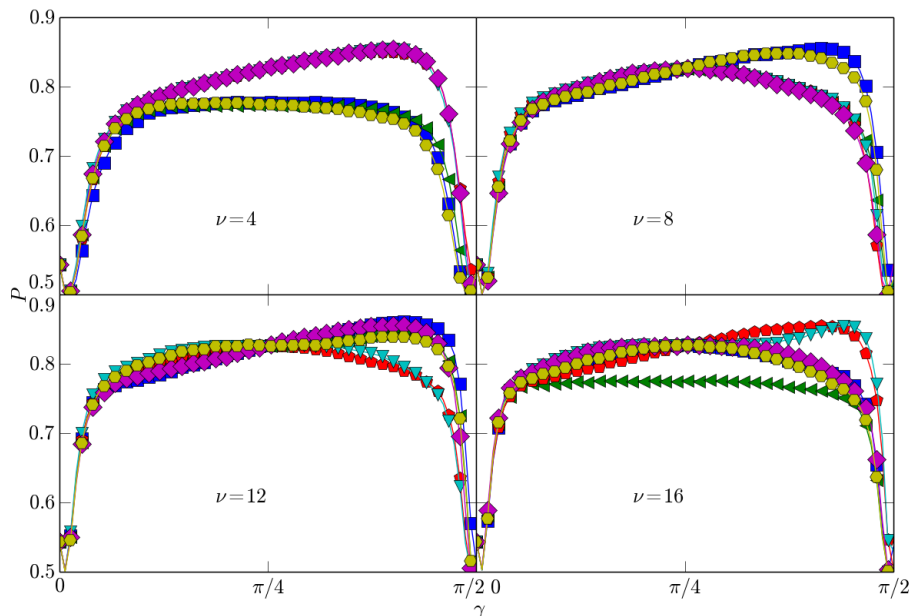
Figure 3.6: *Purity as a function of γ for four different sets of topologies each with a fixed number of connections ν, each curve represents a different randomly selected configuration of connections between environments. We see how the three behaviours are present in the different cases, showing that increasing the number of connections has little effect in the predominance of a specific behaviour.*
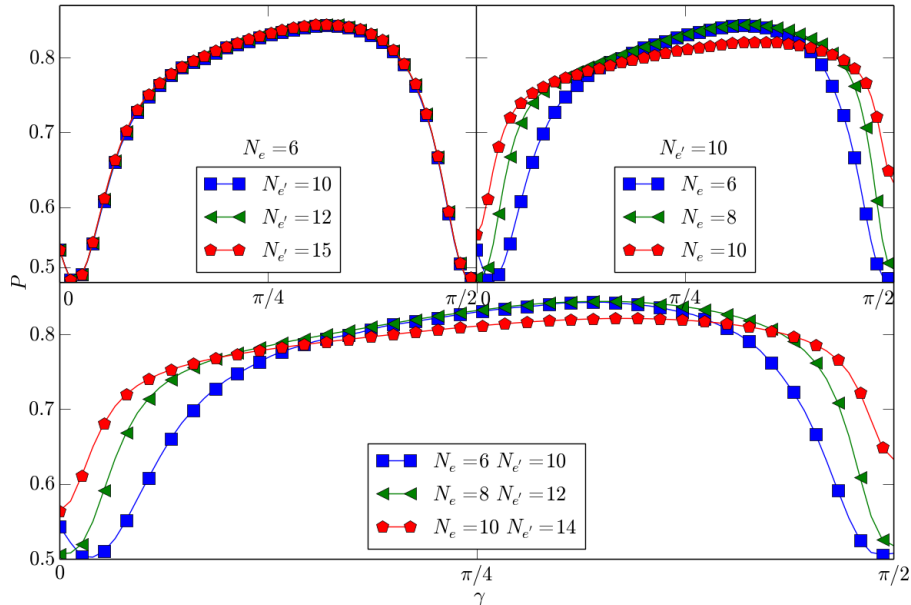
Figure 3.7: Purity as a function of γ for the simple direct connection configuration for different sizes of environments, where $\dim(H_e) = 2^{N_e}$ *and* $\dim(H_{e'}) = 2^{N_{e'}}$. *We see how increasing the environment sizes does not increases the effect of the phenomena, as it only makes it more persistent over the parameters.*

test we have to look at the λ dependence of the effect; as the interaction of the central system with the near environment is unavoidable, we have to check how small it must be to actually obtain an improvement of coherence if we increase the interaction of the near environment with the far environment. For this purpose we show the purity as a function of λ in Fig.3.8. The effect indeed must disappear as λ reaches one. The fact that the central system does not directly interact with the far environment becomes irrelevant as any initial state will soon mix the excitations of the degrees of freedom of the central system with those of the near environment.

This part of the work evolves around the phenomenon that increasing coupling between near and far environment slows decoherence. The case of small couplings is discussed extensively in the perturbative regime in [60, 123], while the case or strong dissipation is discussed in some generality in [127]. The intermediate region, is at this moment essentially only accessible numerically except for very simple integrable models [128]. We have given a survey of many options for the intermediate region, and we have consistently found the effect under discussion. Yet we have not approached the decoherence free limit but this is may be related to the finite size of our systems. We have restricted our studies to two-body interactions whose convergence for large spaces is known to be as $1/\log N$ and thus for numerical purposes inadequate. Another important point is the restriction to dephasing we used. We can lift this restriction by adding the magnetic field kicks to the central system. In 3.9 we show with parameters otherwise the same as in Fig.3.2, that this slows the decoherence much more than dephasing. Thus, while our findings do not confirm the decoupling in the strong coupling limit between near and far environments, it certainly does not contradict the decoupling.

3.3 Two qubits in a nested environment

As we discussed above, a central system composed of two qubits is of great relevance because it is the building block for universal quantum computation and other important quantum protocols [20]. De-
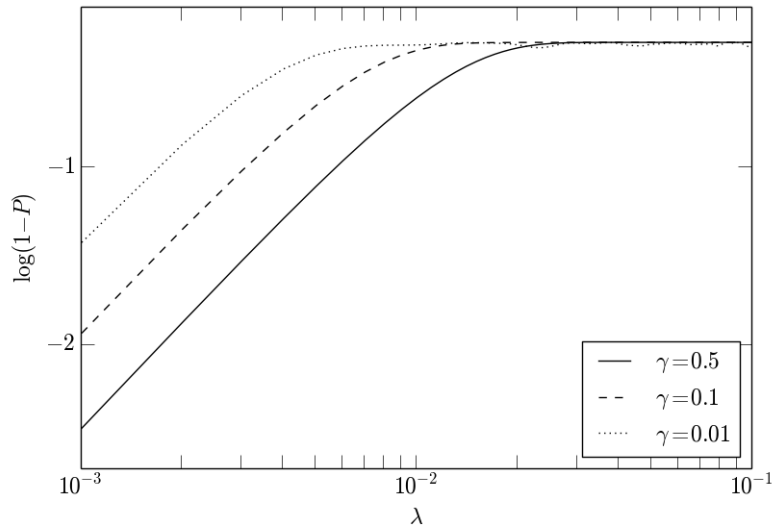
Figure 3.8: The $\log_{10}(1-P)$ as a function of λ for different values of γ. The results show a straight line up to a point where λ becomes relatively large. This is in accordance with previous results that showed how the purity decay is proportional to λ^2 for small λ.
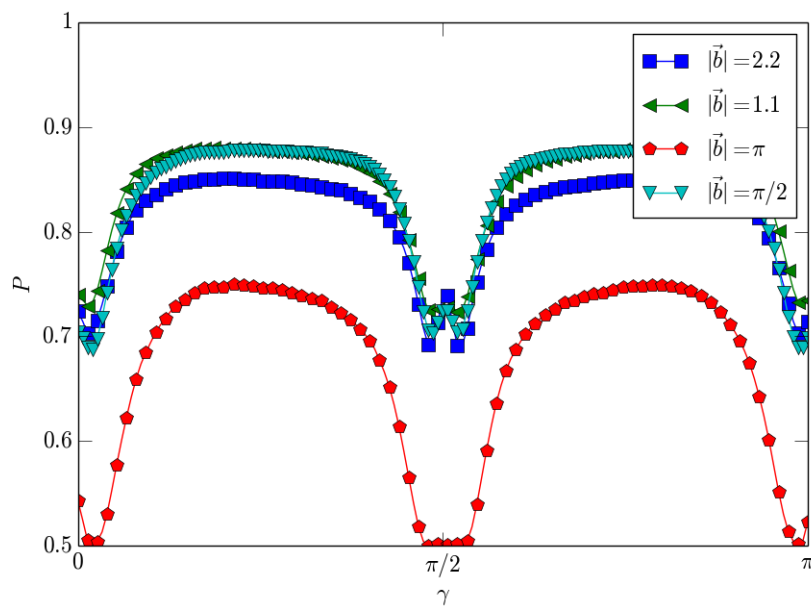
Figure 3.9: Purity at a fixed time, when adding an internal magnetic field $\vec{b}$ at a $pi/4$ angle with respect to Ising. The effect is preserved, i.e. larger couplings imply larger values of purities for the central system, as long as the periodicity in this parameter is not coming to bear. The sensitivity on the magnetic field is large and thus the non-dephasing terms are important.
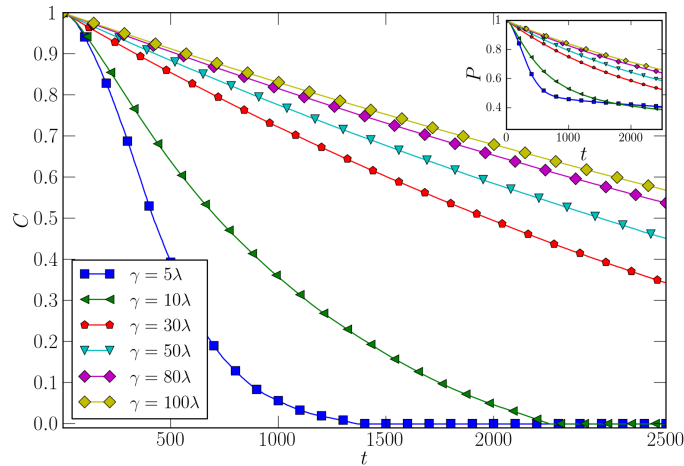
Figure 3.10: Time evolution of the concurrence (main figure) and purity (inset) for different values of γ for an initial Bell state $(|00\rangle + |11\rangle)/\sqrt{2}$ for two-qubits as central system in the spectator configuration. We have implemented this by adding a spectator to the configuration of 3.2. We observe a similar behaviour of slowing down of decoherence as the coupling to the far environment increases. This effect is also reflected in the behaviour of the concurrence in the main figure.

coherence and entanglement shared in a two-qubit system is the subject of many interesting papers, mainly in the context of cavity quantum electrodynamics using Markovian master equations in Lindblad form [129, 130]. The aim of this section is to study the evolution of the internal entanglement in the central system and how it is affected by the presence of a nested environment. If we have two qubits we can think that they are coupled to the same or different environments and also the two couplings being of equal or different strength; in the latter case we have the option that of one of the qubits is not coupled. Such a situation we call *spectator model* [62]. We will focus our attention in this particular configuration in which one of the qubits plays the role of an observer. Furthermore, we assume that the two qubits are non-interacting, avoiding the influence of this internal coupling on the entanglement evolution in the central system. We use as entanglement measure the concurrence defined in Eq. 2.14. In Fig.3.10 we show the evolution of concurrence for an initial Bell pair in a nested environment for the same parameters and configuration of the environments as in Fig.3.2. We see that the behavior is indeed quite similar, which strengthens our point, that this mechanism may actually be appropriate in very general terms to improve conditions for quantum information processing and quantum computing. The phenomenon of entanglement sudden death is present in all the curves so we can actually use the coupling parameter γ in order to delay degradation of entanglement. The inset plot also shows the evolution of purity over time for the Bell pair. The results are similar to the case of one qubit in Fig.3.2. As in the case of a single qubit, it is interesting to see the evolution of the concurrence for fixed couplings varying the number of connections ν between near and far environment as shown in Fig.3.11. The connections have been varied in the same manner as in 3.2. Notice that the scaling of γ is still valid for this configuration, showing the robustness of the effect and essentially the same behavior for the evolution of the concurrence.

3.3.1 Conncurrence-Purity diagram

A useful tool to characterize the decoherence process of a two-qubit system is the so called concurrence-purity diagram or *C-P* plane [42]. One point on this diagram gives the value of mixedness and entanglement simultaneously. Those quantum states that for a definite value of the purity can reach the maximum degree of entanglement are known as maximally entangled mixed states [131]. Looking at the behaviour on the *C-P* plane of an initial pure maximally entangled state under a local quantum channel (which
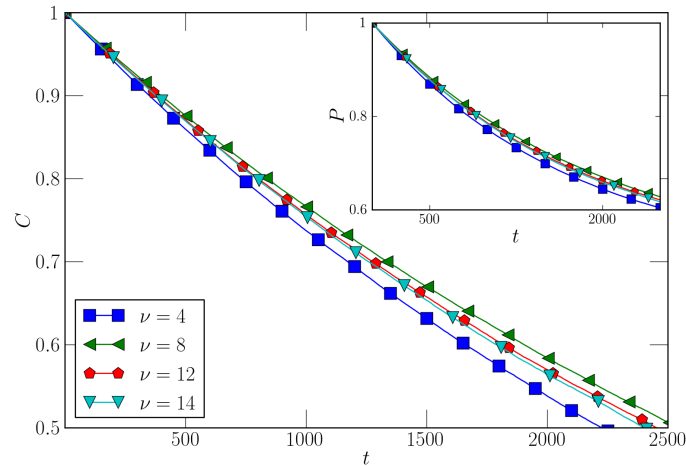
Figure 3.11: Time evolution of the concurrence (main figure) and purity (inset) for an initial Bell state $(|00\rangle + |11\rangle)/\sqrt{2}$ for two-qubits as central system in spectator configuration varying the number of connections ν between environments (near and far). In each case the rescaled parameter $\gamma' = \gamma/\sqrt{\nu}$ is used. We observe that the scaling observed in 3.4 is also approximately valid for the case of a two-qubit system.

is the case of the spectator configuration) we can in principle characterize the corresponding quantum process suffered by the system [42]. Under the action of unital channels, Bell states are mapped to the region between the corresponding to Werner states and the one corresponding to the action of dephasing channels, over Bell states. It is worthwhile to explore the behavior of our system in this plane, when an internal magnetic field is applied (otherwise, we would simply have dephasing, and thus we would lie in the lower curve). In Fig.3.12 we show a set of typical *C-P* diagrams with fixed λ and varying γ. The first observation is that the quantum channel induced by the KI for the parameters we have used is actually unital, all the curves are in the region of unital channels. The top figure shows that the lines tend to follow the Werner state behaviour quite closely as we increase the strength of the interaction between near and far environment (though we should remember, that actually they might not be Werner states). From the bottom figure is clear that for a sufficiently large number of connections between environments, the increasing of γ is no longer effective to improve the coherence in the central system. The saturation is reached faster when there is enough connectivity of the environments.
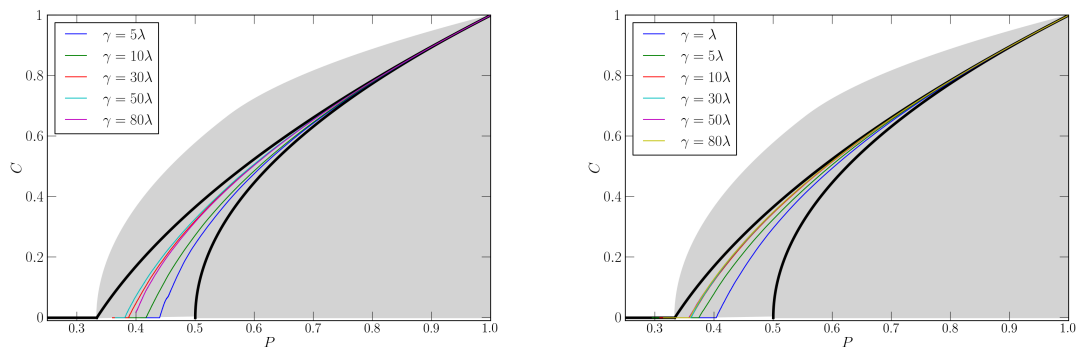
Figure 3.12: C-P diagrams for different values of γ and $t \in [0,4000]$ for an initial Bell state. The light grey area shows the region of all physical states of two qubits, bounded by above by the maximally entangled mixed states. The region bounded by the curves for Werner states and for Bell states under phase damping channels (thick lines) define the image of a Bell pair under the set of local unital operations [42]. The top figure corresponds to the configuration illustrated in 3.2. The bottom figure corresponds to a configuration with $\nu = 16$ connections between environments (near and far). Parameters are the same as in 3.12. We observe that increasing the connectivity diminishes the dispersion of purity for a fixed value of concurrence.

Chapter 4

Decoherence in light-matter interaction

4.1 Two-qubit Tavis-Cummings model

The interaction between two two-level atoms (qubits) A and B with a single mode of the electromagnetic radiation field with frequency v in the dipole and rotating-wave approximations is described by the following Tavis-Cummings Hamiltonian [22] (we set $\hbar = 1$)

$$H_{\text{TC}} = \frac{\omega_0}{2}(\sigma_z^A + \sigma_z^B) + v a^\dagger a + \sum_{j=A,B} g_j(a\sigma_+^j + a^\dagger \sigma_-^j), \tag{4.1}$$

where a, $a^\dagger$ are the usual bosonic operators satisfying $[a,a^\dagger] = 1$, σ_z^j is the z-component of Pauli matrices and $\sigma_\pm^j$ are the rising and lowering operators for atoms A and B. We remark that this model is experimentally realized in circuit QED [23]. Here we will focus on the particular case where $g_B = 0$ and $g_A = g$, i.e., only one of the atoms is interacting with the field. This setting could be realized with the atom B outside of the cavity [70] or with it in a node of the electromagnetic field. In this context the atom B acts as a *probe* from which one can obtain information about the other systems (atom A and/or the field). This is the spectator configuration implemented before. For simplicity, in the following we restrict our analysis to the resonant case $\omega_0 = v$. With the aforementioned considerations it is easy to obtain the exact time evolution operator for the Hamiltonian of Eq. (4.1) in the interaction picture and in the atomic basis $\{|ee\rangle, |eg\rangle, |ge\rangle, |gg\rangle\}$, which reads

$$U(t)_{\text{TC}} = \begin{pmatrix} \cos(gt\sqrt{aa^\dagger}) & -iV\sin(gt\sqrt{a^\dagger a}) \\ -iV^\dagger \sin(gt\sqrt{aa^\dagger}) & \cos(gt\sqrt{a^\dagger a}) \end{pmatrix} \otimes \mathbb{1}_B, \tag{4.2}$$

where $\mathbb{1}_B$ is the identity operator for the qubit B Hilbert space, and we have used the well known expression for the Jaynes-Cummings (JC) time propagator [24] in terms of the Susskind-Glogower operators defined as [132]

$$V = \frac{1}{\sqrt{a^\dagger a + 1}} a = \sum_{n=0}^\infty |n\rangle\langle n+1|, \ V^\dagger = a^\dagger \frac{1}{\sqrt{a^\dagger a + 1}} = \sum_{n=0}^\infty |n+1\rangle\langle n|. \tag{4.3}$$

These operators are non-unitary and satisfy the commutation relation $[V,V^\dagger] = |0\rangle\langle 0|$. In order to investigate the reduced dynamics of the two-qubit system we assume the total initial state as a product state $\rho(0) = \rho_\Psi(0) \otimes \rho_f(0)$ where

$$\rho_\Psi(0) = \frac{1-x}{4}\mathbb{1} + x|\psi\rangle\langle\psi|, \tag{4.4}$$

is a Werner-like state for the central system with purity parameter $x \in [0,1]$, $|\psi\rangle = \sin\phi|ee\rangle + \cos\phi|gg\rangle$ and $\rho_f(0)$ is an arbitrary initial state of the field. Such a state reduces to a Bell-like state when $x = 1$ and is contained in a wider class of two-qubit states known as X states, which are represented by a density matrix having only diagonal and off-diagonal terms different from zero [19]. We focus on two particular field states of interest: the number state and coherent state, which represent the most quantum and the most classical states of the radiation field, respectively.

4.1.1   Field in a number state

In this case we consider the field to be initially in a pure state with a definite number of photons, i.e., $\rho_f(0) = |n\rangle\langle n|$. Using this field state in $\rho(0)$ and tracing over the degrees of freedom of the field we can get the reduced density operator for the central system as

$$\rho(t) = \mathrm{Tr}_f[U(t)\rho(0)U^\dagger(t)]. \tag{4.5}$$

For simplicity we write down only the non zero matrix elements for the reduced density operator

$$
\begin{aligned}
\rho_{11}(t) &= \left(\frac{1-x}{4} + x\sin^2\phi\right)\cos^2(gt\sqrt{n+1}) + \frac{1-x}{4}\sin^2(gt\sqrt{n}), \\
\rho_{22}(t) &= \left(\frac{1-x}{4} + x\cos^2\phi\right)\sin^2(gt\sqrt{n}) + \frac{1-x}{4}\cos^2(gt\sqrt{n+1}), \\
\rho_{33}(t) &= \left(\frac{1-x}{4} + x\sin^2\phi\right)\sin^2(gt\sqrt{n+1}) + \frac{1-x}{4}\cos^2(gt\sqrt{n}), \\
\rho_{44}(t) &= \left(\frac{1-x}{4} + x\cos^2\phi\right)\cos^2(gt\sqrt{n}) + \frac{1-x}{4}\sin^2(gt\sqrt{n+1}), \\
\rho_{14}(t) &= x\sin\phi\cos\phi\cos(gt\sqrt{n+1})\cos(gt\sqrt{n}), \quad \rho_{41}(t) = \rho_{14}(t)^*.
\end{aligned}
\tag{4.6}
$$

Notice that the reduced density operator maintains during the time evolution its initial X structure. With the reduced density matrix of Eq. (4.6) we can calculate at any time the evolution of purity and concurrence for the central system which are standard measurements of decoherence and entanglement. To quantify the loss of coherence trough the degree of mixedness of the two-qubit system we use the purity of a density operator defined earlier. The entanglement shared between two qubits can be quantified using the concurrence, which for a X state of the form of Eq. (4.6), can be easily obtained via [42]

$$C(\rho_X) = 2\max\{0, |\rho_{14}| - \sqrt{\rho_{22}\rho_{33}}\}. \tag{4.7}$$

To get easy to handle explicit expressions of the quantifiers, we analyze the particular case with $x = 1$ and $\phi = \pi/4$, which corresponds to an initial pure Bell state of the two-qubit system. A straightforward calculation shows that purity and concurrence read

$$P(t) = \frac{1}{2} + \frac{1}{8}\left[4\cos^2(gt\sqrt{n})\cos^2(gt\sqrt{n+1}) - 1\right] + \frac{1}{16}\left[\cos(4gt\sqrt{n}) + \cos(4gt\sqrt{n+1})\right]. \tag{4.8}$$

$$C(t) = 2\max\{0, \frac{1}{2}\left(\left|\cos(gt\sqrt{n})\cos(gt\sqrt{n+1})\right| - \left|\sin(gt\sqrt{n})\sin(gt\sqrt{n+1})\right|\right)\}. \tag{4.9}$$

We notice that for $n = 0$ (vacuum field state), purity and concurrence are related via

$$C(t) = \sqrt[4]{2P(t) - 1}, \tag{4.10}$$

which is the typical behaviour that characterizes a homogenization process in a *C-P* diagram [42] and tells us that the two qubits are entangled whenever the purity is larger than $1/2$. This process belongs to a class of non-unital channels (see Sec. 4.4 for details). In Fig. 4.1 we show the evolution of concurrence

by substituting the matrix elements of Eq. (4.6) in Eq. (4.7) with the field in the vacuum state $n=0$ and an arbitrary initial degree of entanglement. The figure shows two cases: (a) pure state ($x = 1$), for which $C(t) = 2\max\{0, |\cos\phi\sin\phi\cos gt|\}$ and (b) mixed state ($x = 0.48$). The time behaviors are in accordance with the non-dissipative case of a single qubit subject to a single-mode radiation field in the vacuum state (zero temperature perfect cavity).
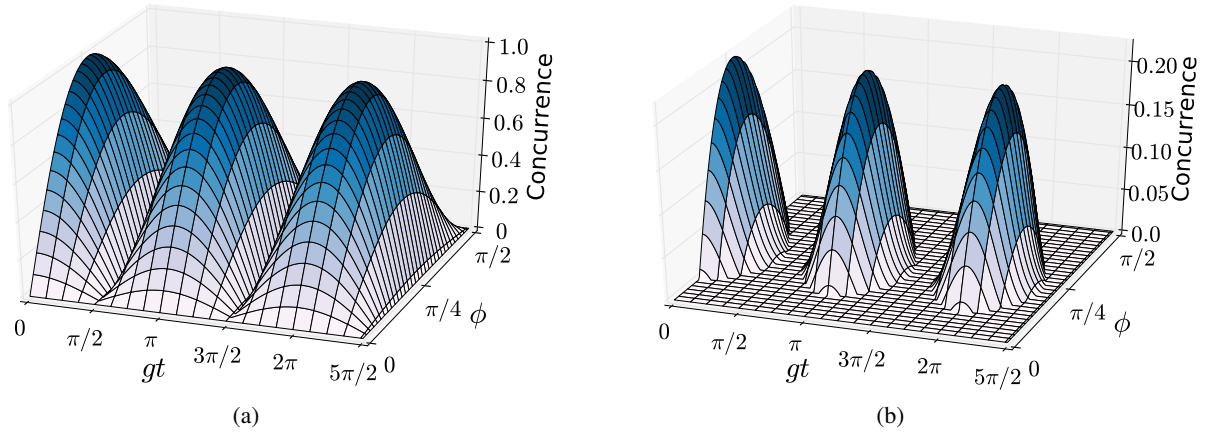
Figure 4.1: Concurrence as a function of scaled time gt and initial degree of entanglement ϕ for the spectator two-qubit TC model in the vacuum state $n = 0$. Two cases are shown: (a) with purity parameter $x = 1$ there is vanishing of entanglement at $gt = (m + 1/2)\pi$, (b) For $x = 0.48$ collapses and revivals of entanglement are observed. This behavior shows a strong dependence on the initial conditions, as reported in Ref. [35].

4.1.2 Field in a coherent state

We now choose the initial radiation field in a coherent state, which is a typical situation in cavity-QED experiments [6]. In this case the field state is given by

$$\rho_f(0) = |\alpha\rangle\langle\alpha|, \text{ with } |\alpha\rangle = \sum_{n=0}^{\infty} p_n|n\rangle, \text{ and } p_n = e^{-|\alpha|^2/2}\frac{\alpha^n}{\sqrt{n!}}. \tag{4.11}$$

The explicit elements of the reduced density operator for $x = 1$ and $\phi = \pi/4$ are

$$\rho_{11} = \sum_n |p_n|^2 \cos^2(gt\sqrt{n+1}), \quad \rho_{13} = i\sum_n p_{n+1}^* p_n \sin(gt\sqrt{n+1})\cos(gt\sqrt{n+2}),$$

$$\rho_{12} = \frac{i}{2}\sum_n p_{n+1}^* p_n \sin(2gt\sqrt{n+1}), \quad \rho_{14} = \sum_n |p_n|^2 \cos(gt\sqrt{n})\cos(gt\sqrt{n+1}),$$

$$\rho_{22} = \sum_n |p_n|^2 \sin^2(gt\sqrt{n+1}), \quad \rho_{23} = \sum_n p_n^* p_{n+2} \sin(gt\sqrt{n+1})\sin(gt\sqrt{n+2}),$$

$$\rho_{33} = \sum_n |p_n|^2 \sin^2(gt\sqrt{n}), \quad \rho_{24} = -i\sum_n p_n^* p_{n+1} \sin(gt\sqrt{n+1})\cos(gt\sqrt{n}),$$

$$\rho_{44} = \sum_n |p_n|^2 \cos^2(gt\sqrt{n}), \quad \rho_{34} = -\frac{i}{2}\sum_n p_{n+1}^* p_n \sin(2gt\sqrt{n+1}), \tag{4.12}$$

where we have omitted the explicit time dependence in the matrix elements $\rho_{jk}(t)$. As in the standard JC model, the sums in Eq. (4.12) cannot be evaluated in a closed form, so analytical expressions for purity and concurrence are too cumbersome to be shown here. In Fig. 4.2 we then show plots of purity and concurrence as functions of time, where the field state is initially in a coherent state with average photon number $\bar{n} = |\alpha|^2 = 15$. Differently from the previous case of initial number state, now entanglement
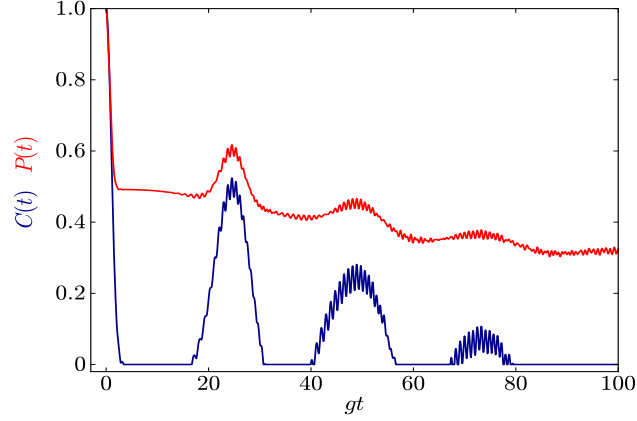
Figure 4.2: Purity (upper red line) and concurrence (lower dark blue line) as functions of scaled time gt for the spectator two-qubit TC model. Bell ($x = 1$, $\phi = \pi/4$) and coherent ($\bar{n} = 15$) initial states were used. Concurrence shows collapses and revivals of entanglement with the envelope eventually decaying at $gt_r \approx 2\pi\sqrt{\bar{n}}$.

and purity eventually decay presenting oscillations during the evolutions. We point out that purity peaks follow entanglement revivals which however does not mean that the larger the purity (or smaller the mixedness), the larger the entanglement. This can be immediately seen by comparing, for instance, the behaviors at the time regions $2 < gt < 18$ (zero entanglement) and $68 < gt < 78$ (entanglement revival).

4.2 Two-qubit Buck-Sukumar model

In this section we consider a variant of the model studied in Sec. 4.1 which is inspired in the so-called Buck-Sukumar (BS) model [133]. In that work the authors propose an exactly solvable qubit-field Hamiltonian which is useful to describe nonlinear interactions. The Hamiltonian for the two-qubit BS model in the spectator configuration is given by

$$H_{\text{BS}} = \frac{\omega_0}{2} \left(\sigma_z^A + \sigma_z^B \right) + \nu a^\dagger a + g \left(a\sqrt{a^\dagger a}\sigma_+^A + \sqrt{a^\dagger a}a^\dagger \sigma_-^A \right), \tag{4.13}$$

Unlike Eq. (4.1) this model allows an intensity-field dependent coupling. In the resonant case the time evolution operator in the interaction picture is

$$U_{\text{BS}}(t) = \begin{pmatrix} \cos\left[gt(a^\dagger a + 1)\right] & -iV\sin\left[gta^\dagger a\right] \\ -iV^\dagger\sin\left[gt(a^\dagger a + 1)\right] & \cos\left[gta^\dagger a\right] \end{pmatrix} \otimes \mathbb{1}_B. \tag{4.14}$$

Using the same initial condition for the two-qubit system Eq. (4.4), the matrix elements for the reduced density operator are analogous to Eqs. (4.6) and (4.12) (except for the square root in the trigonometric functions argument, i.e. $\sqrt{x} \rightarrow x$) for the field in a number and coherent state respectively. Purity and concurrence for the Bell pair ($x=1$, $\phi=\pi/4$) with the field starting in the number state $|n\rangle$ are

$$P(t) = \frac{1}{2} + \frac{1}{8}\left(4\cos^2\left[gtn\right]\cos^2\left[gt(n+1)\right] - 1\right) + \frac{1}{16}\left(\cos\left[4gtn\right] + \cos\left[4gt(n+1)\right]\right), \tag{4.15}$$

$$C(t) = \max\{0, |\cos\left[gtn\right]\cos\left[gt(n+1)\right]| - |\sin\left[gtn\right]\sin\left[gt(n+1)\right]|\}. \tag{4.16}$$

In Fig. 4.3(a) we have plotted Eqs. (4.15) and (4.16) as functions of time with $n = 10$ photons. A behaviour similar to that of Fig. 4.3(a) is found between an isolated atom and a Jaynes-Cummings atom [70]. On the other hand, when the field is initially in a coherent state analytical expressions for $P(t)$ and

$C(t)$ in the two-qubit BS model are cumbersome, as pointed out in the previous section, and we limit to report their plots. Evolutions of purity and concurrence for this case are displayed in Fig. 4.3(b) as functions of scaled time for $x = 1$, $\phi = \pi/4$ and $\bar{n} = 10$. We highlight that now, in contrast to what happened in the JC model with an initial coherent field state (see Fig. 4.2), a complete spontaneous recovery of the initial entanglement can be found due to the nonlinear atom-field interaction. Purity and entanglement again show the same qualitative behavior but now larger values of purities always correspond to larger values of entanglement ($P = 1/2$ when $C = 0$ in the plateaux and $P = 1$ when $C = 1$ in the peak).
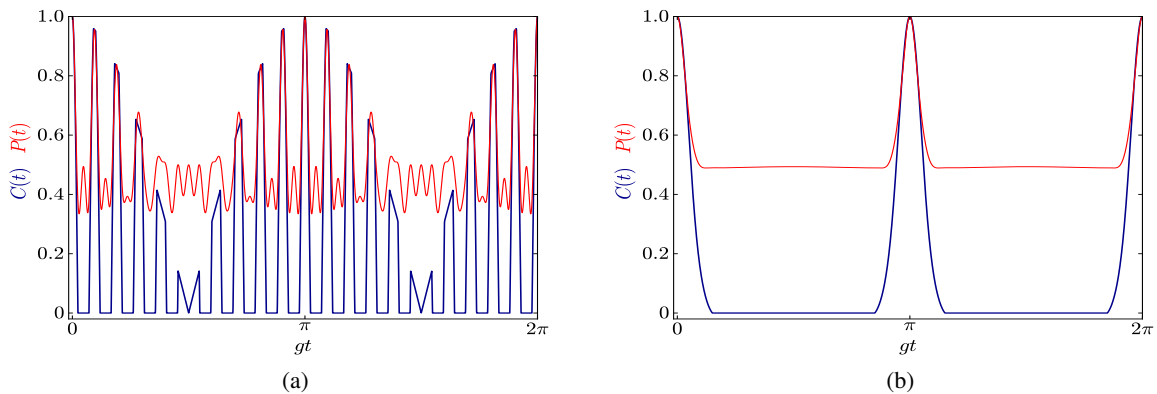
Figure 4.3: Purity (upper red line) and concurrence (lower dark blue line) evolution for the spectator two-qubit BS model. The two qubits start in a Bell state. The field starts in: (a) number state with $n = 10$ and (b) coherent state with $\bar{n} = 10$. A sequence of entanglement dark periods and complete entanglement recoveries occur in both cases due to the nonlinear interaction.

4.3 Two-qubit spin-boson model

The two-qubit spin-boson model describes two spin $1/2$ particles coupled to an environment of M non-interacting quantum harmonic oscillators [10], which can be experimentally realized in cavity and circuit QED [18, 23] and also simulated by all-optical setups with Sagnac interferometers [44, 69]. The pure-dephasing Hamiltonian in the spectator scheme is given by

$$H_{\text{SB}} = \frac{\omega_0}{2} \left(\sigma_z^A + \sigma_z^B \right) + \sum_{j=1}^{M} \omega_j a_j^\dagger a_j + \sigma_z^A \otimes \sum_{j=1}^{M} \left(g_j a_j^\dagger + g_j^* a_j \right). \tag{4.17}$$

Notice that the qubit-environment linear coupling term is an energy conserving interaction since the central system Hamiltonian commutes with H_{SB}. The corresponding time evolution operator in the interaction picture is

$$U_{\text{SB}}(t) = \begin{pmatrix} \prod_j D(\lambda_j(t)) & 0 \\ 0 & \prod_j D(-\lambda_j(t)) \end{pmatrix} \otimes \mathbb{1}_B, \tag{4.18}$$

where $D(\lambda_j(t)) \equiv \exp[(\lambda_j(t) a_j^\dagger - \lambda_j^*(t) a_j)]$ is the usual Glauber displacement operator for each mode and $\lambda_j(t) \equiv (g_j/\omega_j)[1 - \exp(i\omega_j t)]$. If we set all the oscillators in the ground state $\rho_f(0) = \bigotimes_{j=1}^{M} |0\rangle_{jj}\langle 0|$ and the two-qubit system in $\rho_\Psi(0)$, the non-zero matrix elements of the total den-
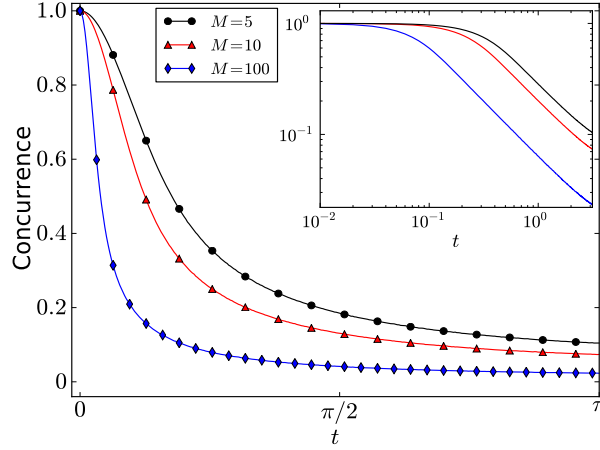
Figure 4.4: Entanglement evolution for the spectator two-qubit SB model. An ensemble average over 10^6 samples was realized using Eq. (4.20), $x=1$, $\phi=\pi/4$, g_j and ω_j were chosen randomly from the interval $[0,1]$, with $M=5$ (black), 10 (red), 100 (blue). The inset shows in log scale the Gaussian (exponential) entanglement decay for short (long) times.

sity operator in the atomic basis are

$$\rho_{11}(t) = \left(\frac{1-x}{4} + x\sin^2\phi\right)\prod_j |\lambda_j(t)\rangle\langle\lambda_j(t)|, \quad \rho_{33}(t) = \frac{1-x}{4}\prod_j |-\lambda_j(t)\rangle\langle-\lambda_j(t)|,$$

$$\rho_{44}(t) = \left(\frac{1-x}{4} + x\cos^2\phi\right)\prod_j |-\lambda_j(t)\rangle\langle-\lambda_j(t)|, \quad \rho_{22}(t) = \frac{1-x}{4}\prod_j |\lambda_j(t)\rangle\langle\lambda_j(t)|,$$

$$\rho_{14}(t) = \rho_{14}(t)^* = x\sin\phi\cos\phi\prod_j |\lambda_j(t)\rangle\langle-\lambda_j(t)|, \tag{4.19}$$

where $|\lambda_j(t)\rangle \equiv D(\lambda_j(t))|0\rangle_j$ is the coherent state for the j-th oscillator. As we have done in previous sections, we trace out over the environment in order to obtain the reduced density operator of the central system: $\rho_{11}(t) = (1-x)/4 + x\sin^2\phi$, $\rho_{22}(t) = \rho_{33}(t) = (1-x)/4$, $\rho_{44}(t) = (1-x)/4 + x\cos^2\phi$ and $\rho_{14}(t) = \rho_{41}(t) = x\sin\phi\cos\phi\exp[-\Gamma(t)]$, where $\Gamma(t) = \sum_j 4|g_j|^2(1-\cos(\omega_i t))/\omega_j^2$ is the decoherence factor. From the Eqs. (2.10) and (4.7) it is trivial to obtain purity and concurrence for the central system. For instance, the explicit expression for concurrence is

$$C(t) = \max\left\{0, x|\sin 2\phi|e^{-\Gamma(t)} - (1-x)/2\right\}. \tag{4.20}$$

For $x=1$ purity and concurrence are related via

$$C(t) = \sqrt{2P(t) - 2(\sin^4\phi + \cos^4\phi)}, \tag{4.21}$$

which is a generalized form of the expression describing a dephasing process induced by a local operation acting on a Bell state given by $C = \sqrt{2P-1}$. From Eq. (4.20), one finds that entanglement vanishes whenever $\Gamma(t) = -\ln((1-x)/(2x|\sin 2\phi|))$. Assuming all the modes to be identical ($g_j=g$, $\omega_j=\omega$), with $\phi=\pi/4$, the time when entanglement disappears is $t_d = \arccos\left[1 + \frac{1}{M}\frac{\omega^2}{4|g|^2}\ln((1-x)/(2x))\right]$. In Fig. 4.4 we plot concurrence of Eq. (4.20) as a function of time for several realizations of g_j and ω_j which are randomly chosen from interval $[0,1]$. M stands for different dimensions of the environment. We emphasize that this time behavior is non-Markovian, meaning that its decay is not exponential at short times, a situation reminiscent of pure-dephasing evolution in the solid state due to inhomogeneous broadening [134, 135].

4.4 Discussions

In this section we discuss the results for the evolution of purity and concurrence for the models studied in previous sections of this chapter.

General aspects on the time behaviors

For the two-qubit TC model with the field starting in the vacuum state, concurrence (and also purity) is a periodic function of time as can be seen in Fig. 4.1. We have explored two different initial conditions for the two-qubit system (4.4): pure entangled state Fig. 4.1 (a) and entangled state with a degree of mixedness Fig. 4.1(b). In both cases we observe the expected decay of correlations at short times in the initial entangled state due to the interaction with the field. Fig. 4.1(a) shows complete entanglement revivals at times given by $gt = n\pi$. A similar behaviour is shown in Fig. 4.1(b) but in this case the entanglement remains zero for finite intervals of time, identified as entanglement dark periods [19], followed by complete entanglement recoveries as time goes by. In the case under consideration, the TC interaction permits only zero photons or one photon to reside in the cavity, i.e., the cavity acts effectively as a two-level system, so the Hilbert space available for the environment is finite and gives rise to entanglement rebirths in the central system. When entanglement completely disappears in the central system, quantum correlations must be contained in other bi-partitions [136, 137], for instance between the isolated qubit and the field or the central system and the field. This effective three-qubit system is a convenient framework for understanding the dynamical mechanisms of entanglement sharing among the parts of a composite system with a quantum reservoir [19, 50]. Dynamical behaviors qualitatively similar to those obtained in the case when both qubits are open [19, 35] have been here found. This implies that the spectator configuration is able to reproduce general dynamical features exhibited by more complex systems, provided that each qubit of the system is locally interacting with its own environment. Concerning the second initial condition for the environmental state in the TC model, i.e. the field prepared in a coherent state, we notice that this is the situation in which the Hilbert space is formed by an infinite basis of number states. In principle it is possible that entanglement can be shared in arbitrary multipartitions of the Hilbert space not allowing the complete backflow of information to the central system. This sort of local coherent-state control leads to revivals of entanglement whose amplitude eventually decays, as predicted for the case of two open qubits [36, 37]. Purity and concurrence evolution for the central system have been plotted in Fig. 4.2 when the average photon number of the field coherent state is $\bar{n} = 15$. Both quantities oscillate but the periodicity in both quantities is no longer maintained. This time behaviour resembles the evolution of the atomic inversion in the standard one-qubit JC model where non-complete revivals are consequence of constructive quantum interference between states in the Fock basis [6]. Since we have used the spectator configuration it is easy to see that the time of entanglement revival is given by $gt_r \approx 2\pi\sqrt{\bar{n}}$. Successively, considering the intensity-dependent field interaction described by the two-qubit BS Hamiltonian in Eq. (4.13), we have plotted purity and concurrence with the field in a number ($n = 10$) and a coherent state ($\bar{n} = 15$) in Figs. 4.3(a) and 4.3(b), respectively. In contrast to what was observed for the TC model, $C(t)$ and $P(t)$ are now π-periodic functions independent of the number of photons. Interestingly, when the radiation field is initially in a coherent state there are complete entanglement revivals (see Fig. 4.3(b)) regardless that we are dealing with an infinite number of available states associated to the coherent field. In Fig. 4.4 we have finally shown the entanglement evolution for the two-qubit SB model. Aiming at revealing general features of entanglement deterioration in this system, we have performed an ensemble average over 10^6 samples applying Eq. (4.20) with $x = 1$, $\phi = \pi/4$ and random values of g_j and ω_j taken from interval $[0, 1]$. As we see, increasing the environmental modes results in a faster decay of entanglement. As expected, for short (long) times a Gaussian (exponential) behaviour is observed [10]. Due to both the initial Bell state of the central system and the dephasing local interaction, there is no entanglement sudden death, as we can deduce from Eq. (4.20).

4.4.1   Concurrence-Purity Analysis

As we have discussed in Sec.3.3.1 a useful way to characterize bipartite quantum states is given by the concurrence-purity diagram or *C-P* plane [42]. In Fig. 4.5 we show for convenience a typical concurrence-purity diagram specifying the relevant regions. A point on this diagram gives the value of mixedness and entanglement at the same time. Those quantum states for which a definite value of purity can reach the maximum degree of entanglement are known as maximally entangled mixed states (MEMS) [131]. MEMS are represented by curve 1 (C_{MEMS}) in the *C-P* plane. The area below the MEMS curve specifies the region of physical quantum states. Werner states ($\phi = \pi/4$ in Eq. (4.4)) are depicted by curve 2 (C_W). Curve 3 (C_D) is given by Eq. (4.21) with $\phi = \pi/4$ which corresponds to a decoherence process induced by a dephasing interaction. In light of the dynamical results we have obtained for purity
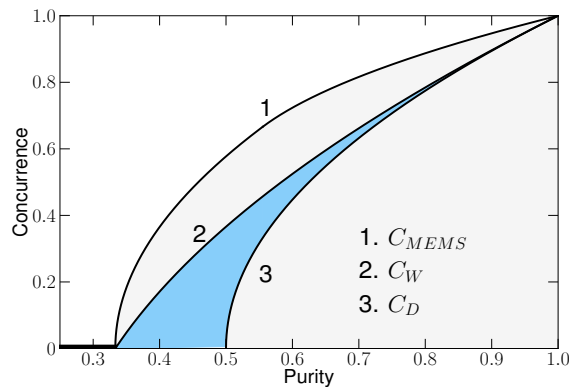
Figure 4.5: C-P plane for two qubits. Curve 1 corresponds to maximally entangled mixed states (MEMS). Curve 2 is for Werner states. The area coloured in blue is the region allowed for maximally entangled pure two-qubit states when they are under the action of a unital quantum local channel. This region has a lower and upper bound given by C_D and C_W respectively [42].

and concurrence, we analyze their relation using the *C-P* diagram. We first make some remarks about the nature of the quantum operations involved in our models. We emphasize that the spectator configuration is a physical example of a local quantum operation (channel) acting on a bipartite quantum state (the state of the two-qubit central system). In this sense, environment performs operations (trough the interaction) on one of the two qubits. These local operations can be *unital* or *non-unital*. Unital channels are maps that leave invariant the uniform state, i.e., the total mixture state. It is known [42] that initial Bell states under the action of unital channels lie in the region bounded by curves 2 and 3 in the *C-P* plane (blue shadow) of Fig. 4.5. Characterizing the behaviour of our quantum channels within this diagram is therefore desirable and can provide new overall insights on concurrence-purity dynamical relations. In Fig. 4.6 (a) we show the behaviour of the channel acting on a Bell state generated by the two-qubit TC dynamics in the spectator scheme. The starting point is the right upper corner in the plane. Two representative cases for the initial state of the environment are shown: *i*) $n = 0$ and *ii*) $n = 5$. For the vacuum state a simple analytical relation between purity and concurrence can be obtained Eq. (4.10): $C = \sqrt[4]{2P-1}$ (red line), which for a long interval of time is outside of the unital region. This channel is related to the homogenization process describing exponential decay of correlations in which the vacuum state is the fixed point of the dynamics. The case $n = 5$ is shown in blue and gives rise to a rich loop structure due to immeasurability and non-Markovian behaviour in the evolution of purity and concurrence. It must be mentioned that the associated *C-P* line for the vacuum state is also a loop over itself reaching zero entanglement at times $gt = (m+1/2)\pi$. These loops are exceptions to the rule that lines in the *C-P* plane must be non-increasing if they are generated by Markovian semigroup dynamics. Hence, the appearance of this loops is due to the non-Markovian evolution considered in this work as we were able to obtain the exact reduced density operator for the central system. It should be noted that similar results (not shown) for the Buck-Sukumar interaction in the *C-P* diagram can be obtained; in contrast to the spec-
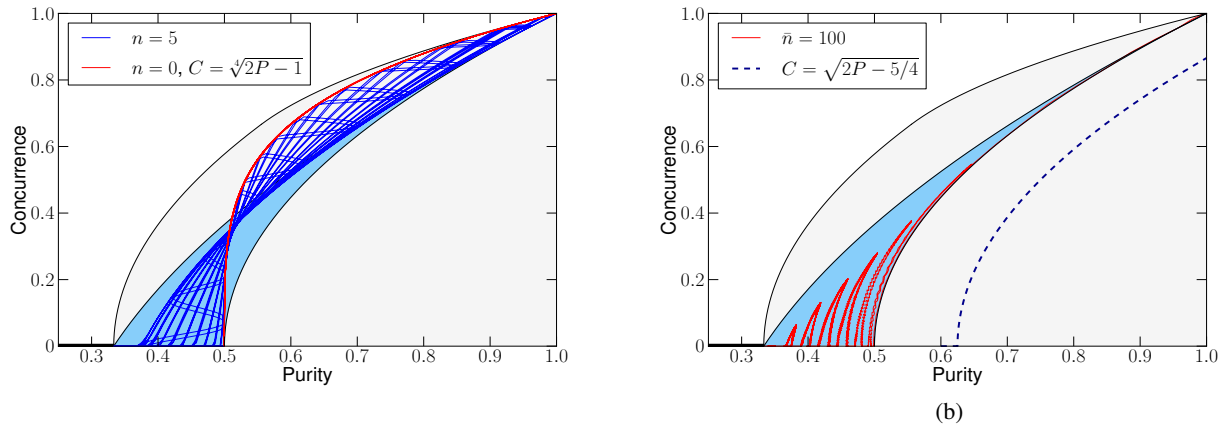
Figure 4.6: C-P plane representation for the local operation induced by Tavis-Cummings interaction. The central system starts in a Bell state and the field in: (a) Fock state n=5 (blue lines) and n=0 (red line), (b) coherent state $\bar{n}$=100 (red line). Dashed line in (b) corresponds to a dephasing channel generated by the SB interaction (see text).

tator two-qubit TC model, closed loops emerge due to the π-periodicity in the purity and concurrence. At this point it is interesting to see the *C-P* dynamics for an initial coherent state for the environment using the results of subsection 4.1.2. For an average number of field excitation $\bar{n} = 100$, signatures of long-time entanglement revivals are obtained before their occurrence (see Fig. 4.6(b)). Almost all the action of the local operation is contained in the unital region except for a small part generated by the short time dynamics near to the upper right corner. The corresponding *C-P* representation for the spectator two-qubit SB dynamics is also shown in Fig. 4.6(b) (dashed line) using the obtained generalized expression in Eq. (4.21) with $\phi = \pi/6$. As expected we observe a typical decoherence process induced by dephasing, this process being represented as a rescaled C_D curve.

4.4.2 Operational use of the concurrence-purity relations

We now briefly discuss on the possible usefulness to have quantitative relations between concurrence and purity for implementing some specific protocols. It is known that entanglement must overcome some quantitative thresholds, for a given value of state purity, in order to allow quantum processes, such as teleportation [64, 65], entanglement swapping [66] and entanglement percolation [67]. Our results under specific dynamical conditions allow to only measure purity of the system state at a given time t for obtaining the value of concurrence and then checking if it is sufficient for the desired task. Such a procedure will in turn provide the time regions within which the task can be performed. We focus on the recently reported concurrence threshold for entanglement necessary to realize a teleportation protocol with quantum speedup [65]. Such a threshold is equal to $C_{\text{th}} = (\sqrt{\rho_{22}} - \sqrt{\rho_{33}})^2$ in the case when the entangled state shared between the two parties is a X state, which is just the one we have during the evolutions here considered. For instance, for the SB dephasing model, where $\rho_{22}(t) = \rho_{33}(t)$, one immediately gets $C_{\text{th}} = 0$ at any time. The system state can be thus exploited for teleportation until $C(t) > 0 = C_{\text{th}}$, which in turn means whenever purity is above its minimum value $P(t) > P_{\text{th}} \equiv \sin^4 \phi + \cos^4 \phi$ (see Eq. (4.21)). For the plot of Fig. 4.6(b) it must be $P(t) > 5/8$. Instead, for the TC model with the vacuum field state and the two qubits initially prepared in a Bell state, the entanglement threshold is time-dependent, namely $C_{\text{th}}(t) = (1/2) \sin^2(gt)$. Quantum teleportation is then achievable at those times such that $C(t) = |\cos(gt)| > C_{\text{th}}(t)$, which in terms of state purity also means $P(t) > P_{\text{th}}(t) \equiv [1 + C_{\text{th}}^4(t)]/2$ according to Eq. (4.10).

4.5 Microscopic dissipation in light-matter interaction

The Jaynes-Cummings (JC) model [138], describing the interaction of a single bosonic mode with a two-level system, plays a key role in our understanding of interaction between radiation and matter. It is of central importance for the description of quantum effects, for example, the existence of Rabi oscillations for Fock boson field states [138] and the collapse and revival of the atomic inversion in the presence of coherent fields [139], and constitutes a basic building block for the implementation of quantum gates [140]. The model has been implemented in a variety of experimental platforms [7, 141, 142], where the unavoidable effect of the environment over closed-system dynamics is observed as a deterioration, or even complete suppression, of the expected quantum phenomena [143–146]. Thus, an adequate description of loss-mechanisms in different physical scenarios becomes essential to compare with experimental results, and lead to the proposal and study of different decoherence and dissipation models in the literature [147–154]. Here, we are interested in the microscopic approach to field dissipation in the standard Jaynes-Cummings model. The microscopic approach has demonstrated fundamental dynamical differences with the usual phenomenological approach for the single excitation manifold of the Jaynes-Cummings at zero [155] and finite [156] temperature. Both, the microscopic and phenomenological models of dissipation make use of the Born-Markov approximation, that considers a memory-less environment that couples weakly to the system. They differ on the fact that the microscopic approach uses the dressed state basis that diagonalizes the JC model in order to derive the effective master equation, while the phenomenological approach uses the microscopic master equation derived for just a dissipative field mode. In the following, we review the microscopic master equation for field dissipation in the Jaynes-Cummings model, and provide a new closed-form analytical expression for the state evolution of any given pure single-excitation state, which agrees with previous results in the corresponding limits. Then, we numerically compare the dynamics under this master equation and the standard phenomenological approach beyond the single excitation manifold at zero and finite temperature with a flat environment. In particular, we demonstrate the time evolution due to initial number and coherent field states through standard observables, like atomic inversion, mean photon number, entropy-related measures, such as purity, and phase space quantities, like quadratures of the field and Husimi Q-function.

4.5.1 Microscopic approach for the open JC model

We follow the formal microscopic derivation of the Markovian master equation for the JC model [155], and start from the standard JC Hamiltonian [138],

$$H_{JC} = \frac{\omega_0}{2}\sigma_z + \omega a^\dagger a + g\left(a\sigma_+ + a^\dagger\sigma_-\right), \tag{4.22}$$

describing a two-level system, a qubit, with transition frequency ω_0 and modeled by the standard atomic inversion operator, σ_z, and lowering (raising), σ_- (σ_+), operators, interacting with a boson field with frequency ω, described by the annihilation (creation) operator a ($a^\dagger$); the strength of the interaction is provided by the coupling parameter g. The JC model assumes near resonance, $\omega \sim \omega_0$, and weak coupling, $g \ll \omega, \omega_0$. It relates to experimental realizations in cavity-QED [141], trapped-ion-QED [7], circuit-QED and more [142], Fig 4.7. The JC model is a typical example of an integrable system, it conserves the total number of excitations $N = a^\dagger a + (1 + \sigma_z)/2$. It has a ground state provided by the boson vacuum and the qubit ground state,

$$|\varepsilon_0\rangle = |0,g\rangle, \tag{4.23}$$
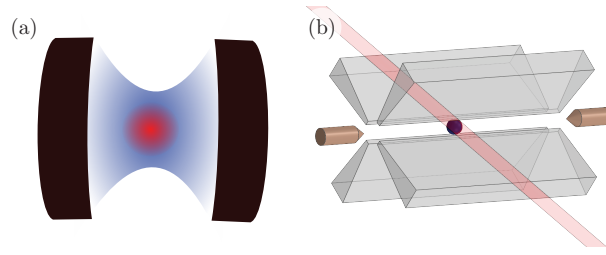
Figure 4.7: Schematics for two experimental realizations of the Jaynes-Cummings model, (a) cavity-QED, and (b) ion-trap-QED.

with zero total excitation number, $\langle N \rangle = 0$, and the rest of eigenstates are given by the dressed state basis [157],

$$
\begin{aligned}
|\varepsilon_{n,+}\rangle &= c_n|n,e\rangle + s_n|n+1,g\rangle, \\
|\varepsilon_{n,-}\rangle &= -s_n|n,e\rangle + c_n|n+1,g\rangle,
\end{aligned}
\tag{4.24}
$$

which define subspaces with mean total excitation $\langle N \rangle = n+1$, for integer index $n = 0, 1, 2, \ldots$. The normalization coefficients are given by $c_n = \cos(\theta_n/2)$, $s_n = \sin(\theta_n/2)$, and the rotation angle $\theta_n = \arctan 2g\sqrt{n+1}/\Delta$, where the detuning is defined by $\Delta = \omega_0 - \omega$. The energy spectrum,

$$
\begin{aligned}
\varepsilon_0 &= -\frac{\omega_0}{2}, \\
\varepsilon_{n,\pm} &= \left(n+\frac{1}{2}\right)\omega \pm \frac{\Omega_n}{2},
\end{aligned}
\tag{4.25}
$$

is given in terms of the Rabi frequency, $\Omega_n = \sqrt{\Delta^2 + 4g^2(n+1)}$.

Now, we follow the standard formalism for open quantum systems described earlier in chapter 2 (see Sec.2.2) in order to arrive to a mircroscopic master equation. We model the environment as a collection of non-interacting bosons, $H_B = \sum_k \omega_k b_k^\dagger b_k$, that bilinearly couple to the field via the interaction Hamiltonian, $H_I = X \otimes X_B$ with $X = a^\dagger + a$ and $X_B = \sum_k g_k \left(b_k^\dagger + b_k\right)$. Then, we use the eigenmode decomposition, $X(v) = \sum_v \Pi(\varepsilon) X \Pi(\varepsilon')$, in terms of the projection operator $\Pi(\varepsilon)$ onto the dressed subspace with effective frequency ε and frequency difference $v = \varepsilon' - \varepsilon$,

$$
X(v) = \sum_{\varepsilon'-\varepsilon=v} \langle \varepsilon|X|\varepsilon'\rangle \, |\varepsilon\rangle\langle\varepsilon'|.
\tag{4.26}
$$

This provides us with the explicit form of the boson field operator X, in terms of the Bohr eigenfrequencies of the central system, such that the jump operators for the JC ladder become,

$$
\begin{aligned}
X(\varepsilon_{0,\pm} - \varepsilon_0) &= s_0|\varepsilon_0\rangle\langle\varepsilon_{0,+}| + c_0|\varepsilon_0\rangle\langle\varepsilon_{0,-}|, \\
X(\varepsilon_{n',+} - \varepsilon_{n,+}) &= \delta_{n,n'-1}\left[c_n c_{n+1}\sqrt{n+1} + s_n s_{n+1}\sqrt{n+2}\right]|\varepsilon_{n,+}\rangle\langle\varepsilon_{n+1,+}|, \\
X(\varepsilon_{n',-} - \varepsilon_{n,-}) &= \delta_{n,n'-1}\left[s_n s_{n+1}\sqrt{n+1} + c_n c_{n+1}\sqrt{n+2}\right]|\varepsilon_{n,-}\rangle\langle\varepsilon_{n+1,-}|, \\
X(\varepsilon_{n',\pm} - \varepsilon_{n,\mp}) &= \delta_{n,n'-1}\left[s_n c_{n+1}\sqrt{n+2} - c_n s_{n+1}\sqrt{n+1}\right]|\varepsilon_{n,\pm}\rangle\langle\varepsilon_{n+1,\mp}|.
\end{aligned}
\tag{4.27}
$$

Writing down the von Neumann equation for the the total density operator in the interaction picture with the reference free Hamiltonian $H_0 = H_{JC} + H_B$, using the Born-Markov and rotating wave approximations (RWA), and taking the average over the degrees of freedom of the environment trough the partial trace

operation, we can obtain the following master equation in the Schrdinger picture,

$$
\begin{aligned}
\dot{\rho}(t) &= -i[H_{JC}, \rho(t)] + \sum_{v>0} \gamma(v) \left[X(v)\rho(t)X^{\dagger}(v) - \frac{1}{2}\{X^{\dagger}(v)X(v), \rho(t)\} \right] \\
&\quad + \sum_{v>0} \gamma(-v) \left[X^{\dagger}(v)\rho(t)X(v) - \frac{1}{2}\{X(v)X^{\dagger}(v), \rho(t)\} \right].
\end{aligned}
\tag{4.28}
$$

Note that the RWA is valid only for couplings larger than the decay rate, $2g \gg \gamma$. The effective frequency-dependent decay rates are given by the Fourier transform,

$$
\begin{aligned}
\gamma(v) &= \int_0^{\infty} ds\, e^{ivs}\, \mathrm{Tr}_B \left[X_B^{\dagger}(s)X_B(0) \right], \\
&= \begin{cases} |g(v)|^2 D(v)[1+\bar{n}(v)], & v > 0 \\ |g(|v|)|^2 D(|v|)\bar{n}(|v|), & v < 0, \end{cases}
\end{aligned}
\tag{4.29}
$$

with the continuum coupling distribution, $g(v)$, and the density of modes, $D(v)$, providing the environment spectral density, $|g(v)|^2 D(v)$; for example, a flat environment has a constant spectral density equal to the common decay rate, $|g(v)|^2 D(v) = \gamma$. Finally, the average number of thermal bosons in the environment is defined by $\bar{n}(v) = 1/\left(e^{v/k_B T} - 1\right)$, with Boltzmann constant k_B and finite temperature T.

In order to provide an explicit working form, we consider the microscopic master equation for the JC model interacting with a flat thermal bath at finite temperature,

$$
\begin{aligned}
\dot{\rho}(t) &= -i[H_{JC}, \rho(t)] + \gamma_1 s_0^2 \hat{\mathscr{D}}(|\varepsilon_0\rangle\langle\varepsilon_{0,+}|) + \gamma_2 c_0^2 \hat{\mathscr{D}}(|\varepsilon_0\rangle\langle\varepsilon_{0,-}|) \\
&\quad + \sum_{n=0}^{\infty} \gamma_3 a_n^2 \hat{\mathscr{D}}(|\varepsilon_{n,+}\rangle\langle\varepsilon_{n+1,+}|) + \sum_{n=0}^{\infty} \gamma_4 b_n^2 \hat{\mathscr{D}}(|\varepsilon_{n,-}\rangle\langle\varepsilon_{n+1,-}|) \\
&\quad + \sum_{n=0}^{\infty} \gamma_5 d_n^2 \hat{\mathscr{D}}(|\varepsilon_{n,-}\rangle\langle\varepsilon_{n+1,+}|) + \sum_{n=0}^{\infty} \gamma_6 d_n^2 \hat{\mathscr{D}}(|\varepsilon_{n,+}\rangle\langle\varepsilon_{n+1,-}|) \\
&\quad + \tilde{\gamma}_1 s_0^2 \hat{\mathscr{D}}(|\varepsilon_{0,+}\rangle\langle\varepsilon_0|) + \tilde{\gamma}_2 c_0^2 \hat{\mathscr{D}}(|\varepsilon_{0,-}\rangle\langle\varepsilon_0|) \\
&\quad + \sum_{n=0}^{\infty} \tilde{\gamma}_3 a_n^2 \hat{\mathscr{D}}(|\varepsilon_{n+1,+}\rangle\langle\varepsilon_{n,+}|) + \sum_{n=0}^{\infty} \tilde{\gamma}_4 b_n^2 \hat{\mathscr{D}}(|\varepsilon_{n+1,-}\rangle\langle\varepsilon_{n,-}|) \\
&\quad + \sum_{n=0}^{\infty} \tilde{\gamma}_5 d_n^2 \hat{\mathscr{D}}(|\varepsilon_{n+1,+}\rangle\langle\varepsilon_{n,-}|) + \sum_{n=0}^{\infty} \tilde{\gamma}_6 d_n^2 \hat{\mathscr{D}}(|\varepsilon_{n+1,-}\rangle\langle\varepsilon_{n,+}|),
\end{aligned}
\tag{4.30}
$$

where we have used the standard notation for dissipators $\hat{\mathscr{D}}(O) = O\rho O^{\dagger} - \{O^{\dagger}O, \rho\}/2$. The energy ladder in Fig.4.8 indicates the different decay and excitation channels induced by the non-unitary part of Eq.4.30. The auxiliary coefficients are defined trough the relations,

$$
\begin{aligned}
a_n &= c_n c_{n+1}\sqrt{n+1} + s_n s_{n+1}\sqrt{n+2}, \\
b_n &= s_n s_{n+1}\sqrt{n+1} + c_n c_{n+1}\sqrt{n+2}, \\
d_n &= s_n c_{n+1}\sqrt{n+2} - c_n s_{n+1}\sqrt{n+1}.
\end{aligned}
\tag{4.31}
$$

Decay rates, assuming a flat environment with constant spectral density, are defined by the expressions $\gamma_i = \gamma[1 + \bar{n}(v_i)]$ and $\tilde{\gamma}_i = \gamma\bar{n}(v_i)$. The average number of thermal photons is given by Planck distribution, $\bar{n}(v_i) = 1/\left(e^{\hbar v_i/k_B T} - 1\right)$, where the characteristic Bohr frequencies, v_i, are the absolute value of the differences between energy levels in the dressed states ladder, ε_0 and $\varepsilon_{n,\pm}$. For example, in a harmonic oscillator there is a unique Bohr frequency provided by the natural frequency of the system. This is not the case in the JC model, however the rotating wave approximation (RWA) on the Hamiltonian allows us to take the field frequency as central Bohr eigenfrequency for the sake of simplicity, $v_i \sim \omega$. It is important to mention that the master equation presented above was derived under a rotating wave approximation performed on the dissipator [156, 158], $\Omega_0 \gg \gamma$.
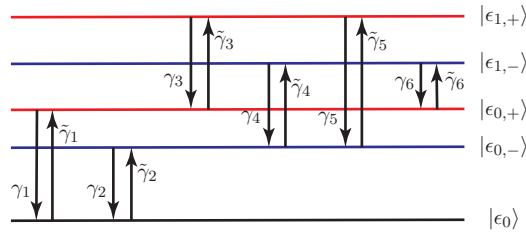
Figure 4.8: A schematic example of some allowed transitions in the dressed energy ladder, decay and excitation channels, due to a finite temperature environment.

On the other hand, dissipation in the JC model is commonly described by a phenomenological master equation of the form [159, 160],

$$\dot{\rho}_{\text{ph}}(t) = -i[H_{JC}, \rho_{\text{ph}}(t)] + \gamma[\bar{n}(\omega) + 1]\hat{\mathscr{D}}(a) + \gamma\bar{n}(\omega)\hat{\mathscr{D}}(a^\dagger), \tag{4.32}$$

which is valid for a broader range of parameters provided that coupling is small compared to the free field and qubit frequencies, $\omega, \omega_0 \gg \gamma$.

4.5.2 Single-excitation manifold at zero temperature

Rabi oscillations are a signature in JC model dynamics; they show the periodic exchange of excitations between the qubit and the field mode in the absence of losses. In real cavity-QED experiments [146], the cavity is in fact open and subject to decoherence, making Rabi oscillations decay and eventually disappear with the inevitable scape of the excitation to the environment. Single-excitation dynamics at zero temperature under the microscopic approach [155] are described by the following simplified form of Eq. (4.30),

$$\dot{\rho}(t) = -i[H_{JC}, \rho(t)] + \gamma\left[s_0^2\hat{\mathscr{D}}(|\varepsilon_0\rangle\langle\varepsilon_{0,+}|) + c_0^2\hat{\mathscr{D}}(|\varepsilon_0\rangle\langle\varepsilon_{0,-}|)\right]. \tag{4.33}$$

Here, decay of the two bare states $|e, 0\rangle$ and $|g, 1\rangle$ to the ground state is allowed, in contrast to the phenomenological description where only the bare state $|g, 1\rangle$ provides a decay channel to the ground state. In the following, we provide a closed-form analytic solution for the case of pure initial states in the single-excitation manifold, $|\psi(0)\rangle = c_{0e}|0, e\rangle + c_{1g}|1, g\rangle$ with $|c_{0e}|^2 + |c_{1g}|^2 = 1$, with the aid of the damping basis technique [161],

$$\begin{aligned}
\rho(t) = &\left\{1 - \left[|c_{1g}|^2(2s_0^2 - 1) + c_0^2 - 2c_0s_0\operatorname{Re}(c_{1g}c_{0e}^*)\right]e^{-\gamma s_0^2 t} + \right.\\
&\left. - \left[|c_{1g}|^2(1 - 2s_0^2) + s_0^2 + 2c_0s_0\operatorname{Re}(c_{1g}c_{0e}^*)\right]e^{-\gamma c_0^2 t}\right\}|\varepsilon_0\rangle\langle\varepsilon_0| + \\
&+ \left[|c_{1g}|^2(2s_0^2 - 1) + c_0^2 - 2c_0s_0\operatorname{Re}(c_{1g}c_{0e}^*)\right]e^{-\gamma s_0^2 t}|\varepsilon_{0,-}\rangle\langle\varepsilon_{0,-}| + \\
&+ \left[|c_{1g}|^2(1 - 2s_0^2) + s_0^2 + 2c_0s_0\operatorname{Re}(c_{1g}c_{0e}^*)\right]e^{-\gamma c_0^2 t}|\varepsilon_{0,+}\rangle\langle\varepsilon_{0,+}| + \\
&+ e^{-\gamma t/2}\left\{\left[\left(1 - 2|c_{1g}|^2\right)c_0s_0 + c_{1g}^*c_{0e}c_0^2 - c_{1g}c_{0e}^*s_0^2\right]e^{i\Omega_0 t}|\varepsilon_{0,-}\rangle\langle\varepsilon_{0,+}| + \right.\\
&\left. + \left[\left(1 - 2|c_{1g}|^2\right)c_0s_0 + c_{1g}c_{0e}^*c_0^2 - c_{1g}^*c_{0e}s_0^2\right]e^{-i\Omega_0 t}|\varepsilon_{0,+}\rangle\langle\varepsilon_{0,-}|\right\}.
\end{aligned} \tag{4.34}$$

From this solution, we can see that off-resonant interaction makes one of the two decay channels dominant, and provides the opportunity to control the decay to the ground state; for example, as we increase the detuning Δ, the coherent exchange of the excitation is maintained for longer times as expected, Fig. 4.9. Meanwhile, the phenomenological description in the single-excitation manifold,

$$\dot{\rho}_{\text{ph}}(t) = -i[H_{JC}, \rho_{\text{ph}}(t)] + \gamma\hat{\mathscr{D}}(|0, g\rangle\langle 1, g|), \tag{4.35}$$
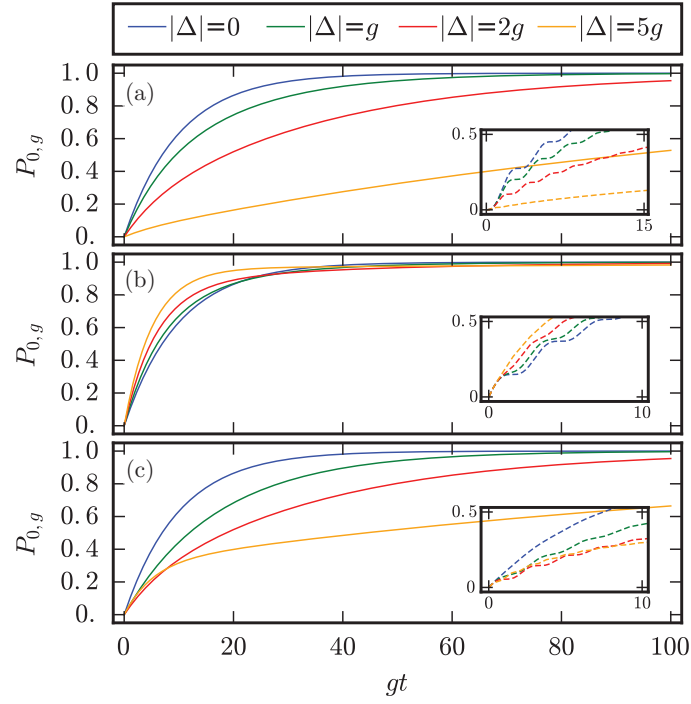
Figure 4.9: *Probability of finding the system in the ground state for initial states (a)* $|\psi(0)\rangle = |0,e\rangle$*, (b)* $|\psi(0)\rangle = |1,g\rangle$*, and (c)* $|\psi(0)\rangle = (|0,e\rangle + |1,g\rangle)/\sqrt{2}$ *under the dynamics provided by the microscopic description of dissipation at zero-T and different detunings. Insets: phenomenological description. Simulation parameters:* $\{\gamma, \omega_0\} = \{0.2, 100\}g$.

shows the direct decay of the state $|1,g\rangle$ to the ground state. We also find convenient to write down an explicit evolution for the same initial state used before,

$$\rho_{\mathrm{ph}}(t) = \left[1 - |a(t)|^2 - |b(t)|^2\right] |\varepsilon_0\rangle\langle\varepsilon_0| + |\Psi(t)\rangle\langle\Psi(t)|, \tag{4.36}$$

where we have used the notation $|\Psi(t)\rangle = [c_0 a(t) + s_0 b(t)] |\varepsilon_{0,+}\rangle + [c_0 b(t) - s_0 a(t)] |\varepsilon_{0,-}\rangle$, with time-dependent functions,

$$a(t) = \left[c_{0e}\cosh\frac{\Omega t}{2} + \frac{c_{0e}(\gamma - 2i\Delta) - 4ic_{1g}g}{2\Omega}\sinh\frac{\Omega t}{2}\right] e^{-\frac{1}{4}(\gamma + 6i\Delta)t},$$

$$b(t) = \left[c_{1g}\cosh\frac{\Omega t}{2} - \frac{c_{1g}(\gamma - 2i\Delta) + 4ic_{0e}g}{2\Omega}\sinh\frac{\Omega t}{2}\right] e^{-\frac{1}{4}(\gamma + 6i\Delta)t}, \tag{4.37}$$

and auxiliary complex frequency $\Omega = \sqrt{\gamma^2 - 16g^2 - 4\Delta(\Delta + i\gamma)}/2$. Our analytic expressions allow general initial states and detuning between the field-qubit frequencies. The difference between the two treatments sits on a high-frequency modulation, at short propagation times, in the decay to the ground state dynamics under the phenomenological description (insets in Fig. 4.9). Fig. 4.9 shows the probability to find the system in the ground state for a near-resonance system, $\omega_0 \sim \omega \gg g$, for different detuning between the qubit and field frequencies for initial states in the single-excited state manifold. An initial qubit in the excited state, $|\psi(0)\rangle = |0,e\rangle$ ($c_{0e} = 1$), produces slower effective decay to the ground state with larger absolute values of the detuning, Fig. 4.9(a), while an initial qubit in the ground state, $|\psi(0)\rangle = |1,g\rangle$ ($c_{1g} = 1$), produces larger effective decay rates to the ground state with larger absolute values of the detuning, Fig. 4.9(b). For a maximally entangled state, $|\psi(0)\rangle = (|0,e\rangle + |1,g\rangle)/\sqrt{2}$ ($c_{0e} = c_{1g} = 1/\sqrt{2}$), these effects provide an effective decay rate that is placed in between those described before, Fig. 4.9(c). The same process is observed in the phenomenological approach with the addition of the higher frequency oscillations mentioned before, insets in Fig. 4.9. The effect of detuning on the qubit-field purity is shown in Fig. 4.10 for the same initial states considered before. On-resonance,

$\Delta = 0$, it is possible to find a simple expression for the purity, namely $P(t) = 1 - 2\left[1 - e^{-\gamma t/2}\right]e^{-\gamma t/2}$, that reaches its minimum at the scaled time $gt = 2\ln 2/\gamma$ for any given initial state in the single excitation manifold. For the initial state with $c_{0e} = 1$, the purity minima appears at longer scaled times for larger absolute values of the detuning, Fig. 4.10(a). A totally different situation is found in the case of an initial state with $c_{1g} = 1$, shown in Fig. 4.10(b), this minimum is slightly shifted back in time as the detuning is increased For a maximal entangled state, $|\psi(0)\rangle = (|0, e\rangle + |1, g\rangle)/\sqrt{2}$ ($c_{0e} = c_{1g} = 1/\sqrt{2}$), the purity minimum behavior is similar to that of the first case, where detuning tends to slow down the purity decay to the ground state but in a less significant way for short times, Fig. 4.10(c). Here, it is not possible to
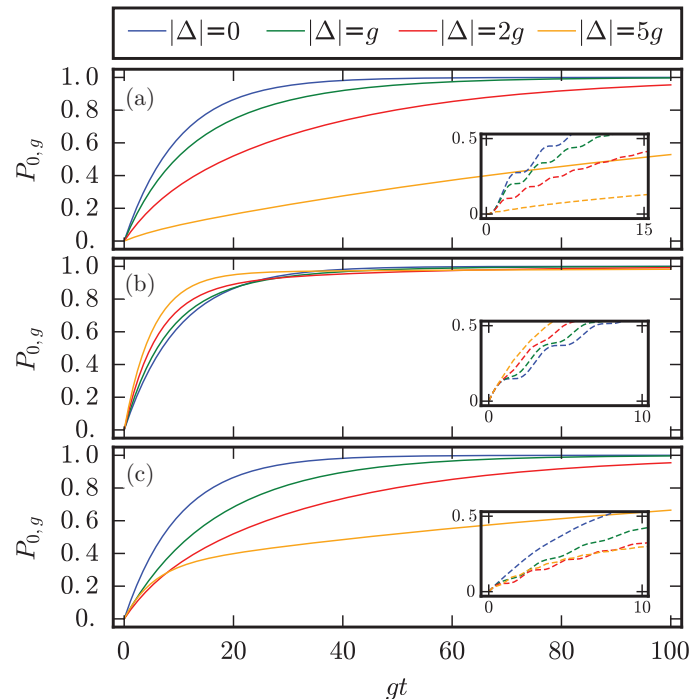
Figure 4.10: Evolution of the qubit-field purity for initial states and parameter values from Fig. 4.9.

express the qubit-field state vector at any time using the appropriate Schmidt decomposition, hence the respective qubit and field entropies are not expected to be equivalents. Actually, in the single-excitation limit, we can think of the field as an effective qubit, and calculate the two-qubit concurrence for the field-matter state. Figure 4.11 shows the dynamics of Wootters concurrence for the effective two-qubit system under the microscopic approach. Figure 4.11(a) and Fig. 4.11(b) shows the evolution starting from separable initial states, $c_{0e} = 1$ and $c_{1g} = 1$ in that order, to an almost maximally entangled at half a Rabi oscillation. Obviously, this will be affected by the environment-induced decoherence. The induced effective decay rates show that an initial state $|\psi(0)\rangle = |0, e\rangle$ produces a higher entangled state for small evolution times and higher detuning, Fig. 4.11(b). An initial pure separable state of the form $|\psi(0)\rangle = |1, g\rangle$ produces and maintains higher concurrence values for lower detuning, Fig. 4.11(a). This is in agreement with the information provided by our previous discussion of the effect of the detuning on the effective decay rates. On-resonance, $\Delta = 0$, and for initial Bell states, in general, the dynamics of the qubit-field correlations can be found by expressing the density operator in the effective two-qubit basis, and applying the analytic expression for concurrence in the case of X-density matrices [42]. It turns out that concurrence decays exponentially with time, $C = e^{-\gamma t/2}$, as shown in Fig. 4.11(c) for an initial state with $c_{0e} = c_{1g} = 1/\sqrt{2}$.
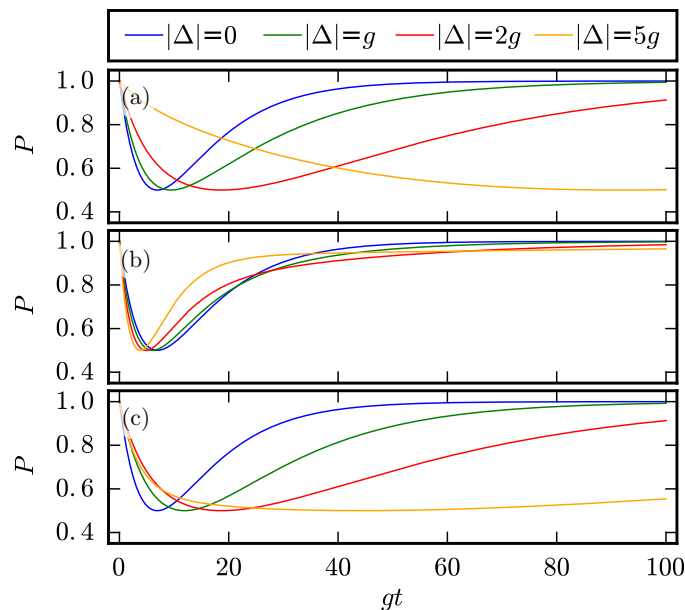
Figure 4.11: *Evolution of the field-qubit concurrence for initial states and parameter values from Fig.* 4.9.

4.5.3   Beyond the single-excitation manifold at finite temperature

As we go beyond the single-excitation manifold, starting with an initial state with more than one total excitation, the oscillations in the ground state probability, $P_{0,g}$, provided by dynamics in the phenomenological description, insets in Fig. 4.9, have larger frequencies and, eventually, make the phenomenological description indistinguishable to the naked eye from that of the microscopic one using the variables presented above. Here, we will show that it is possible to use phase space dynamics to notice the differences between the two approaches. Sadly, it becomes cumbersome and impractical to address analytically the dynamics beyond the single-excitation manifold at zero and finite temperature, and we must resort to numeric simulations in order to create intuition for these systems. In the following, we numerically solve the microscopic master equation, Eq. (4.30), for parameter values related to cavity-QED experiments in the microwave regime [146]. We use two methods, brute force iterative Runge–Kutta methods and direct diagonalization of the Liouvillian [162], and in both cases the dimension of the master equation is truncated once a desired convergence is reached.

Fock states

At zero-T, an initial state in the $\langle N \rangle$-excitation manifold, $|\psi(0)\rangle = |n, e\rangle$ or $|\psi(0)\rangle = |n + 1, g\rangle$, should present similar dissipation dynamics to those described above: the effective decay rate for initial excited and ground state dynamics will differ and be related to the detuning between the qubit and field frequencies. We can see this in the time evolution of the atomic inversion for an initial state $|\psi(0)\rangle = |4, e\rangle$, Fig. 4.12(a), and $|\psi(0)\rangle = |5, g\rangle$, Fig. 4.12(b), but becomes more evident in the qubit-field purity, Fig. 4.12(c) and Fig. 4.12(d). The dynamics provided by the phenomenological approach still have a higher modulating frequency, but it becomes so high that the differences are indistinguishable without further analysis. At finite but low-T, the dynamics are equivalent to those at zero-T with a slight increase of the effective decay rate due to temperature effects and, obviously, the final state of the radiation-matter system, in the asymptotic limit, will reach the thermal equilibrium steady state of the open system. Figures 4.13(a) and 4.13(b) show the time evolution of the atomic inversion, Figs. 4.13(c) and 4.13(d) that of the qubit-field purity of initial states $|\psi(0)\rangle = |4, e\rangle$ and $|\psi(0)\rangle = |5, g\rangle$, in that order for each case, under JC dynamics interacting with a low-T thermal environment with average thermal photons $\bar{n} = 0.1$ that
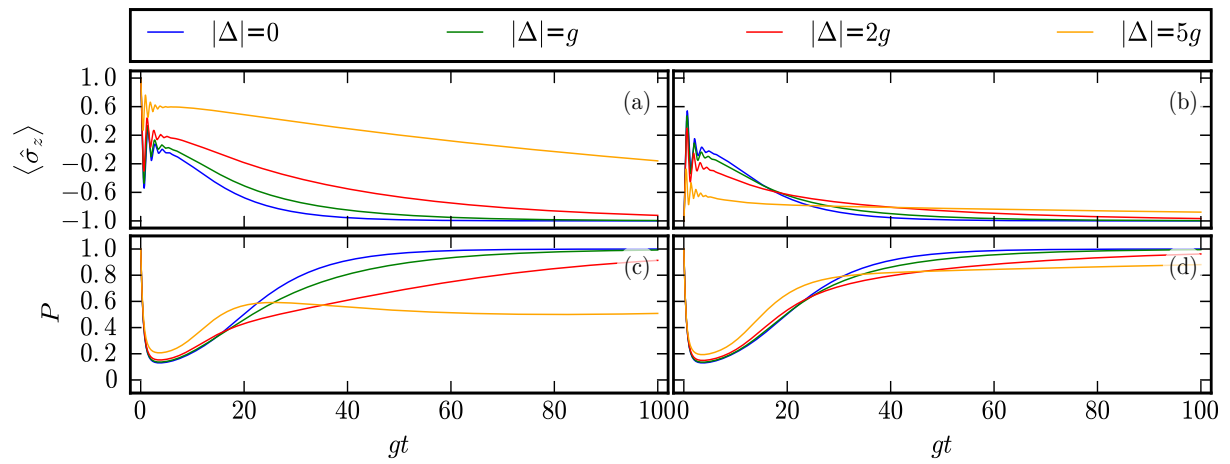
Figure 4.12: Time evolution of the atomic inversion (first row) and qubit-field purity (second row) for initial states $|\psi(0)\rangle = |4,e\rangle$ (left column) and $|\psi(0)\rangle = |5,g\rangle$ (right column), under dynamics provided by the microscopic approach to dissipation at zero-T for different detuning between the qubit and field frequencies. Simulation parameters: $\{\gamma, \omega_0\} = \{0.2, 100\}g$
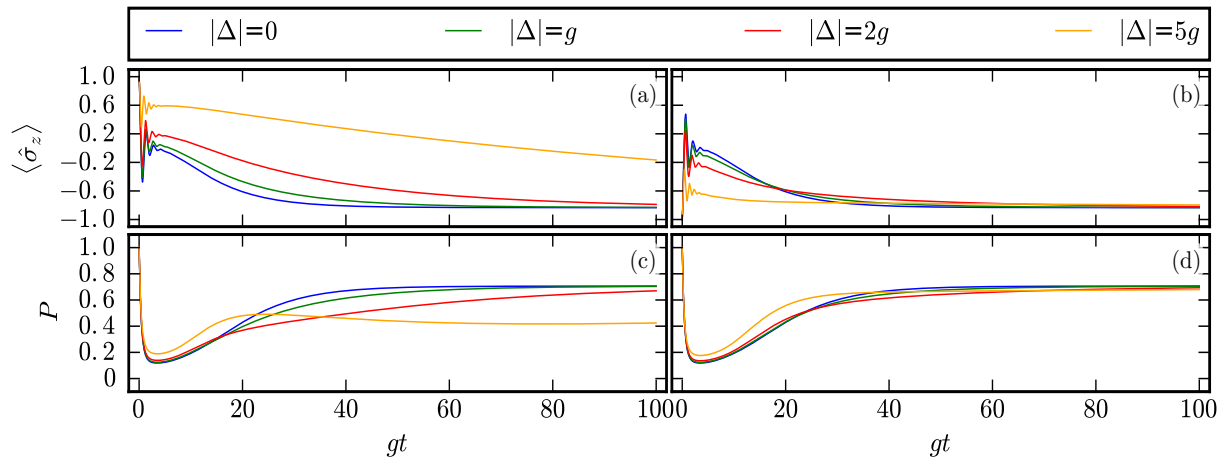
Figure 4.13: Time evolution of the atomic inversion (first row) and qubit purity (second row) for initial states $|\psi(0)\rangle = |4,e\rangle$ (left column) and $|\psi(0)\rangle = |5,g\rangle$ (right column), under dynamics provided by the microscopic approach to dissipation at low-T, for different detuning between the qubit and field frequencies. Simulation parameters: $\{\gamma, \omega_0, \bar{n}\} = \{0.2g, 100g, 0.1\}$.

corresponds to a temperature $T \sim 1$ K for a central Bohr eigenfrequency in the range of a microwave field frequency $\omega \sim 2\pi$ 51 GHz for cavity-QED experiments [153, 154].

Coherent states

In order to study more complex dynamics, let us consider initial states involving coherent states of the field, As we know these are the most classical quantum states in which a field mode can be prepared. For the sake of simplicity, we start from a pure and separable initial state, $|\psi(0)\rangle = |\alpha, g\rangle$, that shows collapse and revival of the atomic inversion at the approximate scaled revival time $gt_r \sim 2\pi|\alpha|$ for the closed system. Figure 4.14 shows the atomic inversion and mean photon number evolution under the microscopic and phenomenological approaches to dissipation for a single revival time. Cavity losses slightly affect the initial collapse of the atomic inversion, but heavily suppress the revival, Fig. 4.14(a), in agreement with previous results employing the phenomenological approach. It is possible to observe differences between the two approaches at short times, but the dynamics seem to become identical as the
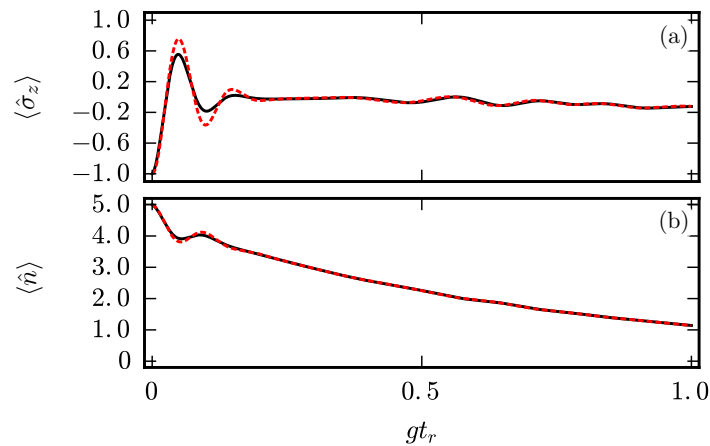
Figure 4.14: Time evolution of the (a) atomic inversion and (b) mean photon number for an initial state composed of a coherent field with $\alpha = \sqrt{5}$ and the atom in the ground state on-resonance, $\Delta = 0$, under dynamics ruled by microscopic (black solid lines) and phenomenological (dotted red lines) approaches to dissipation. Simulation parameters: $\{\gamma, \omega_0, \bar{n}\} = \{0.1g, 100g, 0\}$.

system evolves. Note that care must be exerted to use simulation parameters that satisfy the restrictions mentioned above for each model. Obviously, the effects of detuning at each and every manifold with constant total excitation number described above will survive, but it is not at all obvious that an initial state composed by a coherent field and the two-level system in the ground state, $|\psi(0)\rangle = |\alpha, g\rangle$, will have a lower effective decay rate for larger detuning, Fig. 4.15(a). Figure 4.15(b) shows the atomic inversion evolution, on-resonance for different decay rates, where we can observe that the collapse dynamics, for times shorter than half the revival time, are barely modified while the revival dynamics is strongly suppressed for increasing decay rate. A substantial deviation between the two approaches is easier to detect using the time evolution of the field quadratures, $q = \left(a + a^\dagger\right)/2$ and $p = \left(a - a^\dagger\right)/2i$, whose mean values for a coherent state are equivalent to the real and imaginary part of the analogue classical complex field amplitude. Interestingly enough, the microscopic approach to dissipation provides us with an intuitively expected, spiral decay evolution of the field quadratures, Fig. 4.16(a), similar to the one obtained by the phenomenological approach for just a dissipative cavity. The time evolution for the field quadratures under the phenomenological approach shows the differences and high frequency modulation in the form of deviations from the spiral decay of the free dissipative field, Fig. 4.16(b). Furthermore, the effect of finite-T, which increases the effective decay rate, is more evident in the microscopic approach, Fig. 4.16(c), than in the phenomenological approach, Fig.4.16(d), both in short- and moderate-time scales. Here, we consider a thermal environment with average number of photons $\bar{n} = 1$ that corresponds to a temperature $T \sim 3$ K for a central Bohr eigenfrequency in the microwave regime $\omega \sim 2\pi\ 51$ GHz. The variances of the field quadratures, $\langle \Delta x \rangle = \langle x^2 \rangle - \langle x \rangle^2$, for the microscopic, Fig. 4.17(a) and Fig. 4.17(c), and the phenomenological approaches, Fig. 4.17(b) and Fig. 4.17(d), show an even greater difference on the open system dynamics provided by the two approaches. Under the microscopic approach to dissipation, the initial coherent state of the field stops minimizing the uncertainty relation for the field quadratures in a shorter time than under phenomenological open dynamics. Furthermore, open microscopic dynamics predict lower fluctuations in the variances of the field quadratures, leading to a smoother transition to the steady state, than the one predicted by phenomenological open dynamics. These differences in the mean values of the quadratures and their variances can also be observed in phase space thorough quasi-probability distributions, like Husimi Q-function, $Q(\alpha) = \langle \alpha | \hat{\rho} | \alpha \rangle / \pi$, shown in Fig. 4.18. The dynamics of the Q-function under a microscopic description of dissipation starts from a well defined Gaussian phase space distribution corresponding to a coherent state that, smoothly and quickly, becomes a donut-shaped distribution whose radius starts diminishing until it takes the Gaussian distribution form of coherent vacuum. Fig. 4.18(a)-Fig. 4.18(d). Meanwhile, the evolution
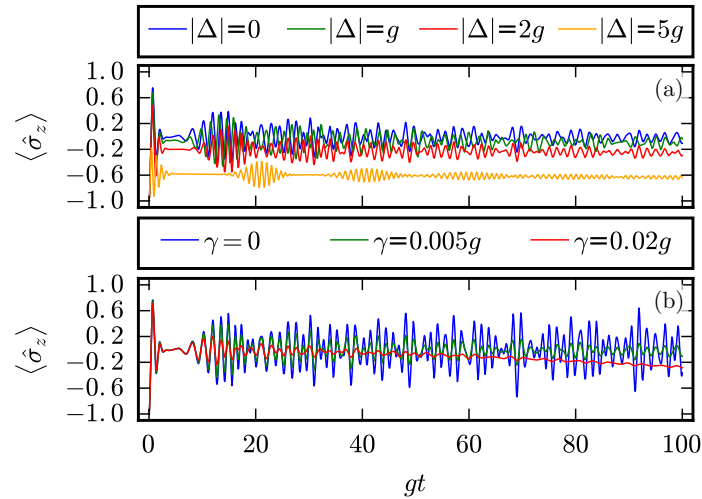
Figure 4.15: *Time evolution of the atomic inversion for an initial state composed of a coherent field with $\alpha = \sqrt{5}$ and the atom in the ground state, $|\psi(0)\rangle = |\alpha, g\rangle$. (a) Varible detuning with fixed decay rate γ, simulation parameters: $\{\gamma, \omega_0\} = \{0.005, 100\}g$, (b) variable decay rate on-resonance, simulation parameters: $\omega_0 = \omega = 100g$.*
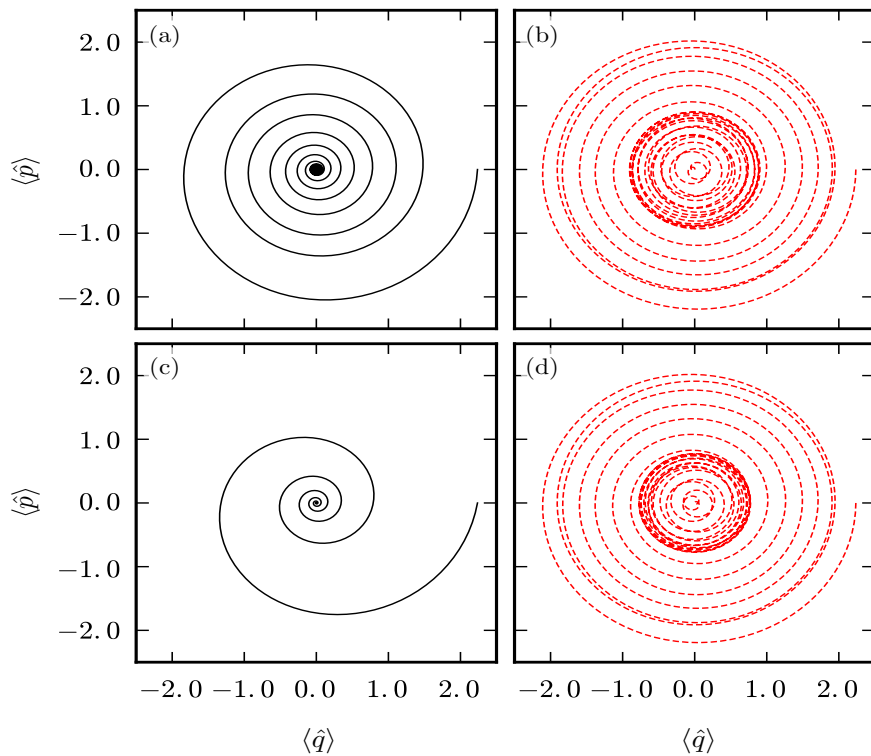
Figure 4.16: *Time evolution of the mean value of the field quadratures for an initial state $|\psi(0)\rangle = |\alpha, g\rangle$ with $\alpha = \sqrt{5}$ under the microscopic (left column) and phenomenological approaches (right column) to dissipation at zero-T (first row), simulation parameters: $\{\gamma, \omega_0\} = \{0.1, 100\}g$, and finite-T (second row), simulation parameters: $\{\gamma, \omega_0, \bar{n}\} = \{0.1g, 100g, 1.0\}$. All cases consider a simulation scaled time interval $[0, 2gt_r]$.*
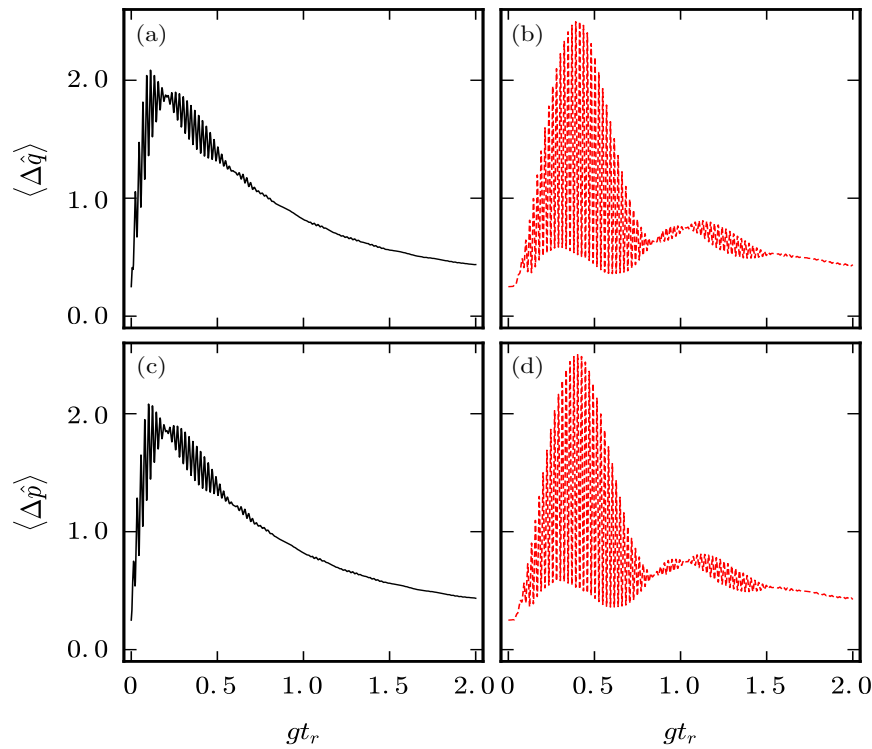
Figure 4.17: Time evolution of the field quadratures variances for an initial state $|\psi(0)\rangle = |\alpha, g\rangle$ with $\alpha = \sqrt{5}$ under the microscopic (left column) and phenomenological approaches (right column) to dissipation at zero-T, simulation parameters: $\{\gamma, \omega_0\} = \{0.1, 100\}g$.

of the Q-function under the phenomenological description follows a more complicated dynamics that might look like a decaying spiral to the coherent vacuum. As visualization help, the reader can find animations for both processes in http://www.hambrientosvagabundos.org/mpg/Micro.mp4 and http://www.hambrientosvagabundos.org/mpg/Pheno.mp4. We conducted an analysis for initial squeezed coherent states of the field but the dynamics are similar to those for coherent states, the mean value of the quadratures follow a spiral decay to the coherent vacuum and, at short times, the variances of the quadratures equalize and follow a behaviour equivalent to that of coherent states.
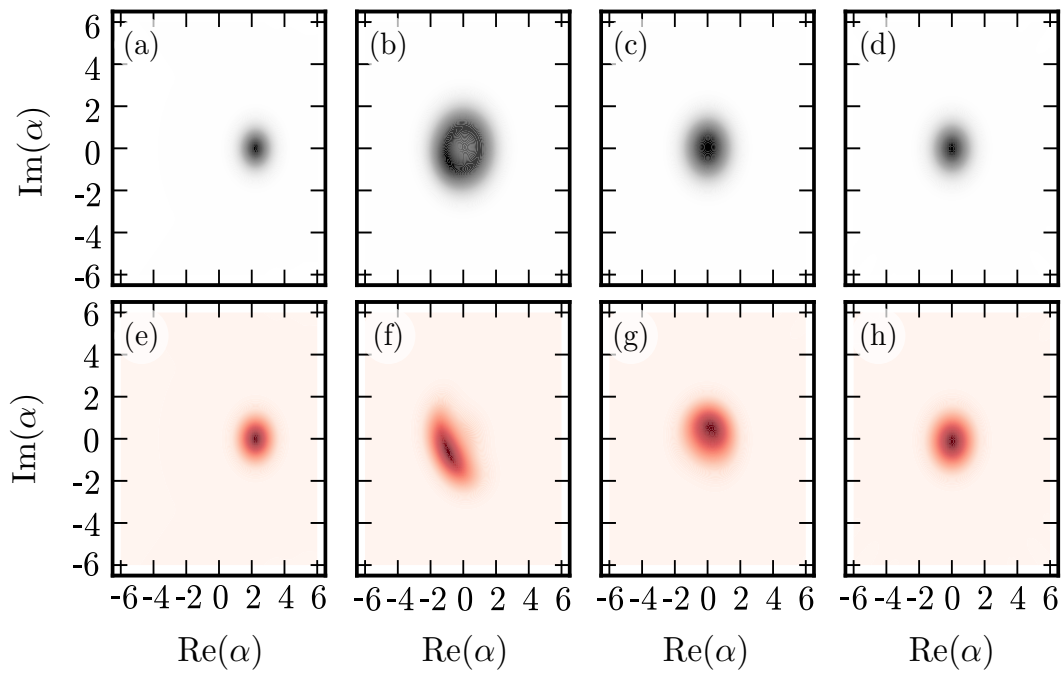
Figure 4.18: Snapshots of Husimi Q-function for different evolution times of an initial state $|\psi(0)\rangle = |\alpha, g\rangle$ with $\alpha = \sqrt{5}$ under the microscopic (top row) and phenomenological approaches (bottom row) to dissipation at zero-T at scaled times (a),(e) $gt = 0$, (b),(f) $gt = 2gt_r/3$, (c),(g) $gt = 4gt_r/3$, and (d),(h) $gt = 2gt_r$ with simulation parameters: $\{\gamma, \omega_0\} = \{0.1, 100\}g$.

Chapter 5

Quantum information based on light-matter interaction

This chapter is devoted to the implementation of quantum information protocols employing light-matter interactions models like the ones presented in chapter 4. In particular we focus our attention in the possibility to perform Bell measurements on atomic qubits using postselection schemes [101].

5.1 The two-photon model

In this section we briefly review the Dicke model in the rotating wave approximation at two-photon resonance with two identical three-level atoms (A and B) that interact with one mode of the quantized electromagnetic field inside an optical cavity. The field couples an intermediate level $|i\rangle$ with the ground $|g\rangle$ and the excited state $|e\rangle$ as depicted in Fig. 5.1. The frequency difference between ground and excited state is assumed to be tuned at twice the frequency of the cavity mode. Choosing units in which $\hbar = 1$, the Hamiltonian describing the dynamics of the system can be written as

$$H = \omega a^{\dagger} a + 2\omega S_{ee} + (\omega + \Delta) S_{ii} + V. \tag{5.1}$$

The first term in the Hamiltonian describes the energy of the optical field and is written in terms of the bosonic annihilation and creation operators a and $a^{\dagger}$. The second and third term represent the atomic energy of the excited and intermediate states, respectively. They are expressed trough the atomic collective operators

$$S_{\mu\nu} = |\mu\rangle\langle\nu|_A + |\mu\rangle\langle\nu|_B, \quad \mu, \nu \in \{g, i, e\}. \tag{5.2}$$

The last term in Eq. (5.1), V, describes the atom-field interaction which is assumed to fulfill the rotating-wave approximation (RWA) and therefore can be written as

$$V = g_g a S_{ig} + g_e a S_{ei} + \text{H.c.} \tag{5.3}$$

where g_e and g_e are the corresponding atom-field coupling strengths. The detuning Δ between the frequency of the intermediate state and the frequency of the mode is assumed to be large compared with both coupling strengths that we consider of the same order of magnitude, namely $\Delta \gg g_g \sim g_e$. In this particular situation, it can be shown that the intermediate level can be approximately decoupled from the dynamics. To show this, we follow the method introduced in [90] and perform a small rotation of the Hamiltonian with the transformation

$$e^{iG} H e^{-iG}, \quad G = \frac{g_g}{\Delta} a S_{ig} - \frac{g_e}{\Delta} a S_{ei} - \text{H.c.} \tag{5.4}$$

Using the Baker-Campbell-Hausdorff (BCH) expansion and neglecting terms of the order $g_e(g_e\sqrt{\langle a^\dagger a\rangle}/\Delta)^2$, one can obtain the following effective Hamiltonian

$$H \approx \omega I + S + W, \tag{5.5}$$

which includes a two-photon interaction term

$$W = g\left(a^2 S_{eg} + a^{\dagger 2} S_{ge}\right), \quad g = -g_e g_e/\Delta. \tag{5.6}$$

Furthermore, the expansion also produces a Stark-shift contribution of the form

$$S = -2\frac{g_g^2}{\Delta}I - \frac{g_e^2 - g_g^2}{\Delta}aa^\dagger S_{ee}, +3\frac{g_g^2}{\Delta}S_{ee}. \tag{5.7}$$

One can verify that the first term in Eq. (5.7) is a constant of motion that is given by

$$I = a^\dagger a + 2S_{ee}. \tag{5.8}$$

In principle, I should also contain the term S_{ii}, however one can safely omit it if the intermediate state is not initially populated. The effective Hamiltonian in (5.5) can be verified with the commutation relations $[G, S_{ii}] = -V$ and $[G, V] = 2W + 2S$ that follows from $[S_{\mu\nu}, S_{\mu'\nu'}] = \delta_{\nu\mu'}S_{\mu\nu'} - \delta_{\nu'\mu}S_{\mu'\nu}$ using Eq. (5.2). Taking into account the order of the neglected terms, one can accurately describe the dynamics of the system using the effective Hamiltonian subjected to the following restriction in time

$$g_e t \ll \Delta^2/g_e^2\langle a^\dagger a\rangle. \tag{5.9}$$

In order to further simplify the interaction, one can find conditions for which the photon-dependent
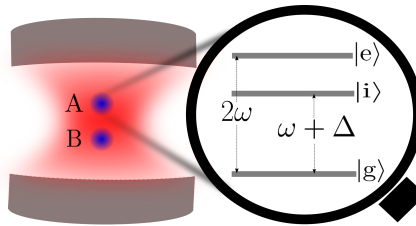
Figure 5.1: Pictorial illustration of two three-level atoms (A and B) interacting at two-photon resonance with one mode of the radiation field inside an optical cavity. For large enough detuning Δ between the lower transition frequency and the frequency of the field, the intermediate state is decoupled from the dynamics leading to an effective two-photon interaction involving only states $|g\rangle$ and $|e\rangle$ of the atoms.

Stark-shift term, second in Eq. (5.7), does not contribute to the dynamics. This part can be neglected if it is smaller than the omitted expressions in the truncated BCH expansion leading to the effective Hamiltonian in Eq. (5.5), which reduces to the condition $|g_e^2 - g_g^2| < g_e^3/\Delta$ quantifying the closenesses between g_g and g_e. With this in mind, the photon-independent Stark-shift, third in (5.7), is of the order of g, which can be neglected for large photon numbers compared with the order of W given by $g\langle a^\dagger a\rangle$. Under these assumptions, one can reduce the Hamiltonian in Eq. (5.1) simply to

$$H \approx (\omega + 2g)I + W. \tag{5.10}$$

As this Hamiltonian effectively describes the dynamics of the two atoms restricted to levels $|g\rangle$ and $|e\rangle$, in what follows we will solve the Schödinger equation for this Hamiltonian in the interaction picture with respect to the constant of motion $(\omega + 2g)I$ exploiting the fact that it commutes with the two-photon interaction, i.e., $[I, W] = 0$. We stress that under the aforementioned assumptions the dynamics of the system is well described by the two-photon interaction term W in Eq. (5.6).

5.1.1 Analytic solution for large mean photon numbers

In this section we derive an approximate analytical solution for the time-dependent state vector in the limit of large mean photon numbers. To this end, we consider initial states of the form $|\Psi\rangle = |\psi\rangle \otimes |\alpha\rangle$, where $|\psi\rangle$ is an arbitrary state of two two-level atoms, and where we have considered the photonic coherent state $|\alpha\rangle = \sum_{n=0}^{\infty} p_n |n\rangle$ with $\alpha = |\alpha| e^{i\phi}$. In this situation, the mean photon number is given by $\bar{n} = \langle a^\dagger a \rangle = |\alpha|^2 \gg 1$ and is assumed to be large. In order to find the time-dependent state vector we choose to solve the eigenvalue problem for W using the photon number states $|n\rangle$, the atomic basis $|gg\rangle$, $|ee\rangle$, and the Bell states

$$|\Psi^\pm\rangle = \frac{1}{\sqrt{2}} (|ge\rangle \pm |eg\rangle). \tag{5.11}$$

In this basis an arbitrary initial state of the atoms takes the form

$$|\psi\rangle = c_g |gg\rangle + c_- |\Psi^-\rangle + c_+ |\Psi^+\rangle + c_e |ee\rangle, \tag{5.12}$$

where the probability amplitudes fulfill the normalization condition and with the convention $|ge\rangle = |g\rangle_A |e\rangle_B$. It can be verified by inspection that the set of states $\{|\Psi^-\rangle |n\rangle\}_{n=0}^{\infty}$ are eigenvectors of W with eigenvalue 0. The rest of the eigensystem can be evaluated by diagonalizing 3×3 matrices which in the tripartite basis $\{|gg\rangle |n\rangle, |\Psi^+\rangle |n-2\rangle, |ee\rangle |n-4\rangle\}$, can be written as

$$W_n = g\sqrt{2} \begin{pmatrix} 0 & \sqrt{n^2-n} & 0 \\ \sqrt{n^2-n} & 0 & \sqrt{n^2-5n+6} \\ 0 & \sqrt{n^2-5n+6} & 0 \end{pmatrix}.$$

Although it is possible to diagonalize these matrices in an exact form, the condition of high mean photon number $|\alpha|^2 \gg 1$ will allow us to find compact expressions that are good approximations to the exact results. For instance, the exact nonzero eigenvalues are $w_n^\pm = \pm g\sqrt{(2n-3)^2 + 3}$, but they can be approximated for large values of n by

$$\tilde{w}_n^\pm = \pm g(2n-3). \tag{5.13}$$

In this limit, one can find that the orthogonal transformation which diagonalizes each block W_n takes the simple form

$$\tilde{O}_n = \frac{1}{2} \begin{pmatrix} -\sqrt{2} & 1 & 1 \\ 0 & -\sqrt{2} & \sqrt{2} \\ \sqrt{2} & 1 & 1 \end{pmatrix}. \tag{5.14}$$

The evolution operator can also be expressed in terms of matrices of size 3×3, which can be evaluated using the transformation that diagonalizes the blocks W_n of W, namely

$$\tilde{U}_n(t) = \tilde{O}_n^\mathsf{T} \exp[-i \operatorname{diag}(0, -\tilde{w}_n, \tilde{w}_n)t] \tilde{O}_n, \tag{5.15}$$

where $\operatorname{diag}(v)$ represents a diagonal matrix with the elements of v as non-zero entries.

With these approximations, the evolution operator has a remarkable simple form and is given by

$$
\tilde{U}_n(t) = \begin{pmatrix} \cos^2\left(\frac{\tilde{w}_n t}{2}\right) & \frac{\sin(\tilde{w}_n t)}{i\sqrt{2}} & -\sin^2\left(\frac{\tilde{w}_n t}{2}\right) \\ \frac{\sin(\tilde{w}_n t)}{i\sqrt{2}} & \cos(\tilde{w}_n t) & \frac{\sin(\tilde{w}_n t)}{i\sqrt{2}} \\ -\sin^2\left(\frac{\tilde{w}_n t}{2}\right) & \frac{\sin(\tilde{w}_n t)}{i\sqrt{2}} & \cos^2\left(\frac{\tilde{w}_n t}{2}\right) \end{pmatrix}. \tag{5.16}
$$

Therefore, the time evolution of any initial state can be written as

$$
|\Psi(t)\rangle = a_0|gg,0\rangle + a_1|gg,1\rangle + \sum_{n=2}^{3} \left(a_{n,t}|gg,n\rangle + b_{n,t}|\Psi^+,n-2\rangle\right) + \tag{5.17}
$$

$$
\sum_{n=4}^{\infty} \left(a_{n,t}|gg,n\rangle + b_{n,t}|\Psi^+,n-2\rangle + c_{n,t}|ee,n-4\rangle\right),
$$

where $a_0 = c_e p_0$ and $a_1 = c_e p_1$ are the probability amplitudes of stationary states that are decoupled from the dynamics. The rest of the coefficients can be evaluated with the aid of the evolution operator and are given by

$$
a_{n,t} = \left(\frac{c_+ + d_{2\phi}^+}{2}e^{-i\tilde{w}_n t} - \frac{c_+ - d_{2\phi}^+}{2}e^{i\tilde{w}_n t} + d_{2\phi}^-\right)\frac{e^{-i2\phi} p_n}{\sqrt{2}},
$$

$$
b_{n,t} = \left(\frac{c_+ + d_{2\phi}^+}{2}e^{-i\tilde{w}_n t} + \frac{c_+ - d_{2\phi}^+}{2}e^{i\tilde{w}_n t}\right) p_{n-2}, \tag{5.18}
$$

$$
c_{n,t} = \left(\frac{c_+ + d_{2\phi}^+}{2}e^{-i\tilde{w}_n t} - \frac{c_+ - d_{2\phi}^+}{2}e^{i\tilde{w}_n t} - d_{2\phi}^-\right)\frac{e^{i2\phi} p_{n-4}}{\sqrt{2}}.
$$

In the previous expressions we have introduced for notational convenience the coefficients

$$
d_\phi^\pm = \frac{c_g e^{i\phi} \pm c_e e^{-i\phi}}{\sqrt{2}}, \tag{5.19}
$$

which are the initial probability amplitudes of the maximally entangled states of the two atoms

$$
|\Phi_\phi^\pm\rangle = \frac{1}{\sqrt{2}}\left(e^{-i\phi}|gg\rangle \pm e^{i\phi}|ee\rangle\right). \tag{5.20}
$$

In order to find a simple expression for the state vector, we use the following approximated relation for the photonic probability amplitudes

$$
p_n \approx p_{n-1} e^{i\phi}. \tag{5.21}
$$

With this result one can carry out the summation in Eq. (5.17) in order the arrive to an approximation of the state vector in terms of coherent states and maximally entangled atomic states, namely

$$
|\Psi(t)\rangle = \left(c_-|\Psi^-\rangle + d_{2\phi}^-|\Phi_{2\phi}^-\rangle\right)|\alpha\rangle + \tag{5.22}
$$

$$
\frac{c_+ + d_{2\phi}^+}{2}e^{-igt}\left(|\Psi^+\rangle + |\Phi_{2\phi-4gt}^+\rangle\right)|e^{-i2gt}\alpha\rangle +
$$

$$
\frac{c_+ - d_{2\phi}^+}{2}e^{igt}\left(|\Psi^+\rangle - |\Phi_{2\phi+4gt}^+\rangle\right)|e^{i2gt}\alpha\rangle.
$$

A similar expression to this formula was found in [30] for the two-atom Tavis-Cummings model involving more complicated field states that followed the dynamics of a coherent state, but distorting its shape in time. In contrast, the solution in Eq.5.22 is written in terms of coherent states as a consequence of the linear behavior of the eigenfrequencies of the system for large photon numbers. The full exact solution for the two-photon model was previously reported in Ref. [98] together with a semiclassical approxi-
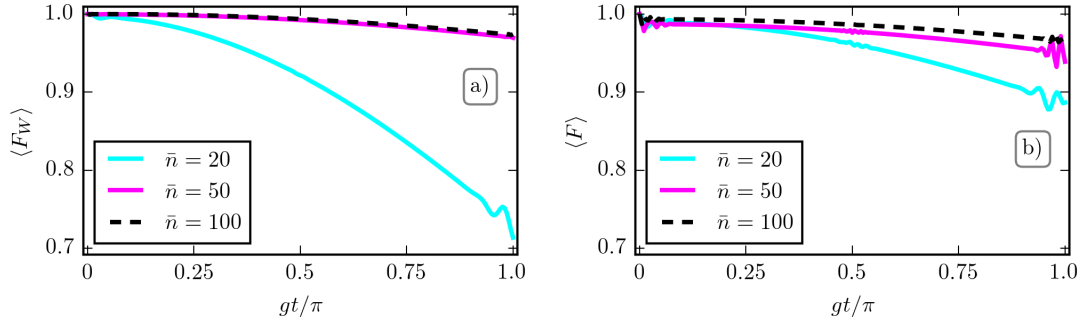
Figure 5.2:   a) Ensemble average of the fidelity $\langle F_W \rangle$ computed from the exact numerical state vector $|\Psi_W(t)\rangle$ for the effective two-photon Hamiltonian W respect to the numerical solution $|\Psi_{\text{exact}}(t)\rangle$ corresponding to the full Hamiltonian (5.1) as a function of the scaled time gt/π. Three cases are shown: $\bar{n} = 20, 50, 100$. b) Ensemble average of the fidelity $\langle F \rangle$ of the approximate solution $|\Psi(t)\rangle$ (Eq. (5.22)) also with reference to the state $|\Psi_{\text{exact}}(t)\rangle$ as function of the scaled time gt with $g_g/\Delta = 0.002$. The ensemble average has been performed over 10^3 initial random pure states uniformly distributed according to the Haar measure of $SU(4)$ with ϕ a random phase drawn from a uniform distribution $\in [0, 2\pi)$.

mation in agreement with our findings. There, however, the form in terms of orthogonal Bell states and coherent states was not identified nor its potential application was stressed.

In order to test the validity of our approximation, we have plotted in Fig. 5.2 a) the fidelity $F_W = |\langle \Psi_{\text{exact}}(t)|\Psi_W(t)\rangle|^2$ of the exact numerical solution evaluated with the full Hamiltonian in Eq. (5.1) with respect to the exact numerical state vector computed with the two-photon Hamiltonian in (5.10) for different values of the average photon number $\bar{n}$. As a comparison we show in Fig. 5.2 b) the fidelity $F = |\langle \Psi_{\text{exact}}(t)|\Psi(t)\rangle|^2$ with respect to the approximate state vector in terms of coherent states of Eq. (5.22). In favor of generality, and for both fidelities, we have performed an ensemble average with 10^3 random initial pure states taken from the uniform distribution of $SU(4)$. The phase ϕ of the coherent state was randomly obtained from a uniform distribution in the interval $[0, 2\pi)$. It can be noted, that the agreement between dynamics is remarkably good for increasing value of the mean photon number in both situations. Having checked its validity, the solution in Eq. (5.22) will be the starting point of our subsequent analysis.

5.1.2   Collapse and revival of Rabi oscillations

A clear manifestation of the coherent shape of the components of the field state is the perfect revivals of the Rabi oscillations of observables such as the mean value of the operator S_{ee}, which can be interpreted as number the atoms in their corresponding excited state. This can be evaluated analytically, for instance for the initial state $|ee\rangle|\alpha\rangle$, using our expression (5.22) as

$$\langle S_{\text{ee}} \rangle = 1 + \text{Re} \left[e^{-|\alpha|^2(1-e^{i2gt})-i3gt} \right], \tag{5.23}$$

where we have employed the overlap between the relevant coherent states $\langle \alpha|\alpha e^{\pm i2gt}\rangle = e^{-|\alpha|^2(1-e^{\pm i2gt})}$ which has a Gaussian envelope $(1 + e^{-2|\alpha|^2 g^2 t^2})/2$ for values of time close to zero and in general to $gt = \pi l$, with $l \in \mathbb{N}$. In Fig. 5.3 we have plotted the numerical exact calculation of $\langle S_{\text{ee}} \rangle$. As in the case of the standard Jaynes-Cummings interaction, collapses and revivals in this atomic observable are present in the dynamics of the two-photon model (apart from an alternating sign). However, they show a different behavior as they appear in a more compact and regular form, showing almost the complete returning to the initial photonic state in the case of large fields [164]. In the two-photon two-atom model,

the time at which revivals appear is independent of $\bar{n}$ and is given by

$$t_r \approx \pi/g. \tag{5.24}$$

In order to attain t_r with the model of Sec. 5.1, the restriction in time of Eq. (5.9) results in the following condition for the parameters of the model: $g_e \bar{n} \pi \ll \Delta$.

The collapse and revival of Rabi oscillations can also be studied in phase space. This gives a relevant pictorial description of the time-evolution of the field state, whose form will corroborate our approximation in terms of coherent states. We choose to visualize the behavior in terms of the Wigner function [165], a quasi-probability distribution defined as

$$W(\beta, t) = \frac{1}{\pi^2} \int \mathrm{Tr} \left\{ \rho_f(t) e^{\zeta a^\dagger - \zeta^* a} \right\} e^{\beta \zeta^* - \beta^* \zeta} d^2\zeta, \tag{5.25}$$

with β and ζ being complex numbers and the reduced density operator of the field obtained after tracing out the atomic degrees of freedom, i.e., $\rho_f(t) = \mathrm{Tr}_{A,B} |\Psi(t)\rangle \langle \Psi(t)|$. In Fig. 5.4 we present the Wigner function of the photonic state for three different values of the interaction time, namely $t = 0$, $t = t_r/4$ and $t = t_r/2$. From this representation one can extract relevant dynamical information of the full system. The
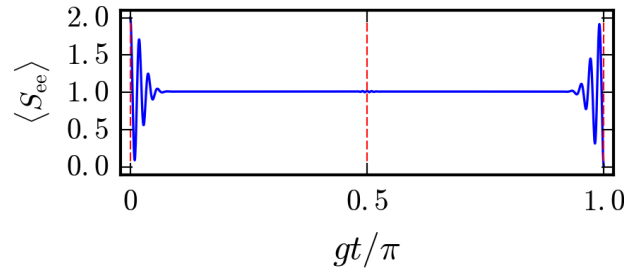
Figure 5.3: *Rabi oscillations generated by the effective Hamiltonian* (5.10) *as a function of the scaled time* gt/π *for the initial state* $|ee\rangle|\alpha\rangle$ *with* $|\alpha|^2 = 50$. *An approximate analytical expression for these oscillations is given in Eq.* (5.23).

initial state for $t = 0$ in Fig. 5.4 a) corresponds to a coherent state and is represented by a Gaussian distribution in the complex plane. For nonzero values of the interaction time, the field evolves as correlated coherent states, without deforming its circular shape, showing no squeezing during the evolution. The correlated feature is manifested by the interference fringes between the maxima at $t_r/4$ in Fig. 5.4 b) that disappear at $t_r/2$ in Fig. 5.4 c). From Eq. (5.22), one can evaluate the state vector at half the revival time

$$\begin{aligned} |\Psi(t_r/2)\rangle &= \left(c_- |\Psi^-\rangle + d_{2\phi}^- |\Phi_{2\phi}^-\rangle \right) |\alpha\rangle \\ &\quad - i \left(c_+ |\Phi_{2\phi}^+\rangle + d_{2\phi}^+ |\Psi^+\rangle \right) |-\alpha\rangle. \end{aligned} \tag{5.26}$$

Tracing over the atomic degrees of freedom, one finds that the field state corresponds to the mixed state

$$\begin{aligned} \rho_f &= \left(|c_-|^2 + |d_{2\phi}^-|^2 \right) |\alpha\rangle\langle\alpha| + \\ &\quad \left(|c_+|^2 + |d_{2\phi}^+|^2 \right) |-\alpha\rangle\langle-\alpha|. \end{aligned} \tag{5.27}$$

This incoherent superposition explains the absence of interference fringes between the two-dimensional Gaussian functions representing opposed coherent states in phase space in Fig. 5.4 c). The complete state of the system at $t_r/2$, half revival time, given in Eq. (5.26) will play a key role in what follows. In the next section we will show that multipartite quantum correlations can be generated during the time evolution leading to the formation of tripartite entangled states.
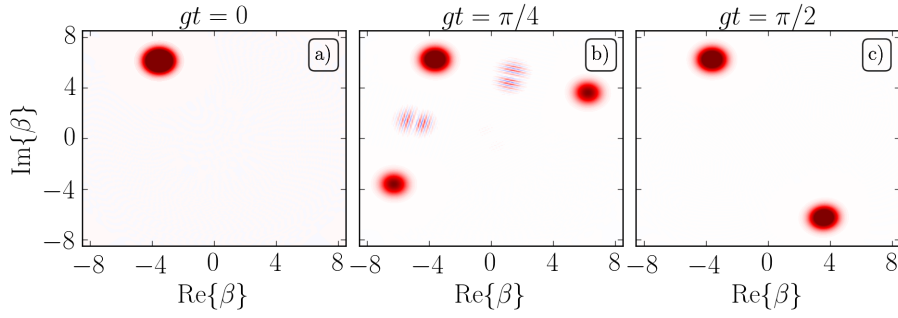
Figure 5.4: Wigner function of the optical field for interactions times a) $t_r = 0$, b) $t_r = 1/4$, c) $t_r = 1/2$. At $t_r = 1/2$ (last snapshot) one can recognize the shape of an incoherent superposition of two coherent states. Parameters are the same as in Fig. 5.3.

5.2   Generation of GHZ states

An immediate application is the possibility to generate maximally entangled three-qubit states using the intrinsic dynamics of the two-photon model. Based on our solution in terms of Bell and coherent states at half revival time in Eq. (5.26) and setting the coefficients $c_- = d_{2\phi}^+ = 0$, and $c_+ = \frac{1}{\sqrt{2}}$, $d_{2\phi}^- = \frac{i}{\sqrt{2}}$, the state vector evaluated at $t_r/2$ takes the following form:

$$|\Psi(t_r/2)\rangle = \frac{i}{\sqrt{2}} \left[|\Phi_{2\phi}^-\rangle |\alpha\rangle - |\Phi_{2\phi}^+\rangle |-\alpha\rangle \right]. \tag{5.28}$$

Looking at the probability amplitudes, the initial state might appear somehow complicated or even entangled, but it is actually an initial tripartite product state with the field in the coherent state $|\alpha\rangle$ and each atom in the state

$$|\varphi_\phi\rangle = \frac{e^{i\pi/4}}{\sqrt{2}} \left(e^{-i\phi} |g\rangle - i e^{i\phi} |e\rangle \right). \tag{5.29}$$

It is therefore a remarkable result that the simple unitary evolution generates a maximally entangled tripartite state with a product state as an input. In order to show that this corresponds to a tripartite entangled state, it is useful to establish an isomorphism between coherent and qubit states for large values $|\alpha|$. Consider the following even and odd Schrödinger cat states:

$$|\alpha, \pm\rangle = \frac{1}{\sqrt{2}} \left(|\alpha\rangle \pm |-\alpha\rangle \right), \tag{5.30}$$

which are eigenstates of the parity operator $\Pi = (-1)^{a^\dagger a}$ with eigenvalues ± 1 that fulfill the condition $\langle \alpha, +|\alpha, -\rangle \approx 0$ for $|\alpha| \gg 1$. Even and odd cat states can then be respectively interpreted as the excited and ground states of a two-level system [166]. In fact, one can easily check that the operators:

$$\Sigma_x = |\alpha, +\rangle\langle\alpha, -| + |\alpha, -\rangle\langle\alpha, +|, \tag{5.31}$$

$$\Sigma_y = i \left(|\alpha, +\rangle\langle\alpha, -| - |\alpha, -\rangle\langle\alpha, +| \right), \tag{5.32}$$

$$\Sigma_z = |\alpha, +\rangle\langle\alpha, +| - |\alpha, -\rangle\langle\alpha, -|, \tag{5.33}$$

satisfy the same $SU(2)$ algebra $[\Sigma_i, \Sigma_j] = 2i\varepsilon_{ijk}\Sigma_k$ and $\{\Sigma_i, \Sigma_j\} = \delta_{ij}$. If we set the phase $\phi = \pi/4$, the state in Eq. (5.28) can be rewritten as

$$|\text{GHZ}\rangle = \frac{1}{\sqrt{2}} \left(|gg\rangle |\alpha, -\rangle + |ee\rangle |\alpha, +\rangle \right), \tag{5.34}$$

which can be immediately recognized as a Greenberger-Horne-Zeilinger (GHZ) state. It is well known that GHZ states contain one of the two types of tripartite entanglement, and they have been experimentally realized in a variety of physical systems, such as photons, trapped ions, and superconducting qubits [104, 105, 167]. These states are characterized by the fact that a measurement performed on the third qubit results in an unentangled qubit pair. However, a very interesting fact is that pairwise en-
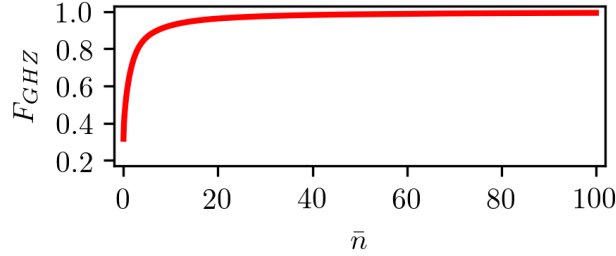
Figure 5.5: Fidelity between the generated GHZ state in Eq. (5.34) and the numerically evaluated state vector, $F_{GHZ} = |\langle \text{GHZ} | \Psi_{\text{exact}}(\pi/2g) \rangle|^2$, as a function of the mean photon number.

tanglement can be obtained by performing an appropriate measurement of the third qubit along some orthogonal direction. From Eq. (5.34) we can see this by projecting onto the coherent states $|\pm\alpha\rangle$, which automatically leaves the qubit pair in one of the entangled states $|\Phi^{\pm}\rangle$. The corresponding fidelity $F_{GHZ} = |\langle \text{GHZ} | \Psi_{\text{exact}}(\pi/2g) \rangle|^2$ between the generated GHZ state in Eq. (5.34) and the exact state vector calculated by numerical means is shown in Fig. 5.5 for increasing mean photon number. As we have shown, almost unit fidelity GHZ states can be efficiently engineered by the appropriate tuning of the initial conditions.

5.3 A novel protocol for Bell measurements

In this section we present a scheme to implement a complete Bell measurement based on atomic postselection by letting the atoms interact with two separate cavities and then measuring the field state as depicted in Fig. 5.6. We elucidate this by first considering the interaction with one cavity for an interaction time equal to half revival time for which the system is left in the state given by Eq. (5.26). At this time, only two coherent states contribute to the photonic state and are correlated with two orthogonal components of the atomic state. As we are considering the limit of high excitation number, these two coherent states are nearly orthogonal as can be noted from their overlap $\langle \alpha | - \alpha \rangle = e^{-2|\alpha|^2}$, and therefore can be distinguished with an appropriate measurement scheme [29, 30, 168]. For our discussion, we assume that one is able to project the field onto the states $|\alpha\rangle$ or $|-\alpha\rangle$. This photonic projections postselect the two-atom state and due to the form of the state in Eq. (5.26) correspond, respectively, to the following measurement operators

$$M_{\phi}^+ = |\Psi^-\rangle\langle\Psi^-| + |\Phi_{2\phi}^-\rangle\langle\Phi_{2\phi}^-|,$$
$$M_{\phi}^- = -i|\Phi_{2\phi}^+\rangle\langle\Psi^+| - i|\Psi^+\rangle\langle\Phi_{2\phi}^+|. \tag{5.35}$$

Therefore, projecting onto the photonic state $|\pm\alpha\rangle$ corresponds to implementing the atomic measurement operator $M_{\phi}^{\pm}$, a rank-two projector and a flip operator, both given in the Bell basis. The appearance of this flip operator is due to the fact that in (5.26) the initial atomic probability amplitudes of the state in the second row are interchanged. For certain atomic probability amplitudes, the above projection postselect the atoms in an entangled state in a similar fashion as in [163]. With the previous result it is not possible to project the atomic states into four orthogonal states,as we have only encountered a rank-two projector and a flip operation in the space of two maximally entangled states. However, one
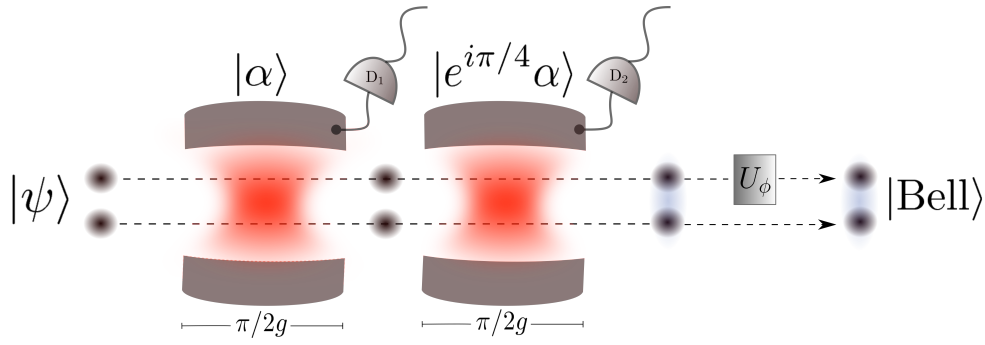
Figure 5.6: Schematic visualization of the Bell measurement scheme. Two matter qubits initially described by an arbitrary state $|\psi\rangle$ enter to a sequence of two independent electromagnetic cavities prepared in coherent states. Both qubits couple to each mode for a time $t_r/2$. At the exit of the cavities, a measurement on the field state is performed by detectors D_1 and D_2. As a final step, a single-qubit unitary U_ϕ is applied on the first qubit resulting in the postselection of a Bell state.

can extend this result with the use of a second cavity, similar to [29, 30]. For this purpose, one has to let the atoms interact with the field prepared in a coherent state of the form $|e^{i\pi/4}\alpha\rangle$, i.e., dephased by $\pi/4$ from the first coherent state. This can be done, for instance, by letting the atoms interact with a second cavity as depicted in Fig. 5.6. After an interaction time of $t_r/2$, one would obtain a similar state to the one in Eq. (5.26), but with rotated coherent states, i.e., ϕ replaced by $\phi + \pi/4$. In this case, projecting onto $|\pm e^{i\pi/4}\alpha\rangle$ would correspond to measuring the atoms with a measurement operator $M^\pm_{\phi+\pi/4}$. Combining this with the previous procedure, one is able to measure the atoms according to the following measurement elements

$$
\begin{aligned}
M^{++} &= M^+_{\phi+\pi/4}M^+_\phi = |\Psi^-\rangle\langle\Psi^-|, \\
M^{+-} &= M^+_{\phi+\pi/4}M^-_\phi = -i|\Phi^+_{2\phi}\rangle\langle\Psi^+|, \\
M^{-+} &= M^-_{\phi+\pi/4}M^+_\phi = |\Psi^+\rangle\langle\Phi^-_{2\phi}|, \\
M^{--} &= M^-_{\phi+\pi/4}M^-_\phi = i|\Phi^-_{2\phi}\rangle\langle\Phi^+_{2\phi}|.
\end{aligned}
\tag{5.36}
$$

where we have considered the following relations

$$
|\Phi^\pm_{\phi+\pi/2}\rangle = -i|\Phi^\mp_\phi\rangle, \quad d^\pm_{\phi+\pi/2} = id^\mp_\phi.
\tag{5.37}
$$

Each measurement element $M^{\pm\pm}$ corresponds to the simultaneous projection onto $|\pm\alpha\rangle$ in the first cavity and onto $|\pm e^{i\pi/4}\alpha\rangle$ in the second cavity. It turns out that all $M^{\pm\pm}$ form the set of measurement operators of a particular positive operator-valued measurement (POVM) [20] that is already good enough to distinguish the four Bell states. However, this does not correspond to a von Neumann measurement, as there are some states that are interchanged during the process. In order to convert this scheme into a von Neumann measurement of the four Bell states, i.e., a Bell measurement, one has to implement a procedure to flip some of the Bell states. Fortunately, this can be accomplished with the help of the following pair of single-atom unitary transformations

$$
\sigma_\phi = e^{i\phi}|e\rangle\langle g| + e^{-i\phi}|g\rangle\langle e|, \quad \sigma_z = |e\rangle\langle e| - |g\rangle\langle g|,
\tag{5.38}
$$

that transform the Bell states according to the following rules

$$
\begin{aligned}
\sigma_{\phi,A}|\Phi^\pm_\phi\rangle &= \pm|\Psi^\pm\rangle, \quad \sigma_{z,A}|\Psi^\pm\rangle = -|\Psi^\mp\rangle \\
\sigma_{\phi,A}|\Psi^\pm\rangle &= \pm|\Phi^\pm_\phi\rangle, \quad \sigma_{z,A}|\Phi^\pm_\phi\rangle = -|\Phi^\mp_\phi\rangle.
\end{aligned}
\tag{5.39}
$$

Applying these single-qubit gates only to qubit-A in a selective way after the field measurement and according to each outcome, one is able to perform the following Bell-state projections

$$
\begin{aligned}
M^{++} &= |\Psi^-\rangle\langle\Psi^-|, \\
i\sigma_{2\phi,A}M^{+-} &= |\Psi^+\rangle\langle\Psi^+|, \\
\sigma_{2\phi,A}\sigma_{z,A}M^{-+} &= |\Phi_{2\phi}^-\rangle\langle\Phi_{2\phi}^-|, \\
i\sigma_{z,A}M^{--} &= |\Phi_{2\phi}^+\rangle\langle\Phi_{2\phi}^+|,
\end{aligned}
\tag{5.40}
$$

that are required in a complete Bell measurement. The implementation of the selective single-qubit gate is represented in Fig. 5.6 by the application of the operation U_ϕ after the interaction with the two cavities. A summary of the protocol with the corresponding single-qubit gate on atom A is presented in table 5.1. In order to test the protocol, we have carried out numerical simulations to evaluate the fidelity

Measured field state in D_1	Measured field state in D_2	Postselected Bell state	Gate U_ϕ on qubit A
$|\alpha\rangle$	$|e^{i\pi/4}\alpha\rangle$	$|\Psi^-\rangle$	$\mathbb{1}$
$|\alpha\rangle$	$|-e^{i\pi/4}\alpha\rangle$	$|\Psi^+\rangle$	$i\sigma_{2\phi}$
$|-\alpha\rangle$	$|e^{i\pi/4}\alpha\rangle$	$|\Phi_{2\phi}^-\rangle$	$\sigma_{2\phi}\sigma_z$
$|-\alpha\rangle$	$|-e^{i\pi/4}\alpha\rangle$	$|\Phi_{2\phi}^+\rangle$	$i\sigma_z$

Table 5.1: *Summary of the quantum protocol indicating the measured field in each cavity, the corresponding post-selected Bell state and the unitary gate that has to be applied to complete a Bell measurement.*

of the postselected atomic states with respect to the corresponding Bell state, i.e., $F_{\text{Bell}} = \langle\psi_{\text{Bell}}|\rho_{\text{at}}|\psi_{\text{Bell}}\rangle$, where $|\psi_{\text{Bell}}\rangle$ stands for one of the four Bell states and ρ_{at} is the reduced density matrix of the two atoms after implementation of the protocol in Fig. 5.6. We have also performed an average over 10^3 initial atomic random pure states from a uniform $SU(4)$ distribution in order to produce generic results for two-qubit systems. In Fig. 5.7 we plot the average fidelity of the numerically obtained Bell states as a function of the mean photon number. We can see that even for relatively small photon numbers, a complete Bell-measurement can be implemented following the proposed protocol. In this case, the only requirement for the mean photon number is to be sufficiently large. This contrasts with previous findings based on the Tavis-Cummings model for which the fidelity of two of the four Bell states is an oscillatory function of the mean photon number, making the protocol functional only for restricted values of the mean photon number [30]. As the protocol is envisioned to work at half of the revival time, it is important to explore the
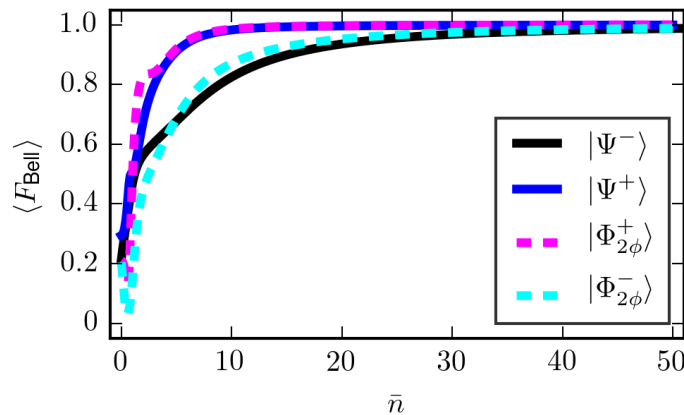
Figure 5.7: *Ensemble average fidelity $\langle F_{\text{Bell}}\rangle$ for each postselected Bell state after the application of the protocol as a function of the mean photon number.*

sensitivity of the Bell measurement when the interaction time is closed but not exactly $t_r/2$. In Fig. 5.8 we

plot the average fidelity in a short time window close to half of the revival time for the four postselected Bell states. In this case we have set the mean photon number $\bar{n} = 50$, for which we know almost perfect fidelity can be obtained. The results show almost unit fidelity for projecting onto the states $|\Psi^-\rangle$ and $|\Phi^+_{2\phi}\rangle$. The first case can be understood in analogy to the Tavis-Cummings model for which one can show that the state $|\Psi^-\rangle$ remains invariant under time evolution [29]. Approximately regular oscillating behavior is found for the other two Bell states near the optimal time $gt = \pi/2$, with a similar effective frequency roughly given by $g(\bar{n}+1)$. In order to get an idea of a deviation ε allowed in the interaction time $t_r/2 \pm \varepsilon$, one can estimate that this possible error must satisfy the condition $|\varepsilon| \ll 1/2\pi g(\bar{n}+1)$ for the protocol to work with nearly optimal fidelity.
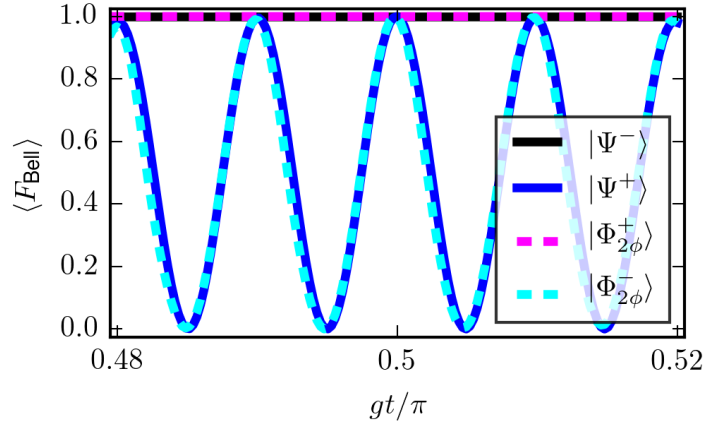
Figure 5.8: Ensemble average fidelity $\langle F_{\mathrm{Bell}} \rangle$ for each postselected Bell state after the application of the protocol around the optimal time $t_r/2$.

5.4 Experimental considerations

We now comment on the possibilities of the experimental realization of the above mentioned protocol. In the cavity-QED scenario, experiments using optical conveyor belts to transport neutral laser-cooled cesium atoms into an optical resonator have been successfully performed [169, 170]. Adapted to our scheme, the idea would be to transport atoms using a standing wave dipole trap into a sequence of two single mode optical cavities. The effects of losses can be neglected, provided the experiment operates in the strong coupling regime, where the condition $g \gg \gamma, \kappa$ holds, i.e., the qubit-field coupling is much larger than the spontaneous decay rate γ of the atoms and the rate accounting for photon losses in the cavities κ. As in our model the revival time is independent of the mean photon number, at the optimal time these conditions are slightly modified to: $g/\gamma \gg \pi/2$ and $g/\kappa \gg \pi/2$, which can met the actual decay rate requirements in cavity-QED experiments.

Similar cavity-based schemes involving coupled cavities and two-level atoms have been also proposed for different applications. For instance, coherence and entanglement protection in the presence of dissipation [171]. The physical realization of these systems seems to fit very well within the context of the circuit quantum electrodynamics architecture (circiut-QED) [172–174], where transmon qubits can be efficiently coupled to coplanar waveguide cavities. High fidelity preparation of entangled input initial states for the protocol can be in principle engineered using a quantum bus trough a transmission line resonator as described in Ref. [175], and the interaction time of the two-qubit system with the resonator mode can also be switched-off after the corresponding projective measurement of the optical mode, thus implementing all the steps of the algorithm in a single on-chip superconducting circuit.

It is worth commenting on the possible implementation in trapped-ion experiments, as they constitute one of the most successful platforms for quantum simulation and quantum information processing [176]. An interesting simulation based on trapped ions has been recently proposed for emulating the dynamics of the two-photon Rabi model in different coupling regimes [97]. As our protocol is supposed to work in the so called strong-coupling regime, where the qubit frequency is assumed to be very small compared with the qubit-field coupling, its implementation in this particular architecture seems to be feasible with current technology. In this context two identical atomic ions with two internal electronic states with level splitting δ placed in a harmonic trap of frequency ν. The Hamiltonian describing this situation in the presence of a driving classical field of Rabi frequency Ω is given by

$$H_I = \frac{\delta}{2}S_{ee} + \nu a^\dagger a + \Omega S_x \left[e^{i(kx - \omega_l t - \varphi)} + \text{H.c.} \right], \tag{5.41}$$

where $x = \sqrt{\frac{1}{2m\nu}}(a + a^\dagger)$ is the position operator describing the displacement of the center of mass of the system of two ions. We can then perform an optical rotating-wave approximation and neglect terms oscillating with frequencies $\delta + \omega_l$. The next step is moving to an interaction frame with respect to the free Hamiltonian, i.e., $\tilde{H}_I = e^{iH_0 t} H_I e^{-iH_0 t}$ with $H_0 = \frac{\delta}{2}S_{ee} + \nu a^\dagger a$, and in the so called Lamb-Dicke regime one can obtain the typical Tavis-Cummings interaction of the two ions with the vibrational mode. Interestingly , an effective two-phonon coupling can be obtained by driving with a laser (second red sideband) at a frequency $\omega_l = \delta - 2\nu$. By applying the vibrational RWA, one can finally get the following trapped-ion Hamiltonian in the interaction picture

$$\tilde{H}_I = -\frac{\Omega}{2}\eta^2 \left(S_{eg} a^2 e^{-i\varphi} + S_{ge} a^{\dagger 2} e^{i\varphi} \right), \tag{5.42}$$

which for $\varphi = 0$ can be immediately recognized as our effective Hamiltonian model in Eq. (5.6) with an effective coupling given by $g_{\text{eff}} = -\Omega\eta^2/2$, being Ω the Rabi frequency of the laser, and η the so-called Lamb-Dicke parameter. The Rabi frequency in trapped-ion experiments lies in the range of kHz and $\eta \sim 10^{-2}$, which leads to a coupling constant of $g_{\text{eff}} \sim 10^2$ Hz. Taking into account these values, it is possible to estimate the optimal time needed to perform the Bell measurement scheme in a trapped-ion setup from the relation $g_{\text{eff}}t/\pi = 1/2$, which results in a simulation time of ~ 10ms. Typical experiments involving, for instance, optical ^{40}Ca$^+$ ions have coherence times of ~ 3ms [177,178]. These times are still small if a Bell measurement based on the proposed protocol is to be performed. However, continuous dynamical decoupling schemes have been recently proposed in order to achieve long-time coherent dynamics by eliminating magnetic dephasing noise in ion-trap simulators [96], making our proposal for Bell state discrimination more realistic and in reach of current technology.

Chapter 6

Conclusions

This dissertation presented the study of decoherence and entanglement evolution in particular two-qubit systems. Ranging from one and two spin qubits in the presence of a spin environment network in the chaotic regime to paradigmatic models of atomic qubits interacting with bosonic fields in optical cavitites. In the first case we have explored various aspects of the effect of nested environments on a central system using the kicked Ising model in chaper 3. Taking advantage of its map structure we have performed simple calculations on relatively large systems. Our departing point was the growing evidence, that for a situation with a central system coupled weakly to a near environment and no (or negligible) direct coupling to a far environment, increasing the coupling between near and far environment slows decoherence of the central system. This effect was confirmed over a wide range of situations for a one-qubit central system with dephasing or more general coupling to the near environment as well as for a two-qubit system in a Bell state with one of the qubits being in a (non-interacting) spectator situation. We demonstrate a similar behaviour for concurrence, which is an essential point for the usefulness of the encountered effect in the context of quantum information. The decoherence of quantum systems is often analyzed from the perspective of Fermis golden rule, which states that the decay rate between two states is proportional to the density of states in the environment. In this work, we are between the Fermi's Golden Rule regime (exponential decay), and the perturbative regime (Gaussian decay). An analysis of how an effective density of states of the near environment changes due to its interaction with the far environment might shed light on general aspects of the effects reported in this thesis. This lies outside of the scope of this work, but it is a promising direction for future research.

In chapter 4 we have presented different exactly solvable models for the dynamics of entanglement and purity of a simple two-qubit central system in the context of light-matter interaction models. We have taken advantage of the spectator configuration, where a qubit is isolated, in order to realize a single local quantum operation acting on a maximally entangled pure state. Furthermore, it allows for straightforwardly find the evolved two-qubit density matrix once the quantum map of the open qubit is known. We have obtained explicit analytical expressions for purity, concurrence and their dynamical relations (Eqs. 4.10 and 4.21) using Tavis-Cummings, Buck-Sukumar and spin-boson type interactions. Our results confirm that even in the spectator scheme the entanglement can disappear at a finite time depending on the initial conditions, as previously found in other open quantum systems [35, 47, 55]. Long-time entanglement revivals appear when a coherent state of the radiation environment is considered, showing that even simpler systems that the ones treated in previous works [12, 19, 36, 37] can reveal general features of entanglement evolution. In fact, the qualitative behaviors of the dynamics of quantum correlations, like entanglement, are analogous for bipartite systems of both open qubits and only one open qubit provided that the qubits are independent and locally interacting with their own environment.

As a further source of information we have exploited the *C-P* diagram to characterize how local actions ruled by the environment affect an initial two-qubit Bell state. For the TC and BS interactions, the two-

qubit state can reach points outside of the unital region which thus demonstrates the non-unital nature of these kind of quantum maps commonly employed in the context of quantum optics. We have also discussed the potentiality of having concurrence-purity dynamical relations to assess quantitative entanglement and purity thresholds at a given time which allow specific quantum tasks, such as teleportation. These results motivate further studies of dynamical characterization of thresholds of purity and entanglement for implementing processes like entanglement swapping [66] and entanglement percolation [67]. For future works, it would be also interesting to consider more realistic models in the spirit of the spectator configuration, for instance introducing spontaneous emission and cavity photon losses by means of Lindblad master equations.

We have also derived the microscopic master equation for the Jaynes-Cummings model under field dissipation at finite temperature and off-resonance. We revisited evolution in the well-known zero-T single-excitation manifold, where the difference in the dynamics under the microscopic and phenomenological approaches appear as a high-frequency modulation of the ground state probability in the phenomenological approach, constructed an analytic closed form for the state evolution, and show the effects of detuning between the qubit and field frequencies on the effective decay rates; for initial states with an excited qubit a larger detuning produces a lower decay rate and the opposite for initial states with the qubit in the ground state. This is obvious, due to the decay channels, and results in an ordering of the qubit-field purity minima. Interestingly, these minima are not observed in the von Neumann entropy for the field (not shown) or the concurrence of the joint qubit-field state. We confirmed numerically these behaviors beyond the single-excitation manifold at finite temperatures for initial Fock states of the field, where the dynamics start in a well-defined excitation manifold, and studied dissipation for initial coherent states, where the dynamics start in an extended superposition of excited manifolds. For initial coherent states of the field, dynamics under the microscopic approach provides a faster suppression of the collapse and revivals of the population inversion than the phenomenological approach, but the real difference is observed in phase-space, where the microscopic approach provides a smooth spiral decay trajectory of the field quadratures, while the phenomenological approach produces more convoluted dynamics with highly oscillating variances in the quadratures. In summary, while a phenomenological treatment makes it simpler to create a building block approach to open systems that does not differ much at short times from the predictions of a formal treatment, a microscopic treatment of dissipation produces smoother dynamics that are closer to what semi-classical intuition might signal. This seems to suggest that it becomes imperative to follow formal approaches to dissipation in order to describe multipartite interaction models.

Chapter 5 of this thesis has focused in the interesting subject of quantum information protocols employing material qubits and their interaction with confined electromagnetic fields. In this context we have presented a Bell measurement scheme on atomic qubits that interact with bosonic fields contained in two separate cavities via two-photon processes in a two-stage Ramsey-type setup. The protocol is based on the two-atom two-photon Dicke model in the limit of large photon number for initial coherent states of the field. Under such conditions, we have derived an approximate solution in terms of atomic Bell states and photonic coherent states, allowing the identification of an appropriate Bell-measurement protocol via coherent state discrimination in two separate cavities. In contrast with previous proposed protocols [29,30] based on multiphoton states, the one presented here allows a complete discrimination of the four atomic Bell states, i.e. a 100%-efficient Bell measurement that we have numerically confirmed by computing the average fidelity over random initial states. The robustness of the protocol as a function of the interaction time has been tested and the corresponding condition for a possible error in terms of the mean photon number was estimated. By analyzing the time-dependent state of the full system, we have also demonstrated that tripartite entangled GHZ states can be naturally generated by the unitary dynamics of the two-photon model, a possibility that can be further exploited in other quantum information protocols. It is worth stressing that the complete projection onto the full Bell basis is possible as a consequence of the perfect discrimination of two separate components of the evolved field which in turn relies on the perfect revivals of Rabi oscillations in the two photon model.

Bibliography

[1] A. G. J. MacFarlane, J. P. Dowling, and G. J. Milburn *Philos. Trans. R. Soc. Lond. A* **361** (2003)

[2] Quantum Manifesto: *A new era of quantum technology* 2016 http://qurope.eu/system/files/u567/Quantum%20Manifesto.pdf

[3] P. W. Shor *Proc. 35th Annual Symposium on Foundations of Computer Science, IEEE Computer Society Press*, Los Alamitos, CA, pp. 124134 1994

[4] Einstein, A. and Podolsky, B. and Rosen, N., *Phys. Rev.*, **47** 777 (1935)

[5] J. Baugh, J. Chamilliard, C. M. Chandrashekar, M. Ditty, A. Hubbard, R. Laflamme, M. Laforest, D. Maslov, O. Moussa, C. Negrevergne, M. Silva, S. Simmons, C. A. Ryan, D. G. Cory, J. S. Hodges, C. Ramanathan *Physics in Canada, Theme Issue - Quantum Computing and Quantum Information*, **63** 197 (2007)

[6] Haroche S 2006 *Exploring the quantum: atoms, cavities, and photons* (Oxford New York: Oxford University Press)

[7] Leibfried D, Blatt R, Monroe C, and Wineland D 2003 *Rev. Mod. Phys.* **75** 281

[8] H. Hffner, C.F. Roos, and R. Blatt. Quantum computing with trapped ions. *Physics Reports*, 469(4):155 – 203, 2008.

[9] M. Brune, E. Hagley, J. Dreyer, X. Maitre, A. Maali, C. Wunderlich, J. M. Raimond, and S. Haroche. *Phys. Rev. Lett.*, 77:4887–4890, Dec 1996.

[10] Schlosshauer M A 2007 *Decoherence and the quantum-to-classical transition* (Springer Science & Business Media)

[11] Rivas Á, Huelga S F and Plenio M B 2014 *Rep. Prog. Phys.* **77** 094001

[12] Aolita L, de Melo F and Davidovich L 2015 *Rep. Prog. Phys.* **78** 042001

[13] Cianciaruso M, Bromley T R, Roga W, Lo Franco R and Adesso G 2015 *Sci. Rep.* **5** 10177

[14] Leggio B, Lo Franco R, Soares-Pinto D O, Horodecki P and Compagno G 2015 *Phys. Rev. A* **92** 032311

[15] Caldeira, A O and Leggett, A J, *Physica*, **587** (1983)

[16] Caldeira , A O, Castro-Neto, A H and Oliveira de Carvalho, T *Phys. Rev. B*, **48** (1993)

[17] Prokof'ev, N V and Stamp, *Rep. on Prog. in Phys.* **63** (2000)

[18] Breuer H P and Petruccione F 2002 *The Theory of Open Quantum Systems* (Oxford, New York: Oxford University Press)

[19] Lo Franco R, Bellomo B, Maniscalco S and Compagno G 2013 *Int. J. Mod. Phys. B* **27** 1345053

[20] M. A. Nielsen and I. Chuang, *Quantum computation and quantum information* (Cambridge University Press, 2000).

[21] Benenti G, Casati G and Strini G 2007 *Principles of quantum computation and information* (Singapore: World Scientific)

[22] Tavis M and Cummings F W 1968 *Phys. Rev.* **170** 379–384

[23] Fink J M, Bianchetti R, Baur M, Göppl M, Steffen L, Filipp S, Leek P J, Blais A and Wallraff A 2009 *Phys. Rev. Lett.* **103** 083601

[24] Moya-Cessa H 2006 *Phys. Rep.* **432** 1–41

[25] Leek P J, Baur M, Fink J M, Bianchetti R, Steffen L, Filipp S and Wallraff A 2010 *Phys. Rev. Lett.* **104** 100504

[26] Amico L, Fazio R, Osterloh A and Vedral V 2008 *Rev. Mod. Phys.* **80** 517-576

[27] Clemens J P and Rice P 2006 Multipartite entanglement in cavity qed *Frontiers in Optics* (Optical Society of America) p LTuD3

[28] Osborne T J and Nielsen M A 2002 *Phys. Rev. A* **66**(3) 032110

[29] J. M. Torres, J. Z. Bernád and G. Alber, Phys. Rev. A **90**, 012304 (2014).

[30] J. M. Torres, J. Z. Bernád and G. Alber, App. Phys. B **122**, 117 (2016).

[31] DiCarlo L *et al.* 2009 *Nature* **460** 240–244

[32] Romero G, Ballester D, Wang Y M, Scarani V and Solano E 2012 *Phys. Rev. Lett.* **108** 120501

[33] Felicetti S, Sanz M, Lamata L, Romero G, Johansson G, Delsing P and Solano E 2014 *Phys. Rev. Lett.* **113** 093602

[34] Yu T and Eberly J H 2004 *Phys. Rev. Lett.* **93** 140404

[35] Cui H, Li K and Yi X 2007 *Phys. Lett. A* **365** 44–48

[36] Yönaç M and Eberly J H 2008 *Opt. Lett.* **33** 270–272

[37] Yönaç M and Eberly J H 2010 *Phys. Rev. A* **82** 022321

[38] Yu T and Eberly J H 2009 *Science* **323** 598–601

[39] Gorin T, Pineda C and Seligman T H 2007 *Phys. Rev. Lett.* **99** 240405

[40] Pineda C, Gorin T and Seligman T H 2007 *New J. Phys.* **9** 106

[41] Carlos Pineda and Thomas H. Seligman Phys. Rev. A 75, 012106 (2007)

[42] Ziman M and Bužek V 2005 *Phys. Rev. A* **72** 052325

[43] Cardoso E S, de Oliveira M C and Furuya K 2005 *Phys. Rev. A* **72** 042320

[44] Almeida M P, de Melo F, Hor-Meyll M, Salles A, Walborn S P, Ribeiro P H S and Davidovich L 2007 *Science* **316** 579–582

[45] Laurat J, Choi K S, Deng H, Chou C W and Kimble H J 2007 *Phys. Rev. Lett.* **99** 180504

[46] Lim H T, Lee J C, Hong K H and Kim Y H 2014 *Opt. Express* **22** 19055–19068

[47] Lo Franco R 2016 *Quantum Inf. Process.* DOI:10.1007/s11128–016–1290–3

[48] Lo Franco R, D'Arrigo A, Falci G, Compagno G and Paladino E 2014 *Phys. Rev. B* **90** 054304

[49] Orieux A, Ferranti G, D'Arrigo A, Lo Franco R, Benenti G, Paladino E, Falci G, Sciarrino F and Mataloni P 2015 *Sci. Rep.* **5** 8575

[50] D'Arrigo A, Lo Franco R, Benenti G, Paladino E and Falci G 2014 *Ann. Phys.* **350** 211

[51] Bellomo B, Lo Franco R, Maniscalco S and Compagno G 2008 *Phys. Rev. A* **78** 060302(R)

[52] Bellomo B, Lo Franco R and Compagno G 2009 *Adv. Sci. Lett.* **2** 459

[53] Bellomo B, Lo Franco R and Compagno G 2007 *Phys. Rev. Lett.* **99** 160502

[54] Man Z X, Xia Y J and Lo Franco R 2015 *Sci. Rep.* **5** 13843

[55] Xu J S *et al.* 2013 *Nature Commun.* **4** 2851

[56] Bellomo B, Lo Franco R, Maniscalco S and Compagno G 2010 *Phys. Scripta* **T140** 014014

[57] Bellomo B, Compagno G, Lo Franco R, Ridolfo A and Savasta S 2011 *Phys. Scr.* **T143** 014004

[58] Bellomo B, Lo Franco R, Andersson E, Cresser J D and Compagno G 2012 *Phys. Scr.* **T147** 014004

[59] Man Z X, Xia Y J and Lo Franco R 2015 *Phys. Rev. A* **92** 012315

[60] H. J. Moreno, T. Gorin, and T. H. Seligman. Improving coherence with nested environments. *Phys. Rev. A*, 92:030104, Sep 2015.

[61] C. González-Gutiérrez, E. Villaseor, C. Pineda and T. H. Seligman, Phys. Scrip. **91**, 083001 (2016).

[62] Carlos Pineda, PhD Thesis, Universidad Nacional Autónoma de México (2007) *Preprint at arXiv:0711.4642*

[63] Mazzola L, Bellomo B, Lo Franco R and Compagno G 2010 *Phys. Rev. A* **81** 052116

[64] Qin M, Li Y B and Wu F P 2014 *Quantum Inf. Process.* **13** 1573

[65] Roa L, Gómez R, Muñoz A and Rai G *Preprint at arXiv:1508.01417*

[66] Roa L, Muñoz A and Grüning G 2014 *Phys. Rev. A* **89** 064301

[67] Acín A, Cirac J I and Lewenstein M 2007 *Nat. Phys.* **3** 256

[68] Shaham A, Halevy A, Dovrat L, Megidish E and Eisenberg H 2015 *Sci. Rep.* **5** 10796

[69] Chiuri A, Greganti C, Mazzola L, Paternostro M and Mataloni P 2012 *Sci. Rep.* **2** 968

[70] Li Z J, Li J Q, Jin Y H and Nie Y H 2007 *J. Phys. B: Atom. Mol. Opt. Phys.* **40** 3401

[71] D. Bouwmeester, J.W. Pan, K. Mattle, M. Eibl, H. Weinfurter and A. Zeilinger, Nature **390**, 575 (1997).

[72] P. van Loock, T. D. Ladd, K. Sanaka, F. Yamaguchi, Kae Nemoto, W. J. Munro and Y. Yamamoto, Phys. Rev. Lett. **96**, 240501 (2006).

[73] S. Pirandola, J. Eisert, C. Weedbrook, A. Furusawa and S. L. Braunstein, Nat. Photonics **9**, 641 (2015).

[74] M. Michler, K. Mattle, H. Weinfurter and A. Zeilinger, Phys. Rev. A **53**, R1209 (1996).

[75] N. Lütkenhaus, J. Calsamiglia and K.-A. Suominen, Phys. Rev. A **59**, 3295 (1999).

[76] J. Calsamiglia and N. Lütkenhaus, App. Phys. B **72**, 67 (2001).

[77] F. Ewert and P. van Loock, Phys. Rev. Lett. **113**, 140403 (2014).

[78] W. P. Grice, Phys. Rev. A **84**, 042331 (2011).

[79] C. H. Bennett, Gilles Brassard, Claude Crépeau, Richard Jozsa, Asher Peres and William K. Wootters, Phys. Rev. Lett. **70** , 1895 (1993).

[80] Y.-H. Kim, S. P. Kulik and Y. Shih, Phys. Rev. Lett. **86**, 1370 (2001).

[81] M. Riebe, H. Häffner, C. F. Roos, W. Hänsel, J. Benhelm, G. P. T. Lancaster, T. W. Körber, C. Becher, F. Schmidt-Kaler, D. F. V. James and R. Blatt, Nature **429**, 734 (2004).

[82] M. D. Barrett, J. Chiaverini, T. Schaetz, J. Britton, W. M. Itano, J. D. Jost, E. Knill, C. Langer, D. Leibfried, R. Ozeri and D. J. Wineland , Nature **429**, 737 (2004).

[83] M. Riebe, M. Chwalla, J. Benhelm, H. Häffner, W. Hänsel, C. F. Roos and R. Blatt, New J. Phys. **9**, 211 (2007).

[84] F. Schmidt-Kaler, H. Häffner, S. Gulde, M. Riebe, G.P.T. Lancaster, T. Deuschle, C. Becher, W. Hänsel, J. Eschner, C.F. Roos and R. Blatt, Appl. Phys. B **77**, 789 (2003).

[85] F. Schmidt-Kaler, H. Häffner, M. Riebe, S. Gulde, G. P. T. Lancaster, T. Deuschle, C. Becher, C. F. Roos, J. Eschner and Rainer Blatt, Nature **422**, 408 (2003).

[86] C. Nölleke, A. Neuzner, A. Reiserer, C. Hahn, G. Rempe and S. Ritter, Phys. Rev. Lett. **110**, 140403 (2013).

[87] J. Z. Bernád, Phys. Rev. A **96**, 052329 (2017).

[88] C.E.A. Jarvis, D.A. Rodrigues, B.L. Györffy, T.P. Spiller, A.J. Short and J.F. Annett, New J. Phys. **11**, 103047 (2009).

[89] J. H. Eberly, N. B. Narozhny and J. J. Sanchez-Mondragon Phys. Rev. Lett. **44**, 1323 (1980).

[90] A. B. Klimov, J. Negro, R. Farias and S. M. Chumakov, J. Opt. B **1**, 562 (1999).

[91] P. Alsing and M. S. Zubairy, J. Opt. Soc. Am. B **4**, 177 (1987).

[92] C. V. Sukumar and B. Buck, Phys. Lett. A **83**, 211 (1981).

[93] A. H. Toor and M. S. Zubairy, Phys. Rev. A **45**, 4951 (1992).

[94] I. Jex, Quantum Opt., **2**, 443 (1990).

[95] M. Brune, J. M. Raimond and S. Haroche, Phys. Rev. A **35**, 154 (1987).

[96] R. Puebla, M.J. Hwang, J. Casanova and M. B. Plenio, Phys. Rev. A **95**, 063844 (2017).

[97] S. Felicetti, D. Z. Rossatto, E. Rico, E. Solano and P. Forn-Díaz, Phys. Rev. A **97**, 013851 (2018).

[98] E. K. Bashkirov Phys. Scr. **82**, 015401 (2010).

[99] C. A. González-Gutiérrez, R. Román-Ancheyta, D. Espitia and R. Lo Franco, Int. J. of Quant. Inform. **14**, 1650031 (2016).

[100] C. A. González-Gutiérrez, D. Solís-Valles and B. M. Rodríguez-Lara, J. Phys. A **51**, 015301 (2018).

[101] C. A. González-Gutiérrez and J. M. Torres, arXiv:1811.06176 (2018) (Summited to Physical Review A).

[102] Ryszard Horodecki, Pawe Horodecki, Micha Horodecki, and Karol Horodecki Rev. Mod. Phys. 81, 865 (2009)

[103] Adil S. Rab *et. al.* Nature Communications **8** 915 (2017)

[104] D. Bouwmeester, J.W. Pan, M. Daniell, H. Weinfurter and A. Zeilinger, Phys. Rev. Lett. **82**, 1345 (1999).

[105] T. Monz, P. Schindler, J. T. Barreiro, M. Chwalla, D. Nigg, W. A. Coish, M. Harlander, W. Hänsel, M. Hennrich and R. Blatt, Phys. Rev. Lett. **106**, 130506 (2011).

[106] Mohan Sarovar, Akihito Ishizaki, Graham R. Fleming, and K. Birgitta Whaley Nature Phys. **6** 462 (2010)

[107] Bell, J. S. Physics. **1** (3) 195 (1964)

[108] Aspect, A. *et al.* Phys. Rev. Lett. 49 (2) 91 (1982).

[109] Florian Mintert, Andr R.R. Carvalho, Marek Ku, and Andreas Buchleitner Phys. Rep. **415** 207 (2005)

[110] Li JL, Qiao CF Sci. Rep. **8** 1442 (2018).

[111] A. Uhlmann. Endlich-dimensionale dichtematrizen. i. *Wissenschaftliche Zeitschrift der Karl-Marx-Universität Leipzig. Mathematisch-Naturwissenschaftliche Reihe*, 21:421–452, 1972.

[112] E. Ruch. *Theor. Chim. Acta*, 38(3):167–183, 1975.

[113] E. Ruch and A. Mead. *Theor. Chim. Acta*, 41(2):95–117, 1976.

[114] W. K. Wootters. Entanglement of formation of an arbitrary state of two qubits. *Phys. Rev. Lett.*, 80:2245–2248, Mar 1998.

[115] T. Prosen. General relation between quantum ergodicity and fidelity of quantum dynamics. *Phys. Rev. E*, 65:036208, Feb 2002.

[116] T. Prosen. Exact time-correlation functions of quantum ising chain in a kicking transversal magnetic field: Spectral analysis of the adjoint propagator in heisenberg picture. *Progress of Theoretical Physics Supplement*, 139:191–203, 2000.

[117] A. Lakshminarayan and V. Subrahmanyam. Multipartite entanglement in a one-dimensional time-dependent ising model. *Phys. Rev. A*, 71:062334, Jun 2005.

[118] Carlos Pineda and Toma Prosen Phys. Rev. E **76**, 061127 (2007).

[119] Haake, F. Quantum Signatures of Chaos, **54** (Springer Science & Business Media, 2010)

[120] I. Pižorn, T. Prosen, S. Mossmann, and T. H. Seligman. The two-body random spin ensemble and a new type of quantum phase transition. *New Journal of Physics*, 10(2):023020, 2008.

[121] Z. Pluhař and A. Weidenmüller, H.˙ Universal quantum graphs. *Phys. Rev. Lett.*, 112:144102, Apr 2014.

[122] C. Pineda, T. Prosen, and E. Villaseor. *New Journal of Physics*, 16(12):123044, 2014.

[123] T. Gorin, H. J. Moreno, and T. H. Seligman. Philos. Trans. A Math Phys Eng Sci. 374(2069): 20150162 (2016)

[124] S. A. Gardiner, J. I. Cirac, and P. Zoller. Quantum chaos in an ion trap: The delta-kicked harmonic oscillator. *Phys. Rev. Lett.*, 79:4790–4793, Dec 1997.

[125] F. Haug, M. Bienert, W. P. Schleich, T. H. Seligman, and M. G. Raizen. Motional stability of the quantum kicked rotor: A fidelity approach. *Physical Review A*, 71(4):043803, 2005.

[126] T Gorin, T. Prosen, T. H. Seligman, and W.T. Strunz. Connection between decoherence and fidelity decay in echo dynamics. *Physical Review A*, 70(4):042105, 2004.

[127] P. Zanardi and L. Campos Venuti. Coherent quantum dynamics in steady-state manifolds of strongly dissipative systems. *Phys. Rev. Lett.*, 113:240406, Dec 2014.

[128] J. M. Torres and T. H. Seligman New J. Phys. 19 113016 (2017)

[129] A.R. Bosco de Magalhes, R. Rossi Jr., and M.C. Nemes. Environment induced quantum zeno effect in coupled microwave cavities. *Physics Letters A*, 375(16):1724 – 1728, 2011.

[130] A. Z. Chaudhry and J. Gong. Decoherence induced by a composite environment. *Phys. Rev. A*, 89:014104, Jan 2014.

[131] S. Ishizaka and T. Hiroshima. Maximally entangled mixed states under nonlocal unitary operations in two qubits. *Phys. Rev. A*, 62:022310, Jul 2000.

[132] Susskind L and Glogower J 1964 *Physics* **1** 49–61

[133] Buck B and Sukumar C 1981 *Phys. Lett. A* **81** 132 – 135

[134] Falci G, D'Arrigo A, Mastellone A and Paladino E 2005 *Phys. Rev. Lett.* **94** 167002

[135] Lo Franco R, D'Arrigo A, Falci G, Compagno G and Paladino E 2012 *Phys. Scr.* **T147** 014019

[136] López C E, Romero G, Lastra F, Solano E and Retamal J C 2008 *Phys. Rev. Lett.* **101** 080503

[137] López C E, Romero G and Retamal J C 2010 *Phys. Rev. A* **81** 062114

[138] Jaynes E T and Cummings F W 1963 *Proc. IEEE* **51** 89

[139] Eberly J H, Narozhny N B, and Sánchez-Mondragón J J 1980 *Phys. Rev. Lett.* **44** 1323

[140] Nielsen M A and Chuang I L 2000 *Quantum computation and quantum information* (Cambridge University Press)

[141] Raimond J M, Brune M, and Haroche S 2001 *Rev. Mod. Phys.* **73** 565

[142] Xiang Z L, Ashhab S, You J Q, and Nori F 2013 *Rev. Mod. Phys.* **85** 623

[143] Rempe G, Walther H, and Klein N 1987 *Phys. Rev. Lett.* **58** 353

[144] Cirac J I, Blatt R, Parkins A S, and Zoller P 1994 *Phys. Rev. A* **49** 1202

[145] Meekhof D M, Monroe C, King B E, Itano W M, and Wineland D J 1996 *Phys. Rev. Lett.* **76** 1796

[146] Brune M, Schmidt-Kaler F, Maali A, Dreyer J, Hagley E, Raimond J M, and Haroche S 1996 *Phys. Rev. Lett.* **76** 1800

[147] Puri R R and Agarwal G S 1986 *Phys. Rev. A* **33** 3610

[148] Eiselt J and Risken H 1989 *Opt. Comm.* **72** 351

[149] Eiselt J and Risken H 1991 *Phys. Rev. A* **43** 346

[150] Barnett S M and Jeffers J 2007 *J. Mod. Opt.* **54** 2033

[151] Chiorescu I, Bertet P, Semba K, Nakamura Y, Harmans C J P M, and Mooij J E 2004 *Nature* **431** 159

[152] Wallraff A, Schuster D I, Blais A, Frunzio L, Huang R S, Majer J, Kumar S, Girvin S M, and Schoelkopf R J 2004 *Nature* **431** 162

[153] Wilczewski M and Czachor M 2009 *Phys. Rev. A* **79** 033836

[154] Wilczewski M and Czachor M 2009 *Phys. Rev. A* **80** 013802

[155] Scala M, Militello B, Messina A, Piilo J, and Maniscalco S 2007 *Phys. Rev. A* **75** 013811

[156] Scala M, Militello B, Messina A, Maniscalco S, Piilo J, and Suominen K A 2007 *J. Phys. A: Math. Theor.* **40** 14527

[157] Gerry C and Knight P L 2005 *Introductory quantum optics* (Cambridge University Press)

[158] Breuer H P and Petruccione F 2002 *The theory of open quantum systems* (Cambridge University Press)

[159] Haroche S 1992 In Dalibard J, Raimond J M, and Zinn-Justin J, editors *Fundamental systems in quantum optics: Proceedings of the Les Houches summer school, session LIII, 1990* Netherlands North-Holland.

[160] Cohen-Tannoudji C, Dupont-Roc J, and Grynberg G 1998 *Atom-Photon Interactions: Basic Processes and Applications* (Wiley)

[161] Briegel H J and Englert B G 1993 *Phys. Rev. A* **47** 3311

[162] Navarrete-Benlloch C 2015 arXiv:1504.05266v2 [quant-ph]

[163] J. Z. Bernád, J. M. Torres, L. Kunz and G. Alber, Phys. Rev. A **93**, 032317 (2016).

[164] R. R. Puri and R. K. Bullough, J. Opt. Soc. Am. B **5**, 2021 (1988).

[165] K. Vogel and H. Risken Phys. Rev. A **40**, 2847(R) (1989).

[166] C. Gerry, Phys. Rev. A **54**, R2529 (1996).

[167] J. Kelly, R. Barends, A. G. Fowler, A. Megrant *et al.*, Nature **519**, 66 (2015).

[168] C. Wittmann, M. Takeoka, K.N. Cassemiro, M. Sasaki, G. Leuchs and U.L. Andersen, Phys. Rev. Lett. **101**, 210501 (2008).

[169] R. Reimann, W. Alt, T. Macha, D. Meschede, N. Thau, S. Yoon and L. Ratschbacher, New J. Phys. **16**, 113042 (2014).

[170] R. Reimann, W. Alt, T. Kampschulte, T. Macha, L. Ratschbacher, N. Thau, S. Yoon and D. Meschede, Phys. Rev. Lett. **114**, 023601 (2015).

[171] Z.-X. Man, Y.-J. Xia and R. Lo Franco, Sci. Rep. **5**, 13843 (2015).

[172] A. Blais, R.-S. Huang, A. Wallraff, S. M. Girvin and R. J. Schoelkopf, Phys. Rev. A **69**, 062320 (2004).

[173] N. T. Bronn, E. Magesan, N. A. Masluk, J. M. Chow, J. M. Gambetta and M. Steffen, IEEE Trans. Appl. Supercond. **25**, 1700410 (2015).

[174] X. Gu, A. F. Kockum, A. Miranowicz, Y-x. Liu and F. Nori, Phys. Rep. **1**, 718 (2017).

[175] L. DiCarlo, J. M. Chow, J. M. Gambetta, Lev S. Bishop, B. R. Johnson, D. I. Schuster, J. Majer, A. Blais, L. Frunzio, S. M. Girvin and R. J. Schoelkopf, Nature **460**, 240 (2009).

[176] D. Leibfried, R. Blatt, C. Monroe and D. Wineland, Rev. Mod. Phys. **75**, 281 (2003).

[177] R. Gerritsma, B. P. Lanyon, G. Kirchmair, F. Zähringer, C. Hempel, J. Casanova, J. J. García-Ripoll, E. Solano, R. Blatt and C. F. Roos, Phys. Rev. Lett. **106**, 060503 (2011).

[178] N. Timoney, I. Baumgart, M. Johanning, A. F. Varn, M. B. Plenio, A. Retzker and Ch. Wunderlich, Nature **476**, 185 (2011).